

**SENSITIVITY OF TURKISH PRECIPITATION TO SEA
SURFACE TEMPERATURE VARIABILITY IN THE
SURROUNDING SEAS**

**M.Sc. Thesis by
Deniz BOZKURT, B.Sc.**

Department: Climate and Marine Sciences

Programme: Earth System Science

JANUARY 2007

**SENSITIVITY OF TURKISH PRECIPITATION TO SEA
SURFACE TEMPERATURE VARIABILITY IN THE
SURROUNDING SEAS**

**M.Sc. Thesis by
Deniz BOZKURT
Environmental Engineer
(601041009)**

**Date of submission: 26 December 2006
Date of defence examination: 29 January 2007**

Supervisor: Assoc.Prof.Dr. Ömer Lütfi Şen

Members of the Examining Committee: Prof.Dr. Mehmet Karaca

Prof.Dr. Mete Tayanç (M.Ü.)

JANUARY 2007

**TÜRKİYE YAĞIŞLARININ ETRAFINDAKİ DENİZLERİN
YÜZEY SICAKLIKLARINDAKİ DEĞİŞİME OLAN DUYARLILIĞI**

YÜKSEK LİSANS TEZİ
Deniz BOZKURT
Çevre Mühendisi
(601041009)

Tezin Enstitüye Verildiği Tarih: 26 Aralık 2006
Tezin Savunulduğu Tarih: 29 Ocak 2007

Tez Danışmanı: Doç.Dr. Ömer Lütfi Şen

Diğer Jüri Üyeleri: Prof.Dr. Mehmet Karaca

Prof.Dr. Mete Tayanç (M.Ü.)

OCAK 2007

ACKNOWLEDGMENTS

I would like to express my deepest gratitude to my research advisor Assoc. Prof. Dr. Ömer Lütfi Şen for suggesting this investigation, for his collaboration, and for encouragement to the completion of this work.

I am also grateful to Prof. Dr. Mehmet Karaca and Dr. Tayfun Kindap for their invaluable help and continuous support.

I would like to thank my roommate and colleague Res. Asst. Ozan Mert Göktürk for his contribution to my background and knowledge and for his motivation. I would also like to thank my other colleagues: Res. Asst. Ali Değer Özbakır, Res. Asst. Kenan Akbayram, and Res. Asst. Taylan Sançar for their support.

I would like to thank Dr. Onur Tan for providing Latex format of ITU used in writing of this thesis.

Many great thanks go to my mother Kıymet, to my brothers Dr. Kutluhan, Assoc. Prof. Dr. Kutsal, Dr. Hüseyin Sancar and to all my families for their outstanding support and understanding.

Deniz Bozkurt

25 December 2006

CONTENTS

ABBREVIATIONS	vi
FIGURE LIST	vii
TABLE LIST	x
1. INTRODUCTION	1
1.1. Introduction	1
1.2. Purpose	2
1.3. Previous studies of SST and precipitation variability	9
2. MODEL DESCRIPTION AND EXPERIMENT DESIGN	13
2.1. Regional Climate Model	13
2.2. Model Description	14
2.2.1. The RegCM Model Vertical and Horizontal Grid	14
2.2.2. Map Projections and Map-Scale Factors	15
2.3. Model Dynamics	15
2.3.1. Horizontal Momentum Equations	16
2.3.2. Continuity and σ Equations	16
2.3.3. Thermodynamic and ω Equations	17
2.3.4. Hydrostatic Equation	17
2.4. Model Physics	17
2.4.1. Radiation Scheme	18
2.4.2. Land Surface Model	18
2.4.3. Planetary Boundary Layer Scheme	18
2.4.4. Convective Precipitation Scheme	19
2.4.5. Large-Scale Precipitation Scheme	19
2.5. Experiment Design	19
2.5.1. Terrain	20
2.5.2. ICBC	23
2.5.3. Running the model and Outputs	24
2.6. Model Performance	28

3. SIMULATION RESULTS	31
3.1. Aegean Sea Sensitivity Experiment	31
3.1.1. Changes in surface parameters	32
3.1.2. Changes in upper level parameters	35
3.1.3. Changes in monthly precipitations	39
3.1.4. Wet and dry years comparison	43
3.2. Eastern Mediterranean Sea Sensitivity Experiment	47
3.2.1. Changes in upper level paramaters	48
3.2.2. Changes in monthly precipitation	50
3.2.3. Wet and dry years comparison	51
3.3. Western Black Sea Sensitivity Experiment	53
3.3.1. Changes in upper level paramaters	53
3.3.2. Changes in monthly precipitation	56
3.3.3. Wet and dry years comparison	57
3.4. Eastern Black Sea Sensitivity Experiment	58
3.4.1. Changes in upper level paramaters	58
3.4.2. Changes in monthly precipitation	60
3.4.3. Wet and dry years comparison	62
3.5. Central Mediterranean Sea Sensitivity Experiment	63
3.5.1. Changes in upper level paramaters	64
3.5.2. Changes in monthly precipitation	66
3.5.3. Wet and dry years comparison	67
4. CONCLUSIONS and DISCUSSION	68
REFERENCES	69

ABBREVIATIONS

AVHRR	:	Advanced Very High Resolution Radiometer
BATS	:	Biosphere-Atmosphere Transfer Scheme
CCM	:	Community Climate Model
CRU	:	Climatic Research Unit
GCM	:	General Circulation Model
GISST	:	Global Sea Surface Temperature
GLCC	:	Global Land Cover Characterization
ICTP	:	International Center for Theoretical Physics
IPCC	:	Intergovernmental Panel on Climate Change
LAM	:	Limited Area Model
NAO	:	North Atlantic Oscillation
NCAR	:	National Center for Atmospheric Research
NCEP	:	National Centers for Environmental Prediction
OISST	:	Optimum Interpolation Sea Surface Temperature
PBL	:	Planetary Boundary Layer
SST	:	Sea Surface Temperature
SUBEX	:	Subgrid Explicit Moisture Scheme

FIGURE LIST

	<u>Page Nr</u>	
Fig. 1.1	Geographical position of Turkey and surrounding seas.	2
Fig. 1.2	Results of trend analysis for winter precipitation of Turkey between the years of 1951 and 2004.	3
Fig. 1.3	Paths of cyclones influencing Turkey (adapted from Karaca et al. (2000)).	4
Fig. 1.4	ONDJFM and DJF average SST of Aegean Sea between the years of 1949 and 2000.	5
Fig. 1.5	Long-term DJF average precipitation of Aegean Region between the years of 1950 and 2004.	6
Fig. 1.6	ONDJFM and DJF average SST of eastern Mediterranean Sea between the years of 1949 and 2000.	7
Fig. 1.7	ONDJFM and DJF average SST of western Black Sea between the years of 1949 and 2000.	8
Fig. 1.8	ONDJFM and DJF average SST of eastern Black Sea between the years of 1949 and 2000.	9
Fig. 1.9	ONDJFM and DJF average SST of Central Mediterranean Sea between the years of 1949 and 2000.	12
Fig. 2.1	Schematic representation of the vertical structure of the model. This example is for 16 vertical layers. Dashed lines denote half-sigma levels, solid lines denote full-sigma levels. (Adapted from the PSU/NCAR Mesoscale Modeling System Tutorial Class Notes and User's Guide.)	14
Fig. 2.2	Schematic representation of the horizontal grid structure of RegCM3 (Adapted from the PSU/NCAR Mesoscale Modeling System Tutorial Class Notes and User's Guide.)	15
Fig. 2.3	Brief schematic description of RegCM3 modeling system used in this study.	20
Fig. 2.4	RegCM3 directory tree. Adapted from workshops on RegCM3 that available at RegCM3 website.	21
Fig. 2.5	The domain and topography used in the RegCM3 simulations. The five rectangles show the regions where SSTs are changed in sensitivity simulations.	22
Fig. 2.6	Land cover and vegetation classes of the domain.	23
Fig. 2.7	10-year ONDJFM (a),(b) and DJF (c),(d) average of 850hPa geopotential height maps from NCEP/NCAR Reanalysis (a),(c) and RegCM3 model output (b),(d).	28

Fig. 2.8	10-year ONDJFM (a),(b) and DJF (c),(d) average of 500hPa geopotential height maps from NCEP/NCAR Reanalysis (a),(c) and RegCM3 model output (b),(d).	29
Fig. 2.9	10-year average precipitation values (mm/day) for ONDJFM and DJF from gridded observations (CRU data) (a),(c) and from RegCM3 model output (b),(d).	30
Fig. 2.10	10-year average SLP values (hPa) for ONDJFM and DJF from NCEP/NCAR Reanalysis (a),(c) and from RegCM3 model output (b),(d).	30
Fig. 3.1	10-year average DJF difference of precipitation between perturbations and control simulation with 850hPa wind vectors of control simulation. (a) (SST-2K)-Control, and (b) (SST+2K)-Control.	31
Fig. 3.2	10-year average DJF difference of 2m-temperature between perturbations and control simulation. (a) (SST-2K)-Control, and (b) (SST+2K)-Control.	33
Fig. 3.3	10-year average DJF difference of sensible heat flux between perturbations and control simulation. (a) (SST-2K)-Control, and (b) (SST+2K)-Control.	34
Fig. 3.4	10-year average DJF difference of latent heat flux between perturbations and control simulation. (a) (SST-2K)-Control, and (b) (SST+2K)-Control.	35
Fig. 3.5	10-year average DJF difference of air temperature at 925hPa between perturbations and control simulation. (a) (SST-2K)-Control, and (b) (SST+2K)-Control.	36
Fig. 3.6	10-year average DJF difference of specific moisture at 925hPa between perturbations and control simulation. (a) (SST-2K)-Control, and (b) (SST+2K)-Control.	37
Fig. 3.7	10-year average DJF difference of air temperature at 925hPa between perturbations and control simulation. (a) (SST-2K)-Control, and (b) (SST+2K)-Control.	38
Fig. 3.8	10-year average DJF difference of specific moisture at 925hPa between perturbations and control simulation. (a) (SST-2K)-Control, and (b) (SST+2K)-Control.	39
Fig. 3.9	10-year average monthly difference of precipitation between SST-2K perturbation and control simulation with 850hPa wind vectors of control simulation.	40
Fig. 3.10	10-year average monthly difference of precipitation between SST+2K perturbation and control simulation with 850hPa wind vectors of control simulation.	41
Fig. 3.11	10-year average December precipitation change with 90% confidence level for both SST-2K (a) and SST+2K (b) perturbations.	42
Fig. 3.12	10-year average monthly precipitation amounts of SST perturbations and control simulation.	43
Fig. 3.13	10-year average relative changes in each month for precipitation.	43
Fig. 3.14	Effects of positive NAO index on North Atlantic and European (http://www.ldeo.columbia.edu/NAO/).	44

Fig. 3.15	Effects of negative NAO index on North Atlantic and European (http://www.ldeo.columbia.edu/NAO/).	44
Fig. 3.16	DJF and ONDJFM index of the NAO 1951-2006.	45
Fig. 3.17	DJF and ONDJFM index of the NAO 1990-2000.	45
Fig. 3.18	Average wet years (1995-1996, 1996-1997, and 1997-1998) difference of precipitation between perturbations and control simulation. (a) (SST-2K)-Control, and (b) (SST+2K)-Control.	46
Fig. 3.19	Average dry years (1992-1993, 1993-1994, and 1994-1995) difference of precipitation between perturbations and control simulation. (a) (SST-2°C)-Control, and (b) (SST+2°C)-Control.	47
Fig. 3.20	10-year average DJF precipitation differences between SST-2K perturbation and control for the region of East Mediterranean.	48
Fig. 3.21	10-year average DJF difference of air temperature at 925hPa between SST-2K and control simulation.	49
Fig. 3.22	10-year average DJF difference of specific moisture at 925hPa between SST-2K and control simulation.	49
Fig. 3.23	10-year average DJF difference of air temperature at 850hPa between SST-2K and control simulation.	50
Fig. 3.24	10-year average DJF difference of specific moisture at 850hPa between SST-2K and control simulation.	50
Fig. 3.25	10-year average monthly difference of precipitation between SST-2K perturbation and control simulation with 850hPa wind vectors of control simulation.	51
Fig. 3.26	Average dry years (1992-1993, 1993-1994, and 1994-1995) (a) and wet years (1995-1996, 1996-1997, and 1997-1998) (b) difference of precipitation between (SST-2K)-Control and control simulation.	52
Fig. 3.27	10-year average DJF precipitation differences between SST-2K perturbation and control for western Black Sea.	53
Fig. 3.28	10-year average DJF difference of air temperature at 925hPa between SST-2K and control simulation.	54
Fig. 3.29	10-year average DJF difference of specific moisture at 925hPa between SST-2K and control simulation.	54
Fig. 3.30	10-year average DJF difference of air temperature at 850hPa between SST-2K and control simulation.	55
Fig. 3.31	10-year average DJF difference of specific moisture at 850hPa between SST-2K and control simulation.	55
Fig. 3.32	10-year average monthly difference of precipitation between SST-2K perturbation and control simulation with 850hPa wind vectors of control simulation.	56
Fig. 3.33	Average dry years (1992-1993, 1993-1994, and 1994-1995) (a) and wet years (1995-1996, 1996-1997, and 1997-1998) (b) difference of precipitation between (SST-2K)-Control and control simulation.	57
Fig. 3.34	10-year average DJF precipitation differences between SST-2K perturbation and control for eastern Black Sea.	58
Fig. 3.35	10-year average DJF difference of air temperature at 925hPa between SST-2K and control simulation.	59

Fig. 3.36	10-year average DJF difference of specific moisture at 925hPa between SST-2K and control simulation.	59
Fig. 3.37	10-year average DJF difference of air temperature at 850hPa between SST-2K and control simulation.	60
Fig. 3.38	10-year average DJF difference of specific moisture at 850hPa between SST-2K and control simulation.	60
Fig. 3.39	10-year average monthly difference of precipitation between SST-2K perturbation and control simulation with 850hPa wind vectors of control simulation.	61
Fig. 3.40	Average dry years (1992-1993, 1993-1994, and 1994-1995) (a) and wet years (1995-1996, 1996-1997, and 1997-1998) (b) difference of precipitation between (SST-2K)-Control and control simulation.	62
Fig. 3.41	10-year average DJF precipitation differences between SST-2K perturbation and control for central Mediterranean Sea.	63
Fig. 3.42	10-year average DJF difference of air temperature at 925hPa between SST-2K and control simulation.	64
Fig. 3.43	10-year average DJF difference of specific moisture at 925hPa between SST-2K and control simulation.	64
Fig. 3.44	10-year average DJF difference of air temperature at 850hPa between SST-2K and control simulation.	65
Fig. 3.45	10-year average DJF difference of specific moisture at 850hPa between SST-2K and control simulation.	65
Fig. 3.46	10-year average monthly difference of precipitation between SST-2K perturbation and control simulation with 850hPa wind vectors of control simulation.	66
Fig. 3.47	Average dry years (1992-1993, 1993-1994, and 1994-1995) (a) and wet years (1995-1996, 1996-1997, and 1997-1998) (b) difference of precipitation between (SST-2K)-Control and control simulation.	67

TABLE LIST

	<u>Page Nr</u>
Table 2.1 Latitude and longitude of each five region in the domain	22
Table 2.2 Domain parameters	23
Table 2.3 Land Cover/Vegetation classes	24
Table 2.4 List of time step variables to be modified in regcm.in file	25
Table 2.5 List of output variables from atmosphere	26
Table 2.6 List of output variables from surface model	27
Table 2.7 List of output variables from radiation model	27

ABSTRACT

This study aims to investigate the linkage between precipitation variability in Turkey and sea surface temperature variability in surrounding seas through sensitivity experiments using a state-of-the-art regional climate model, RegCM3. Sea surface temperatures of five regions including Aegean Sea, Eastern Mediterranean Sea, western half of Black Sea, eastern half of Black Sea, and Central Mediterranean Sea are individually modified by $\pm 2K$ in the model sensitivity simulations, and the results from these simulations are compared with a control simulation to quantify how these changes affect the Turkish precipitation. 10-year sensitivity experiments for all seas are completed and in general, the results of the sensitivity experiments show that the response of Turkish precipitation to sea surface temperature changes in the surrounding seas is limited and mostly confined to the coastal areas in Turkey. Increasing the sea surface temperature usually increases rainfall in the vicinity of the perturbation, and similarly, decreasing it reduces rainfall. Monthly results indicate that Turkish precipitation is mostly affected from perturbations especially in Eastern Mediterranean Sea and Aegean Sea in December which may be related to cyclone tracks and frequency in this month.

ÖZET

Bu çalışmanın amacı, Türkiye yağışlarındaki değişimin etrafındaki denizlerin yüzey sıcaklığındaki değişimle olan ilişkisini, duyarlılık testleri vasıtasıyla güncel bir bölgesel iklim modeli, RegCM3, kullanarak araştırmaktır. Model simülasyonlarında Ege Denizi, Doğu Akdeniz, Batı Karadeniz, Doğu Karadeniz ve Orta Akdeniz'i kapsayan beş bölgenin deniz yüzey sıcaklıkları $\pm 2K$ değiştirildi ve bu değişikliklerin Türkiye yağışlarını nasıl etkilediğini belirlemek için elde edilen sonuçlar kontrol simülasyonu ile karşılaştırıldı. Bütün bölgeler için 10 yıllık duyarlılık testi tamamlandı ve genel olarak, duyarlılık testlerinin sonuçları göstermektedir ki Türkiye yağışlarının etrafındaki denizlerin yüzey sıcaklıklarındaki değişime olan mukabelesi sınırlı olup çoğunlukla kıyı kesimlerde sınırlanmıştır. Deniz yüzey sıcaklığını arttırmak genellikle değişimin yakınındaki yerlerde yağışın artmasına sebep olmaktadır. Tersisi durumda ise yağışın azalması sözkonusudur. Aylık sonuçlar göstermektedir ki, Türkiye yağışları en çok Aralık ayında ve özellikle Ege Denizi ve Doğu Akdeniz'deki değişimlerden etkilenmektedir ve bu sonuç bu aydaki siklon yolları ve frekansları ile ilişkilendirilebilir.

1. INTRODUCTION

1.1. Introduction

The Third Assessment Report of IPCC (2001) stated that a regional scale describing the range of 10^4 to 10^7 km^2 , a temporal scale from sub-daily to multi decadal, and interaction of forcings and circulations are the main components of the process that is used to determine the climate of a given region. Planetary scale (greater than 10^7 km^2) forcings are responsible for the global atmosphere while regional and local scale forcings modulate the spatial and temporal structure of the regional climate signal. Interactions between planetary scale forcings and regional and local scale forcings constitute fundamentals of climatic processes.

In fact, climate models have been used in numerous studies to dynamically downscale atmospheric fields at resolution, from which it is difficult to infer detailed information (Leung et al., 1999; Roads et al., 2003; Takle et al., 1999). It is important to emphasize that general circulation models (GCMs) are not utilizable in order to describe small-scale atmospheric circulations especially occur in land surface in which complex terrain remains in possession. Since demonstrating impacts of climate change especially in mesoscale and small-scale regions crucial for the assessment of climate variability studies, alternative methods have been developed in order to remedy deficiency of GCMs. Nesting a limited-area model (LAM) within a global GCM, or within observational analysis is an alternative process to study mesoscale climate processes (McGregor, 1997). Dickinson et al.(1989) and Giorgi et al.(1993b) came up with an idea that limited area models (LAMs) could be used for regional studies. Since then, regional and mesoscale climate studies with the aid of regional climate models have become widespread.

Regional climate changes in Mediterranean region has been of interest to researchers for many years since it is located in a transitional zone in which mid-latitude and tropical variability play a key role in determining climate characteristics of this region. In addition to this, it has many morphologic, geographical, historical, and societal characteristics that make its climate interesting per se. (Bolle, 2003). Although much of the coastal states have a

Mediterranean climate type, there are also regions that have different climate characteristics due to complex topography, elevation differences, and latitudinal positions.

1.2. Purpose

Turkey, a country in the Eastern Mediterranean, is surrounded by three seas: Black Sea in the north, Aegean Sea in the west, and Mediterranean Sea in the south (Fig. 1.1).

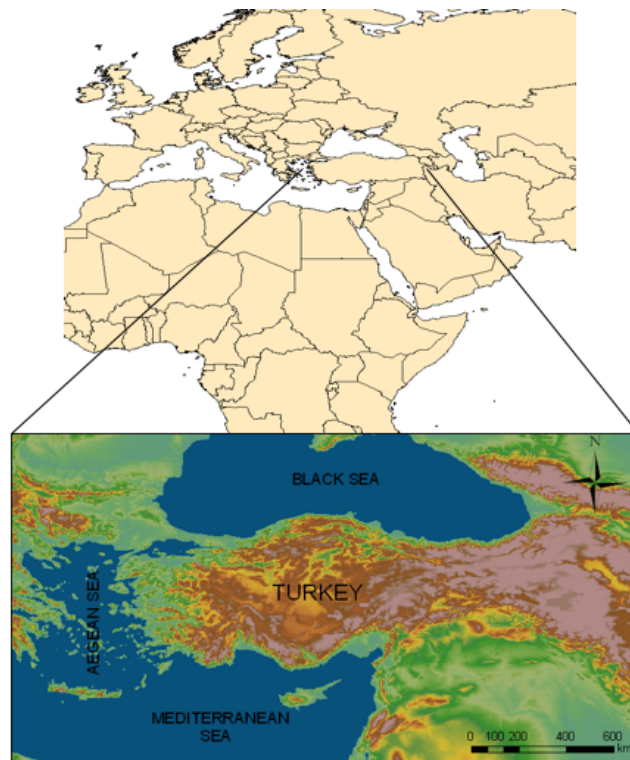


Fig. 1.1. Geographical position of Turkey and surrounding seas.

Complex topography, elevation differences, and geographical position of Turkey make its climate interesting where significant differences from one region to the other take place. The Mediterranean and Aegean coasts have a typical Mediterranean climate with mild, rainy winter and hot, dry summers. Amount of annual average rainfall in these regions varies from 580 to 1300 mm. The inland Anatolian Plateau has limited rainfall, cold winters, and hot summers. Black Sea coasts and northwest regions of Turkey have a moderate climate with colder winters than the Mediterranean and Aegean coasts. Annual average rainfall amount in eastern part of the Black Sea coasts is about 2000-2200 mm and the highest rainfall amount in Turkey.

Long-term winter precipitation records from stations show a decreasing trend in the western provinces of Turkey that constitutes our initial motivation to this study (Fig. 1.2). Changes in cyclone tracks and their frequency and intensity, variations in the sea surface temperature (SST) of surrounding seas of Turkey, and variabilities of the atmospheric teleconnections may be some of the factors that are causing this change in precipitation.

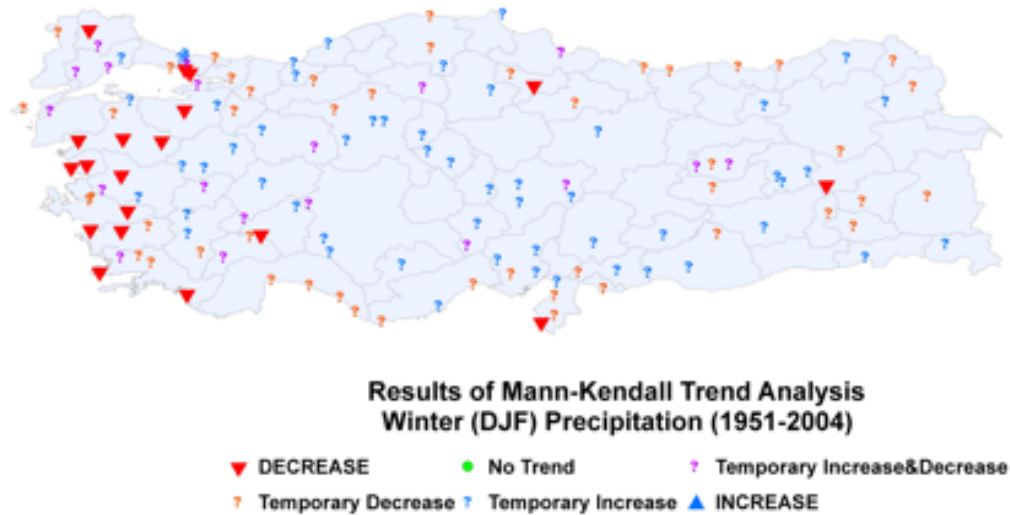


Fig. 1.2. Results of trend analysis for winter precipitation of Turkey between the years of 1951 and 2004.

It is well known that in the cold half of the year, cyclones originating from the North Atlantic region bring over moisture-laden air to Turkey and cause a lot of rainfall, especially in the coastal areas of Turkey due to orographic effects. Cyclones that affect Turkey usually follow four different tracks as identified by Karaca et al. (2000) (Fig. 1.3). There is no doubt that any variation in the intensity and frequency of these cyclones will cause variation in the precipitation in Turkey. Because, the cyclones pass through the surrounding seas before reaching to Turkey, SSTs may play a role in the amount of rainfall in Turkey as they modify the overpassing air masses to some degree. The present study, therefore, investigates whether/how the variations in the SST of the surrounding seas affect the rain falling in Turkey using a state-of-the-art regional climate model, RegCM3. Before defining the model and experiment design it is necessary to present some informations for surrounding seas of Turkey and their long-term annual average SSTs with previous studies concerning with SST and precipitation variability.

Aegean Sea constitutes an arm of Mediterranean Sea off southeast Europe.

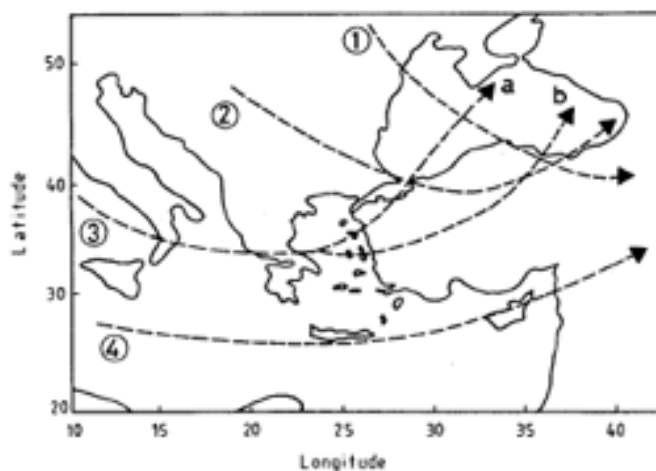


Fig. 1.3. Paths of cyclones influencing Turkey (adapted from Karaca et al. (2000)).

It lies between Greece and Turkey. It has a total area of some 214,000 km^2 and a maximum depth of 3,543 m. It has about 610 km length and 300 km width.

The average SST of Aegean Sea is a few degree lower than those in eastern Mediterranean. There are some reasons that are accounted for this: reduced solar irradiance in North, upwelling of cooler waters due to internal circulations, run-off of cooler river water into the sea, and the intrusion of cold water from the Black Sea through the Marmara Sea and the strait of the Dardanelles (Bolle, 2003).

Long-term ONDJFM and DJF average SST of Aegean Sea is presented in Fig. 1.4. It can be said that there is a decreasing trend in both seasons especially between the years of 1960 and 1990. Increasing trend has taken place after 1990.

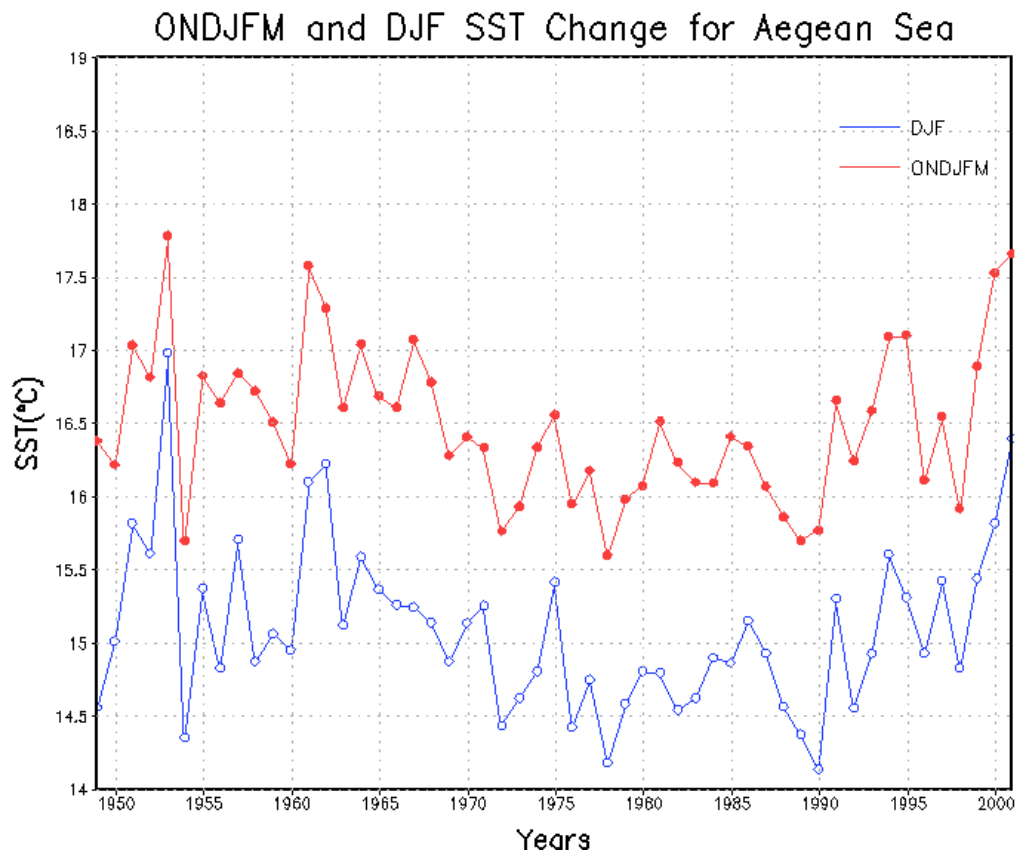


Fig. 1.4. ONDJFM and DJF average SST of Aegean Sea between the years of 1949 and 2000.

Long-term DJF average precipitation trend between 1950 and 2004 from Aegean Region stations indicates the decreasing trend of the precipitation in that region (Fig. 1.5).

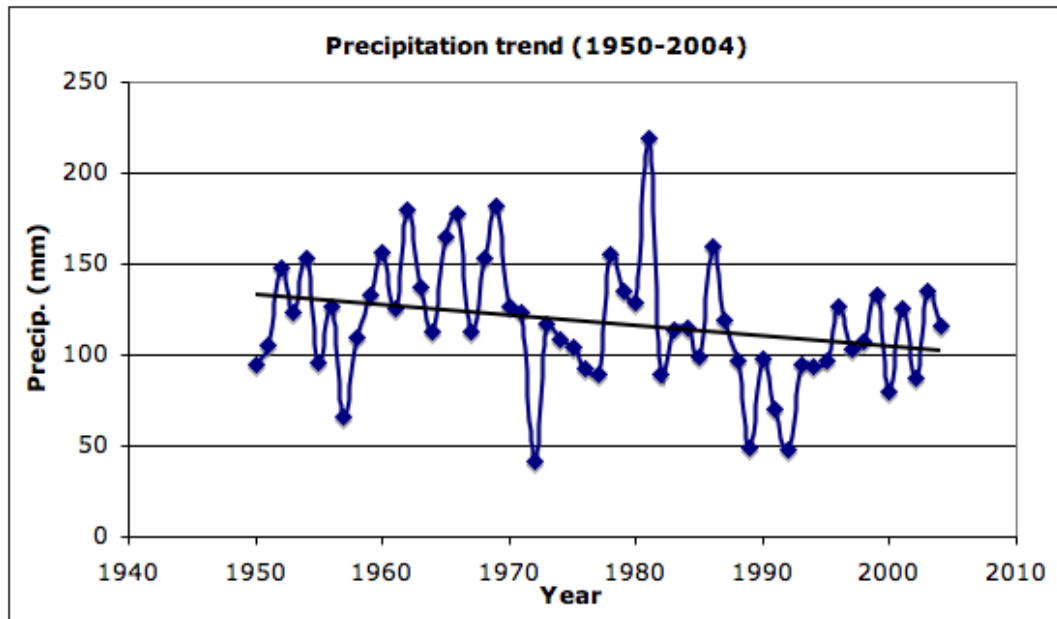


Fig. 1.5. Long-term DJF average precipitation of Aegean Region between the years of 1950 and 2004.

Mediterranean Sea is an inland sea surrounded by Asia to the east, Europe to the north, and Africa to the south. It has an approximate area of 2.5 million km^2 and it is connected to the Atlantic Ocean to the west with Gibraltar Strait. It has an important climatic effect on European-African Mediterranean climate. Surrounding areas of the Mediterranean Sea have negative net radiative flux while the sea itself has positive radiation budget and it behaves as a heat source for surrounding areas that require an influx of heat to compensate for their negative energy budget (Bolle, 2003).

Eastern Mediterranean is surrounded by Turkey to the north, Syria, Lebanon, Israel to the east, and Egypt to the south. High evaporation causes decrease in water level and increase in salinity in eastern Mediterranean (Pinet, 1996).

Long-term ONDJFM and DJF average SST of eastern Mediterranean Sea is presented in Fig. 1.6. A decreasing trend is also seen in here between the years of 1960 and 1990 as same as Aegean Sea. An increasing trend is seen after the year of 1990.

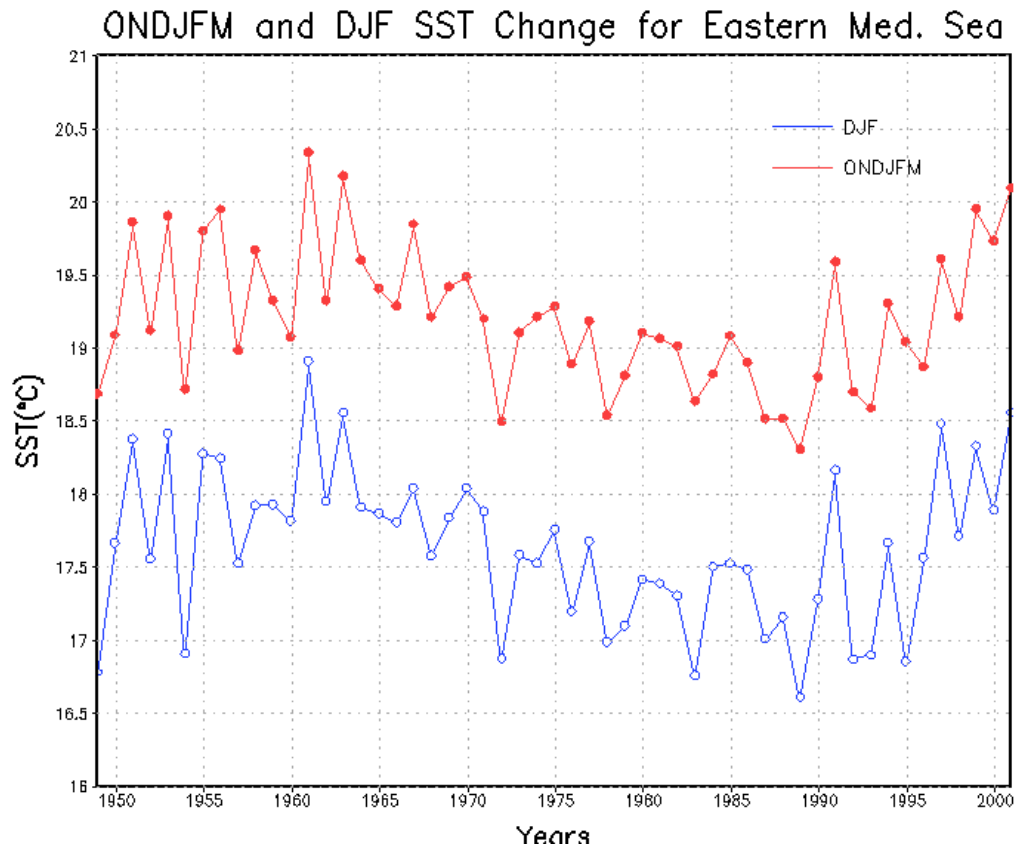


Fig. 1.6. ONDJFM and DJF average SST of eastern Mediterranean Sea between the years of 1949 and 2000.

Black Sea is an inland sea surrounded by Turkey to the south, Bulgaria, Romania, Ukraine to the west, Georgia to the east, and Russia to the north. It has an area of 422,000 km^2 with a maximum depth of 2,210 m. It is connected with Aegean Sea through the Bosphorus, the Sea of Marmara, and the Dardanelles. Oxygen level in Black Sea below 200 meters is very low so marine life is very limited below this depth. It has a low salinity around 0,18‰ since it receives freshwater from rivers in the surrounding areas.

Long-term ONDJFM and DJF average SST of western Black Sea and eastern Black Sea is presented in Fig. 1.7 and Fig. 1.8 respectively.

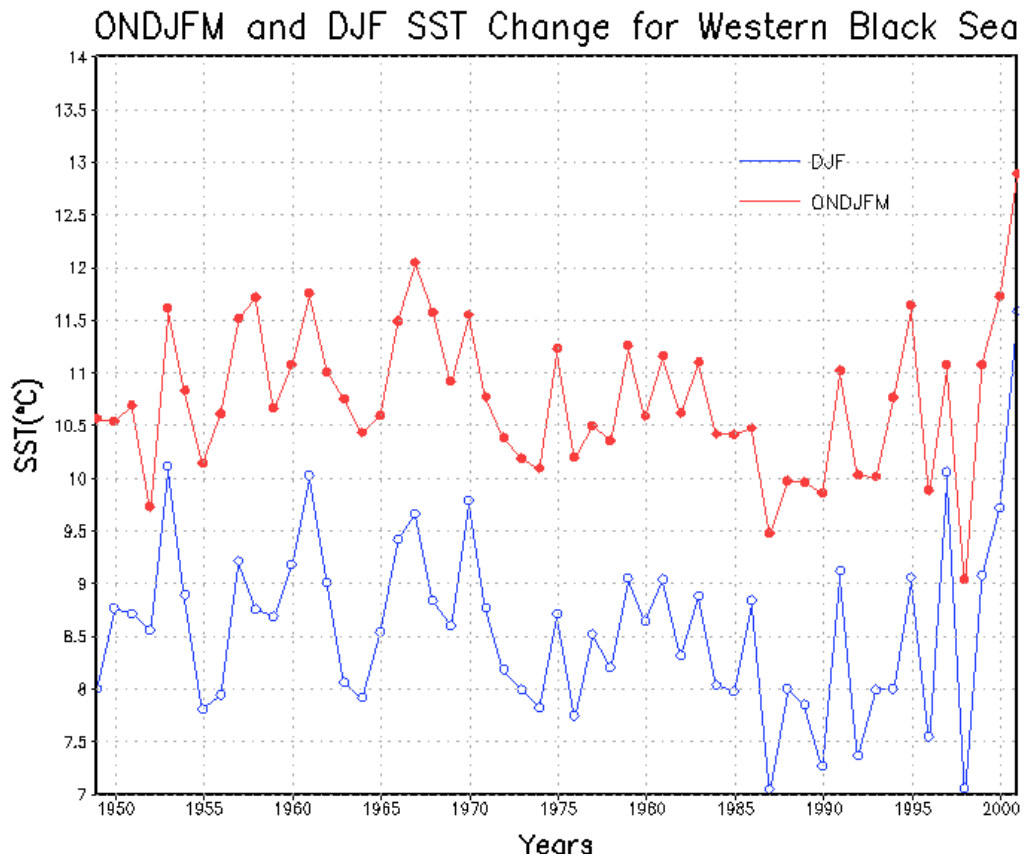


Fig. 1.7. ONDJFM and DJF average SST of western Black Sea between the years of 1949 and 2000.

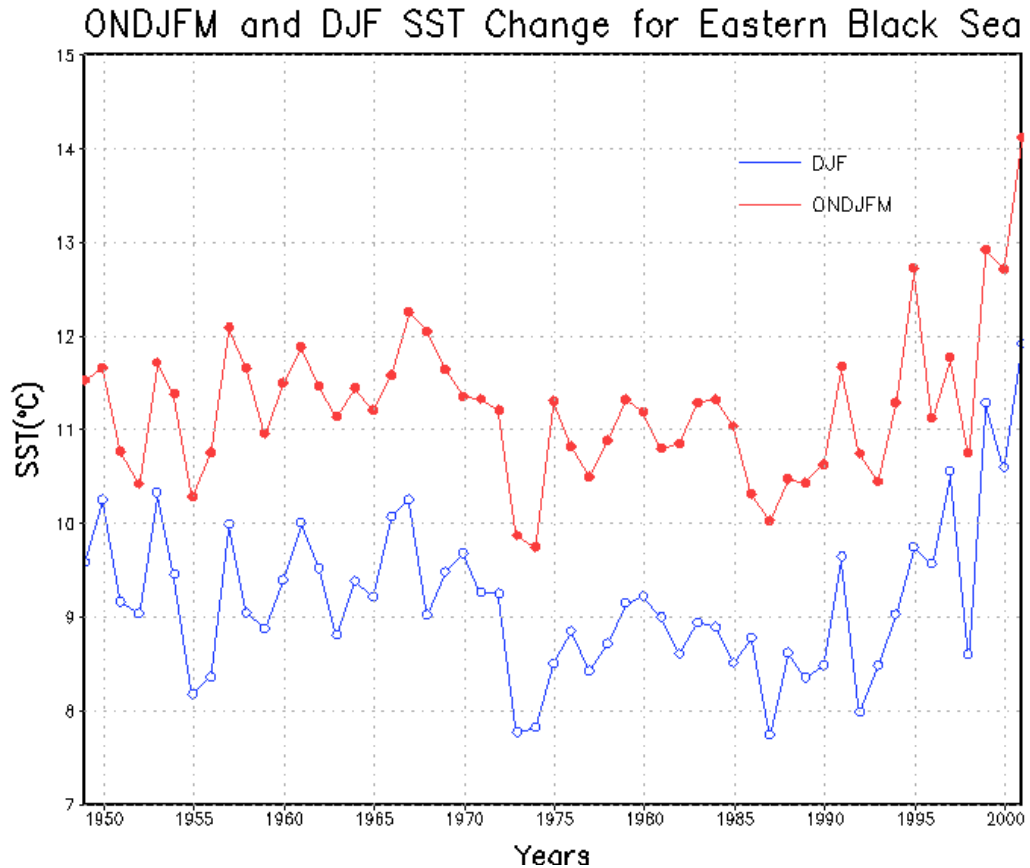


Fig. 1.8. ONDJFM and DJF average SST of eastern Black Sea between the years of 1949 and 2000.

1.3. Previous studies of SST and precipitation variability

Previous and recent studies concerning with regional climate changes, which especially pointing out precipitation variability in Mediterranean region, are mostly focused on large-scale circulation patterns and atmospheric teleconnections (Maheras et al., 2001; Trigo et al., 2000; Trigo and 21 coauthors, 2006; Xoplaki et al., 2004).

Studies concerning with the relationship between SST and precipitation variability have mostly focused on the tropical oceans (Arpe et al., 1998; Janicot et al., 1998; Messenger et al., 2004). Arpe et al. (1998) investigated the variability of Indian monsoon in the ECHAM3 model. Sensitivity of Indian monsoon to SST is one of the subject that they investigated. They confirmed that due to El-Nino effect surface winds over the Arabian Sea is reduced and causing an increase in the SST of the Arabian Sea as there is less mixing and upwelling in the ocean. Higher SST causes more precipitation over India and they performed sensitivity experiment in order to demonstrate effect of North Indian Ocean SST on precipitation variability. They found that

all experiments with increased SST give more precipitation than those with reduced SST. More precipitation over India due to increased SST counteracts the expected decrease from the direct El-Nino effect. They also stated that changes in the SST there within the range of uncertainty (0.5 K) can lead to clear impacts.

Messenger et al. (2004) investigated sensitivity of precipitation to regional SST by using a regional climate model, MAR, during the West African monsoon for two dry years. In addition to simulations for model performance for the years of 1983 and 1984, they performed a hybrid simulation of 1983 in which the SST field is the 1984 SST. They revealed precipitation sensitivity to SST anomalies especially during the high rainy period. They also showed that effect of regional SST on West African monsoon over the inland is modulated by other factors such as orography or surface interactions. According to their results, regional SST is a major factor that determines the rainfall regime during monsoon in dry years over West Africa. They stated that a warmer SST leads to an increase in meridional moisture transport in the lower troposphere resulted in increase in precipitation along the coast.

It is only recently that studies for the relationship between SST and climate variability have been done for the Mediterranean region. Li (2006) studied the atmospheric response to an idealized 2 K cooling of the Mediterranean Sea with a GCM and he demonstrated large-scale atmospheric responses to this cooling. He hypothesized that the Mediterranean Sea could initiate atmospheric teleconnections and thus influence the weather and the climate for remote regions. Rowell (2003) also studied the role of the Mediterranean Sea in the Sahelian rainfall season with a GCM. He found that an increase in moisture transport in the eastern part of the Sahara due to warmer Mediterranean Sea resulting in an increase in the Sahelian summer rainfall.

Maracchi et al. (2000) investigated how SST of Tyrrhenian Sea triggered convective precipitation in Tuscany, Italy. They analysed, four local-scale extreme convective events in Tuscany region resulted in flash floods, gusts, and tornado-like systems. According to their results, there is a positive correlation between SST anomalies of the Ligurian Gulf and frequency and intensity of extreme convective events in Tuscany region. They showed the triggering of convective storms in Tuscany has been enhanced by warm moist air from the Tyrrhenian Sea due to increased sea surface temperature. It is also stated that relationship between SST anomalies and extreme weather events in Mediterranean region are becoming more evident.

Barret (2006) sought the relationship between SST anomalies in the Mediterranean and Black Seas and rainfall in selected sites across Turkey. He computed Pearson correlations coefficients and tested for significance. He revealed that there is an unrelated relationship between SST anomalies in both the Black and Mediterranean Seas and precipitation across Turkey. He also indicated that correlation coefficients were not randomly dispersed throughout the year. Another result of his study presented possible forcings of positive SST anomalies for increased summer precipitation over the central and eastern interior of Turkey due to enhanced convective precipitation resulted from local orography and the greater boundary layer relative humidity.

In this study, we investigate whether/how the variations in the SST of the surrounding seas affect the rain falling in Turkey. In order to achieve our goal, using a state-of-the-art regional climate model, RegCM3, we have conducted sensitivity experiments involving $\pm 2K$ perturbations in SSTs at preselected five regions that fourth of them are in the three seas surrounding Turkey. We have also investigated Central Mediterranean region since it is the intersection point of most cyclones influencing on Turkey. Long-term ONDJFM and DJF average SST of Central Mediterranean Sea is presented in Fig. 1.9.

Section 2 presents the model used in this study and experimental design of the simulations. Model performance is provided in Section 2. Simulation results for sensitivity experiments are presented in Section 3. Finally, summary and some conclusions are given in Section 4.

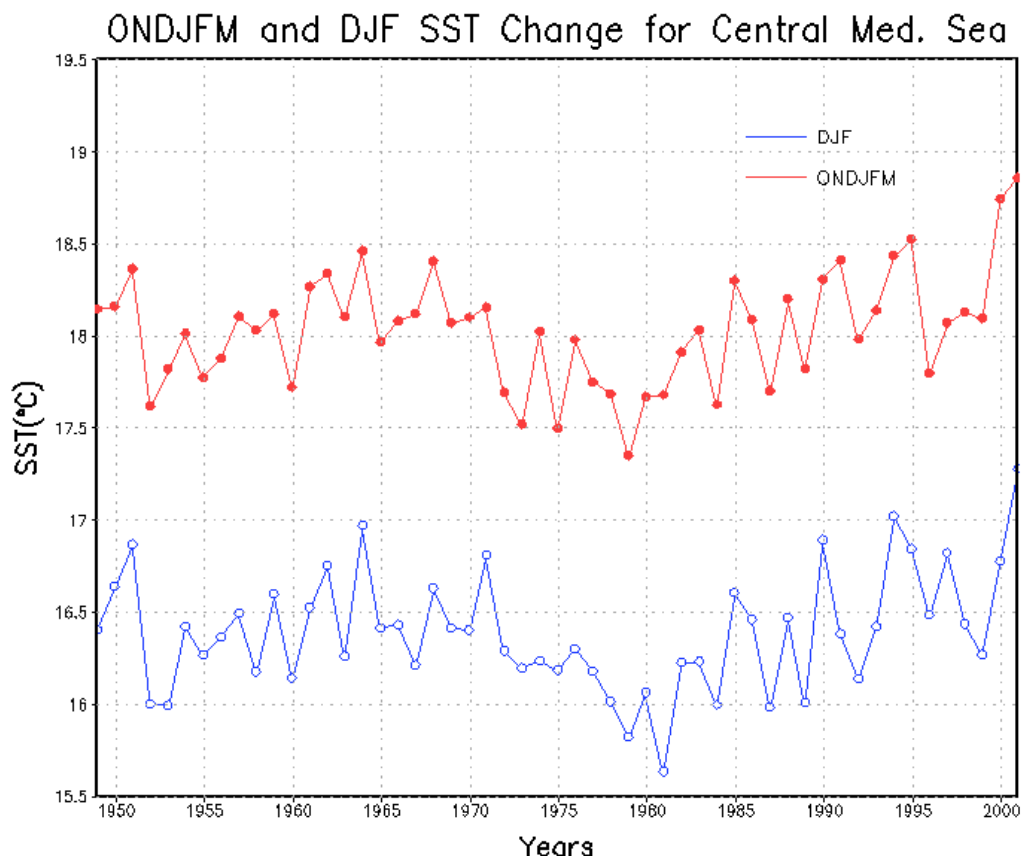


Fig. 1.9. ONDJFM and DJF average SST of Central Mediterranean Sea between the years of 1949 and 2000.

2. MODEL DESCRIPTION AND EXPERIMENT DESIGN

2.1. Regional Climate Model

RegCM3 is the regional model used in this study and it is the third version of a regional climate model developed by and is maintained at the International Centre for Theoretical Physics (ICTP), in Trieste, Italy. The first generation of RegCM included the Biosphere-Atmosphere Transfer Scheme, BATS, (Dickinson et al., 1986) for surface process representation, the radiative transfer scheme of the Community Climate Model version 1 (CCM1), a medium resolution local planetary boundary layer scheme, the Kuo-type cumulus convection scheme of (Anthes, 1977) and the explicit moisture scheme of (Hsie et al., 1984). RegCM was originally built upon the National Center for Atmospheric Research-Pennsylvania State University (NCAR-PSU) Mesoscale Model version MM4, which is a compressible, finite difference model with hydrostatic balance and vertical σ -coordinates in the late 1980s. The model physics and numerical schemes were then upgraded resulting in a second generation of RegCM called as RegCM2 originally developed by Giorgi et al. (1993a,b). The physics of RegCM2 was based on that of the NCAR Community Climate Model version 2 (CCM2) (Hack et al., 1993), and the mesoscale model MM5 (Grell et al., 1994b). Since then, there has been major improvement in the physics of the model and associated software system, including a large-scale cloud and precipitation scheme which accounts for the subgrid-scale variability of clouds (Pal et al., 2000), new parameterizations for ocean surface fluxes (Zeng et al., 1998), and a cumulus convection scheme (Emanuel, 1991; Emanuel and Zivkovic-Rothman, 1999). The main physical parameterizations contained in the RegCM3 used in this study are: radiation scheme of the NCAR Community Climate Model (CCM3) (Kiehl et al., 1996), Biosphere-Atmosphere Transfer Scheme version 1e (BATS1e) (Dickinson et al., 1993), planetary boundary layer scheme (Holtslag et al., 1990), Grell's cumulus convective precipitation scheme (Grell, 1993), and large-scale cloud and precipitation scheme.

2.2. Model Description

Informations describing the model dynamic and physics are based on RegCM3 User's Guide that is available at <http://www.ictp.trieste.it/RegCNET/model.html>.

2.2.1. The RegCM Model Vertical and Horizontal Grid

Vertical grid configuration of the model is based on a dimensionless σ coordinate that is used to define the model levels

$$\sigma = \frac{p - p_t}{p_s - p_t} \quad (2.1)$$

where p is the pressure, p_t is a specified constant top pressure, and p_s is the surface pressure. Since the lower grid levels are under the influence of topography, they are not as flattened as upper grid levels. As the pressure decreases toward the top of the model, intermediate levels progressively flatten (Fig. 2.1).

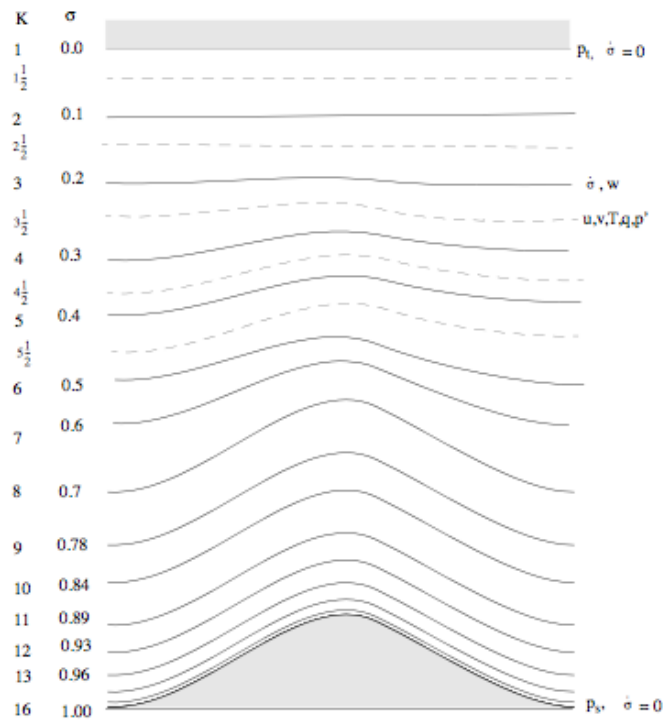


Fig. 2.1. Schematic representation of the vertical structure of the model. This example is for 16 vertical layers. Dashed lines denote half-sigma levels, solid lines denote full-sigma levels. (Adapted from the PSU/NCAR Mesoscale Modeling System Tutorial Class Notes and User's Guide.)

The horizontal grid has an Arakawa-Lamb B-staggering grid with scalar variables such as temperature, mixing ratio, and pressure that are defined at the center of

the grid box referred as cross points, while the eastward (u) and northward (v) components of the velocity vector are defined at the corners of each grid square referred as dot points (Fig. 2.2).

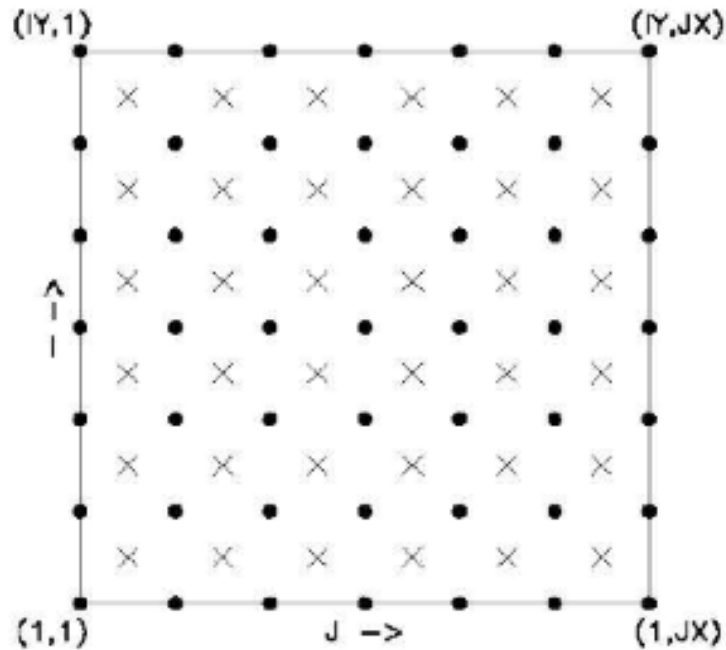


Fig. 2.2. Schematic representation of the horizontal grid structure of RegCM3 (Adapted from the PSU/NCAR Mesoscale Modeling System Tutorial Class Notes and User's Guide.)

2.2.2. Map Projections and Map-Scale Factors

According to studied region, RegCM3 offers four map projections: Lambert Conformal for mid-latitudes, Polar Stereographic for high latitudes, Normal Mercator for low latitudes, and Rotated Mercator for extra choice. The observed wind generally has to be rotated to the model grid since the x and y directions in the model do not correspond to west-east and north-south except for the Normal Mercator projection. In addition to this, the model u and v components need to be rotated before comparison with observations. The map scale factor, m , is defined by ratio of distance on grid to actual distance on earth and its value is usually close to one, varying with latitude.

2.3. Model Dynamics

The model dynamic equations and numerical discretization are described by Grell et al. (1994b).

2.3.1. Horizontal Momentum Equations

$$\begin{aligned} \frac{\partial p^* u}{\partial t} = & -m^2 \left(\frac{\partial p^* u u / m}{\partial x} + \frac{\partial p^* v u / m}{\partial y} \right) - \frac{\partial p^* u \dot{\sigma}}{\partial \sigma} \\ & - m p^* \left[\frac{R T_v}{(p^* + p_t / \sigma)} \frac{\partial p^*}{\partial x} + \frac{\partial \phi}{\partial x} \right] + f p^* v + F_H u + F_V u \end{aligned} \quad (2.2a)$$

$$\begin{aligned} \frac{\partial p^* v}{\partial t} = & -m^2 \left(\frac{\partial p^* u v / m}{\partial x} + \frac{\partial p^* v v / m}{\partial y} \right) - \frac{\partial p^* v \dot{\sigma}}{\partial \sigma} \\ & - m p^* \left[\frac{R T_v}{(p^* + p_t / \sigma)} \frac{\partial p^*}{\partial y} + \frac{\partial \phi}{\partial y} \right] + f p^* u + F_H v + F_V v, \end{aligned} \quad (2.2b)$$

where u and v are the eastward and northward components of velocity, T_v is virtual temperature, ϕ is geopotential height, f is the coriolis parameter, R is the gas constant for dry air, m is the map scale factor for either the Polar Stereographic, Lambert Conformal, or Mercator map projections, $\dot{\sigma} = \frac{d\sigma}{dt}$, and F_H and F_V represent the effects of horizontal and vertical diffusion, and $p^* = p_s - p_t$.

2.3.2. Continuity and Sigmadot($\dot{\sigma}$) Equations

Continuity equation is defined by

$$\frac{\partial p^*}{\partial t} = -m^2 \left(\frac{\partial p^* u / m}{\partial x} + \frac{\partial p^* v / m}{\partial y} \right) - \frac{\partial p^* \dot{\sigma}}{\partial \sigma} \quad (2.3)$$

and in order to compute temporal variation of the surface pressure in the model the vertical integral of Equation 2.3 is used,

$$\frac{\partial p^*}{\partial t} = -m^2 \int_0^1 \left(\frac{\partial p^* u / m}{\partial x} + \frac{\partial p^* v / m}{\partial y} \right) d\sigma \quad (2.4)$$

then the vertical velocity in sigma coordinates($\dot{\sigma}$) is computed at each level in the model by vertical integral of Equation 2.3,

$$\dot{\sigma} = -\frac{1}{p^*} \int_0^\sigma \left[\frac{\partial p^*}{\partial t} + m^2 \left(\frac{\partial p^* u / m}{\partial x} + \frac{\partial p^* v / m}{\partial y} \right) \right] d\sigma' \quad (2.5)$$

where σ' is a dummy variable of integration and $\dot{\sigma}(\sigma=0)=0$.

2.3.3. Thermodynamic and Omega(ω) Equations

The thermodynamic equation is

$$\frac{\partial p^* T}{\partial t} = -m^2 \left(\frac{\partial p^* u T / m}{\partial x} + \frac{\partial p^* v T / m}{\partial y} \right) - \frac{\partial p^* T \dot{\sigma}}{\partial \sigma} + \frac{RT_v \omega}{c_{pm}(\sigma + P_t / p_{ast})} + \frac{p^* Q}{c_{pm}} + F_H T + F_V T, \quad (2.6)$$

where Q is the diabatic heating, $F_H T$ represents the effect of horizontal diffusion, $F_V T$ represents the effect of vertical mixing and dry convective adjustment, and c_{pm} is

$$c_{pm} = c_p(1 + 0.8q_v) \quad (2.7)$$

where c_p is the specific heat at constant pressure for dry air and q_v is the mixing ratio of water vapor. Omega(ω) equation is

$$\omega = p^* \dot{\sigma} + \sigma \frac{dp^*}{dt}, \quad (2.8)$$

and $\frac{dp^*}{dt}$ is computed by

$$\frac{dp^*}{dt} = \frac{\partial p^*}{\partial t} + m \left(u \frac{\partial p^*}{\partial x} + v \frac{\partial p^*}{\partial y} \right) \quad (2.9)$$

2.3.4. Hydrostatic Equation

Geopotential heights from the virtual temperature T_v is computed by using the hydrostatic equation,

$$\frac{\partial \phi}{\partial \ln(\sigma + p_t / p^*)} = -RT_v \left[1 + \frac{q_c + q_r}{1 + q_v} \right]^{-1}, \quad (2.10)$$

where q_v , q_c , and q_r are the water vapor, cloud water or ice, and rain water or snow, mixing ratios. T_v is computed by

$$T_v = T(1 + 0.608q_v) \quad (2.11)$$

2.4. Model Physics

The main physical parameterizations contained in the RegCM3 used in this study are: radiation scheme of the NCAR Community Climate Model (CCM3) (Kiehl et al., 1996), Biosphere-Atmosphere Transfer Scheme version 1e (BATS1e) (Dickinson et al., 1993), planetary boundary layer scheme (Holtslag et al., 1990), Grell's cumulus convective precipitation scheme (Grell, 1993), and large-scale cloud and precipitation scheme. Brief description of these schemes are given

below. Detailed informations and other physical parameterizations are available at www.ictp.trieste.it/RegCNET/model.html.

2.4.1. Radiation Scheme

The radiation scheme of the RegCM3 is the same as that of the NCAR Community Climate Model (CCM3). δ -Eddington approximation (Kiehl et al., 1996) is used for solar radiation component that accounts for the effect of O_3 , H_2O , CO_2 , and O_2 . The cloud scattering and absorption parameterizations are also included in order to determine cloud influence on solar radiation. The infrared calculation accounts for effect of CO_2 , H_2O , O_3 gases.

2.4.2. Land Surface Model

The interactions between the soil, vegetation, and atmosphere are parameterized using Biosphere-Atmosphere Transfer Scheme version 1e (BATS1e) which is described in detail by Dickinson et al. (1993). BATS describe the role of vegetation and interactive soil moisture in modifying the surface-atmosphere exchanges of momentum, energy, and water vapor. 20 vegetation types are available in the present version.

For the water content of the soil layers the soil hydrology calculations are performed. The soil hydrology calculations include predictive equations accounted for precipitation, snowmelt, canopy foliage drip, evapotranspiration, surface runoff, infiltration below the root zone, and diffusive exchange of water between soil layers for the water content of the soil layers. The near surface turbulent fluxes of sensible heat, moisture, and momentum are calculated using a standard surface drag coefficient formulation based on surface-layer similarity theory. The atmospheric stability in the surface layer and the surface roughness length are the factors that affect the drag coefficient.

2.4.3. Planetary Boundary Layer Scheme

The planetary boundary layer (PBL) scheme of the (Holtslag et al., 1990) is the scheme used in the RegCM3 model. The scheme is used for calculation of turbulent transports of sensible heat, momentum, and water vapor in the PBL over land and ocean. The PBL scheme is based on non-local diffusion that takes into account countergradient fluxes resulting from large-scale eddies in an unstable, well-mixed atmosphere. Refer to (Holtslag et al., 1990), (Holtslag and Boville, 1993), and RegCM3 User's Guide for a more detailed description.

2.4.4. Convective Precipitation Scheme

There are three convective schemes in order to compute convective precipitation: Grell scheme (Grell, 1993), Modified-Kuo scheme (Anthes, 1977), and MIT-Emanuel scheme ((Emanuel, 1991), (Emanuel and Zivkovic-Rothman, 1999)). Grell's cumulus convection parameterization is used as convective precipitation scheme in this study. In this scheme, clouds are defined as two steady state circulations; an updraft and a downdraft. There is no direct mixing between the cloudy air and the environmental air except at the top and bottom of the circulations.

The Grell scheme convective closure assumption can be of two types. In the (Fritsch and Chappell, 1980) closure assumption (FC80) convection removes the available buoyant energy at a given time scale. It is designed to represent convections which typically occur in mid-latitudes. In the (Arakawa and Schubert, 1974) closure assumption (AS74) convection stabilizes the environment as fast as the large-scale destabilizes it. It is designed to represent convections which tend to be the most common form of convection.

2.4.5. Large-Scale Precipitation Scheme

The subgrid explicit moisture scheme (SUBEX) developed by Pal et al. (2000) is used as large-scale precipitation scheme in RegCM3. SUBEX considers the subgrid variability in clouds by linking the average grid cell relative humidity to the cloud fraction and cloud water following the work of Sundqvist (1989). For a more detailed description and formulation of SUBEX refer to Pal et al. (2000).

2.5. Experiment Design

Before performing the model it is necessary to complete two pre-processing steps in Terrain and ICBC sub-directory (Fig. 2.3).

In the Terrain sub-directory, the domain with grid intervals is defined and landuse and elevation data are interpolated to the model grid. In the ICBC sub-directory, files used for the initial and boundary conditions are generated. The input data used by the Terrain and ICBC programs are stored in the DATA sub-directory Fig. 2.4.

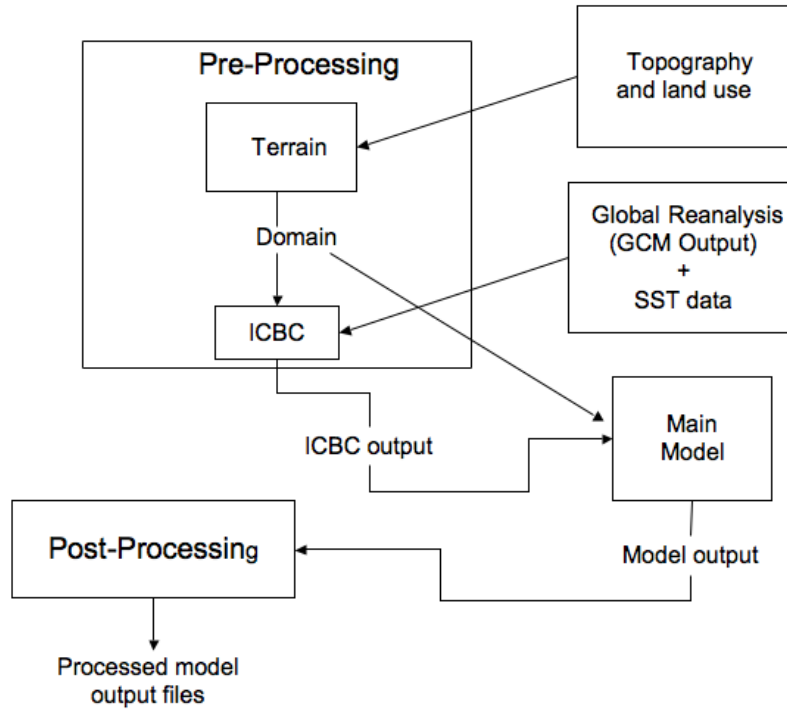


Fig. 2.3. Brief schematic description of RegCM3 modeling system used in this study.

2.5.1. Terrain

The landuse and elevation data from a latitude-longitude grid to the cartesian grid of the chosen domain are horizontally interpolated by the Terrain program. The elevation data used is from the United States Geological Survey (USGS). Both the landuse and elevation data files are available at 60, 30, 10, 5, 3, and 2 minute resolutions. In this study the topography and land use are interpolated to the model grid points from a global dataset at 10 minute resolution.

In regional climate studies, the choice of model domain play a key role in simulation results. The model domain should capture global patterns while it is able to demonstrate small-scale changes. Parameters such as domain size, input data, and length of simulation are defined by the user. There are some important factors when selecting a domain:

1. Choose the map projection most suitable for the studied region.
2. Boundaries should be placed where driving data is trusted.
3. Boundaries should avoid complex topography.

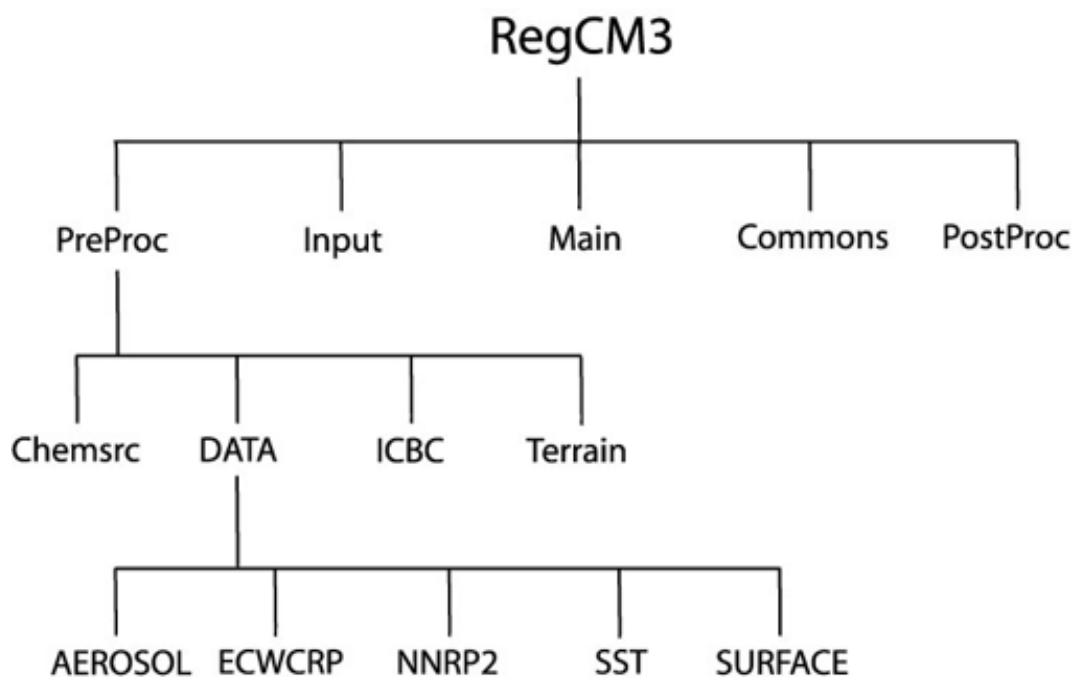


Fig. 2.4. RegCM3 directory tree. Adapted from workshops on RegCM3 that available at RegCM3 website.

In this study, RegCM3 has been set up for a domain centered at 40°N , 32°E with 135×85 grid cells, which have 30 km spatial resolution, using a Lambert Conformal projection (Fig. 2.5).

For each of the five different regions depicted Fig. 2.5, we have devised to carry out three simulations including a control, an SST+2K perturbation and an SST-2K perturbation. Control simulations involve no change to SST, however, the perturbation simulations involve changes in SST at these regions. The simulations are planned to cover the 6-month period from October to March between the years of 1990 and 2000.

We firstly treated Aegean Sea (1^{st} region) and completed the 10-year simulations for all three cases (control, SST-2K, SST+2K). In addition to surrounding seas of Turkey, we also investigated Central Mediterranean Sea since it is the intersection point of most cyclones influencing on Turkey. One of the results of Aegean Sea sensitivity experiment is that there is a quasi-linear relationship between change in precipitation due to SST-2K perturbation and SST+2K perturbation. For that reason and due to inadequate hardware, just SST-2K perturbations and control simulations were performed for the other seas.

The latitude and longitude of each five region and domain parameters are given in Table 2.1 and Table 2.2.

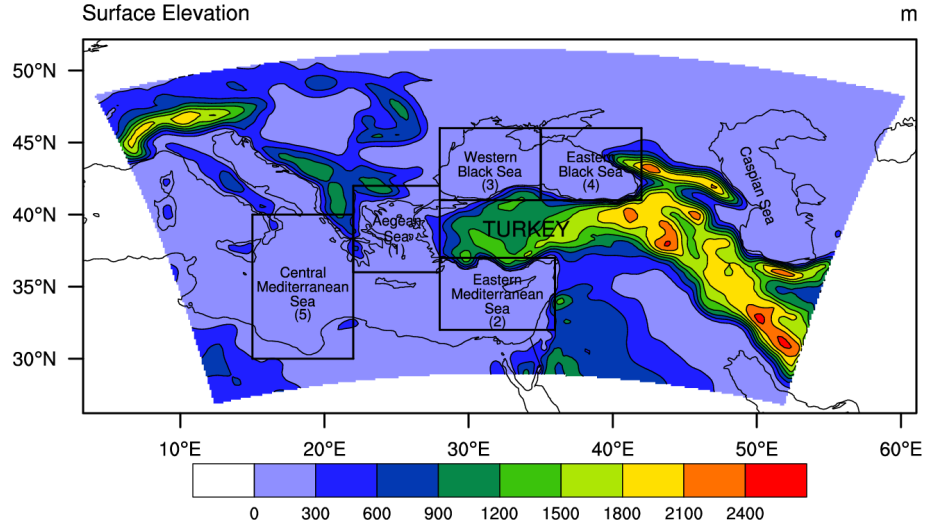


Fig. 2.5. The domain and topography used in the RegCM3 simulations. The five rectangles show the regions where SSTs are changed in sensitivity simulations.

Table 2.1. Latitude and longitude of each five region in the domain

	Latitude	Longitude
Region 1	$36^{\circ}N-42^{\circ}N$	$22^{\circ}E-28^{\circ}E$
Region 2	$32^{\circ}N-37^{\circ}N$	$28^{\circ}E-36^{\circ}E$
Region 3	$41^{\circ}N-46^{\circ}N$	$28^{\circ}E-35^{\circ}E$
Region 4	$41^{\circ}N-46^{\circ}N$	$35^{\circ}E-42^{\circ}E$
Region 5	$30^{\circ}N-40^{\circ}N$	$15^{\circ}E-22^{\circ}E$

Land cover and vegetation classes of the domain is important for determining atmospheric properties of the domain. Atmospheric parameters such as temperature, precipitation and moisture are affected by not only the topography of the domain but also land cover of the domain. The Global Land Cover Characterization (GLCC) datasets are used for the vegetation/landuse data. The GLCC dataset is derived from 1 km Advanced Very High Resolution Radiometer (AVHRR) data spanning April 1992 through March 1993, and is based on the vegetation/land cover types defined by Biosphere Atmosphere Transfer Scheme (BATS). Fig. 2.6 shows landuse pattern over the domain. The land use type of the domain consists of 20 classes (Table 2.3).

Table 2.2. Domain parameters

Parameter	Value	Description
iy	85	number of grid points in y direction (i)
jx	135	number of grid points in x direction (j)
kz	18	number of vertical levels (k)
ds	30	grid point separation in km
ptop	5.0	pressure of model top in cb
clat	40.00	central latitude of model domain in degrees
clon	32.00	central longitude of model domain in degrees
ntypec	10	resolution of the global terrain and land-use data
iproj	'LAMCON'	map projection
igrads	1	true=output GrADS control file
SSTTYP	'OLWK'	SST dataset
DATTYP	'NNRP2'	global analysis dataset
NPROC	'1'	number of processors

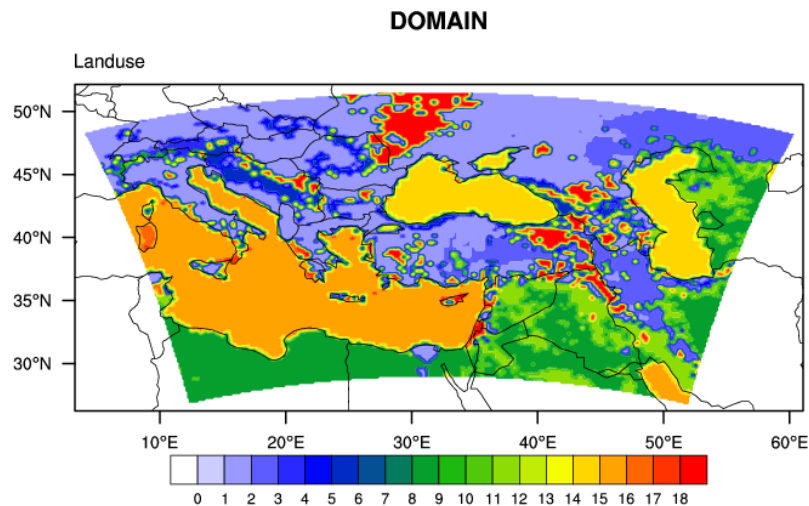


Fig. 2.6. Land cover and vegetation classes of the domain.

2.5.2. ICBC

The ICBC program interpolates global reanalysis and SST data to the model grid. These files are used for the initial and boundary conditions during the simulation.

The initial and boundary conditions are prescribed using the National Center for Environmental Prediction (NCEP) Reanalysis datasets with $2.5^\circ \times 2.5^\circ$ grid resolution and 17 pressure levels. The pressure levels begin from 1000mb for surface and exist for the levels of 925, 850, 700, 600, 500, 400, 300, 250, 200, 150, 100, 70, 50, 30, and 10mb. Model inputs at these pressure levels are geopotential heights (m), temperature (K), u and v components of wind (m/s), relative humidity, specific humidity (kg/kg), and vertical velocity (Pa/s). Model inputs at surface are surface pressure (Pa) and surface geopotential ($m^2 s^2$). Model

Table 2.3. Land Cover/Vegetation classes

1.	Crop/mixed farming
2.	Short grass
3.	Evergreen needleleaf tree
4.	Deciduous needleleaf tree
5.	Deciduous broadleaf tree
6.	Evergreen broadleaf tree
7.	Tall grass
8.	Desert
9.	Tundra
10.	Irrigated Crop
11.	Semi-desert
12.	Ice cap/glacier
13.	Bog or marsh
14.	Inland water
15.	Ocean
16.	Evergreen shrub
17.	Deciduous shrub
18.	Mixed Woodland
19.	Forest/Field mosaic
20.	Water and Land mixture

inputs cover the periods of October to March from of 1990 and 2000.

There are several options for SST data that are defined by the user in the Pre-processing. The Global Sea Surface Temperature (GISST) one-degree monthly gridded data (1871-2002) and the Optimum Interpolation Sea Surface Temperature (OISST) one-degree (1981-2005) at both weekly and monthly time scales are the data used for SST. In this study, OISST with weekly time scales is used as SST data.

2.5.3. Running the model and Outputs

Domain file from the Terrain process and ICBC outputs from the ICBC process are used in main model in order to start simulations. The model is started by selecting start/end dates of simulation, time steps, model output frequencies, and modifying physics options. At that point, selecting the model time step is very important. If the time step is too small, the simulation will take longer. If the time step is too large, the model will crash. Commonly, the timestep in seconds should be approximately three times the spatial resolution of the model. In addition, all of the physics timesteps must be a multiple of the main model time step. The necessary modifications are done in regcm.in file (Table 2.4).

The model generates three main outputs files in binary format from atmosphere (ATM.YYYYMMDDHH) (Table 2.5), surface model

Table 2.4. List of time step variables to be modified in regcm.in file

Parameter	Value	Description
idate0	YYYYMMDDHH	start date of first simulation
idate1	YYYYMMDDHH	restart date
idate2	YYYYMMDDHH	end date of simulation
radfrq	30	time step for radiation model, min
abemh	18	LW absorption/emissivity time step, hr
abatm	270	Land surface time step, sec
dt	90	Main model time step, sec
ibdyfrq	6	Lateral boundary condition time step, hr

(SRF.YYYYYMMDDHH)(Table 2.6), and radiation model (RAD.YYYYYMMDDHH) (Table 2.7).

The RegCM postprocessor converts these model output files to new output files of averaged variables in commonly used formats such as NetCDF or GrADS.

Table 2.5. List of output variables from atmosphere

Variables	Description
u	Zonal wind (m/s)
v	Meridional wind (m/s)
w	Omega (hPa)p-velocity
t	Temperature (K)
qv	Mixing ratio (g/kg)
qc	Cloud mixing ratio (kg/kg)
psa	Surface pressure (hPa)
tpr	Total precipitation (mm/day)
tgb	Ground temperature (K)
swt	Total soil water (mm)
rno	Base flow (mm/day)

Table 2.6. List of output variables from surface model

Variables	Description
u10m	Westerly wind at 10m (m/s)
v10m	Southerly wind at 10m(m/s)
uvdrag	Surface drag stress
tgb	Ground temperature (K)
tlef	Foliage temperature (K)
t2m	Air temperature at 2m (K)
q2m	Specific humidity at 2m (kg/kg)
ssw	Upper layer soil water (mm)
rsw	Root zone soil water (mm)
tpr	Total precipitation (mm/day)
evp	Evapotranspiration (mm/day)
scv	Snow water equivalent (mm)
sena	Sensible heat flux (W/m^2)
flw	Net infrared energy flux (W/m^2)
fsw	Net absorbed solar energy flux (W/m^2)
flwd	Downward infrared energy flux (W/m^2)
sina	Incident solar energy fluw (W/m^2)
prcv	Convective precipitation (mm/day)
psb	Surface Pressure (hPa)
zpbl	Planetary Boundary Layer height (m)
tgmax	Maximum ground temperature (K)
tgmin	Minimum ground temperature (K)
t2max	Maximum 2m air temperature (K)
t2min	Minimum 2m air temperature (K)
w10max	Maximum 10m wind speed (m/s)
psmin	Minimum surface pressure (hPa)

Table 2.7. List of output variables from radiation model

Variables	Description
cld	Cloud fractinal cover (fraction)
clwp	Cloud liquid water path (g/m^{-2})
qrs	Solar heating rate (K/s)
qrl	Longwave cooling rate (K/s)
frsa	Surface absorbed solar flux (W/m^2)
frla	Longwave cooling of surface (W/m^2)
clrst	Clearsky total column absorbed solar flux (W/m^2)
clrss	Clearsky surface absorbed solar flux (W/m^2)
clrlt	Clearsky net upward LW flux at top(W/m^2)
clrls	Clearsky LW cooling at surface (W/m^2)
solin	Instantaneous incident solar (W/m^2)
sabtp	Total column absorbed solar flux (W/m^2)
firtp	Net upward LW flux at top (W/m^2)

2.6. Model Performance

Before demonstrating the sensitivity experiment results, it is important to present model performance in simulating large-scale circulation and precipitation patterns.

Fig. 2.7 and Fig. 2.8 show 10-year December-January-February (DJF) and October-November-December-January-February-March (ONDJFM) average of 850hPa and 500hPa geopotential height maps from NCEP/NCAR Reanalysis and RegCM3 model output. It seems that the model is able to reproduce 850hPa and 500hPa geopotential height fairly well.

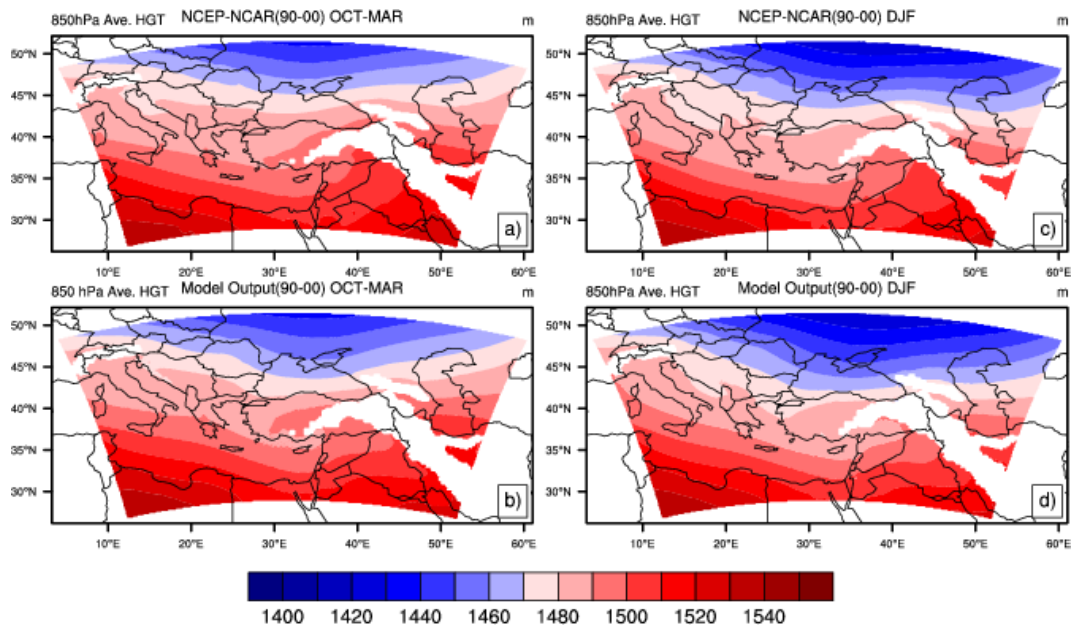


Fig. 2.7. 10-year ONDJFM (a),(b) and DJF (c),(d) average of 850hPa geopotential height maps from NCEP/NCAR Reanalysis (a),(c) and RegCM3 model output (b),(d).

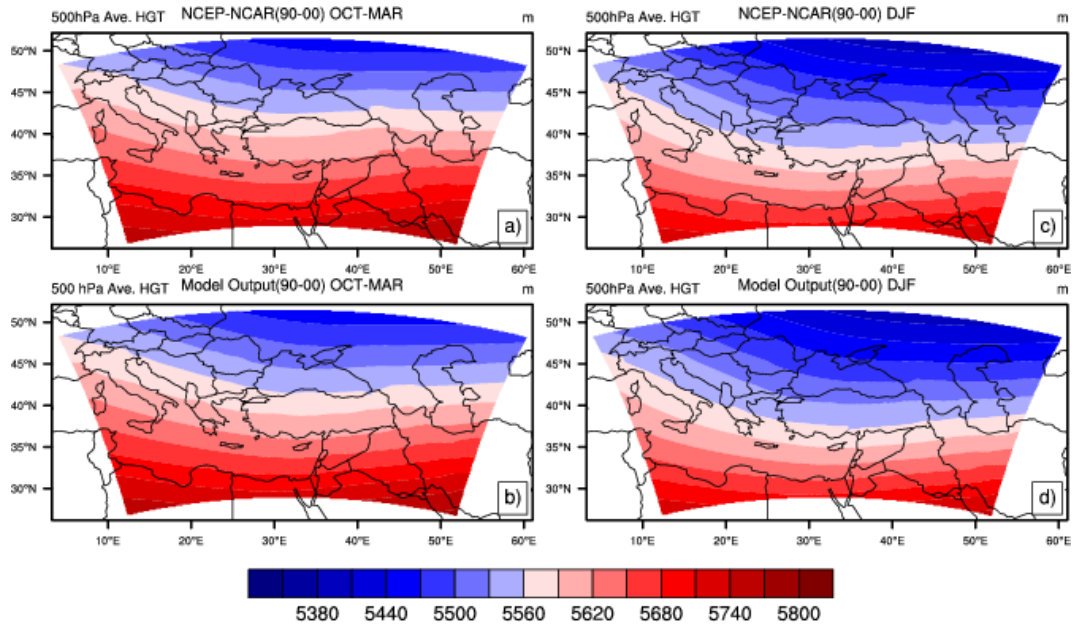


Fig. 2.8. 10-year ONDJFM (a),(b) and DJF (c),(d) average of 500hPa geopotential height maps from NCEP/NCAR Reanalysis (a),(c) and RegCM3 model output (b),(d).

Fig. 2.9 shows 10-year average precipitation values (mm/day) for ONDJFM and DJF from gridded observations (CRU data) and model output. In general the model captures the primary features of the rainfall distribution across the domain. It seems that the CRU data are somehow missing the high precipitation amounts at the mountainous eastern Black Sea region. The model on the other hand gives more reasonable estimations of precipitation in these areas.

Fig. 2.10 shows 10-year average sea level pressure (SLP) (hPa) values for ONDJFM and DJF from NCEP/NCAR Reanalysis and RegCM3 model output. Both seasons of simulation period are characterized by influence of high pressure that is well simulated in model output.

After comparing model outputs with observed and reanalysis data, it is deemed that the model performance is adequate to carry out sensitivity experiments that investigate the effects of SST perturbations in the surrounding seas of Turkey on its precipitation.

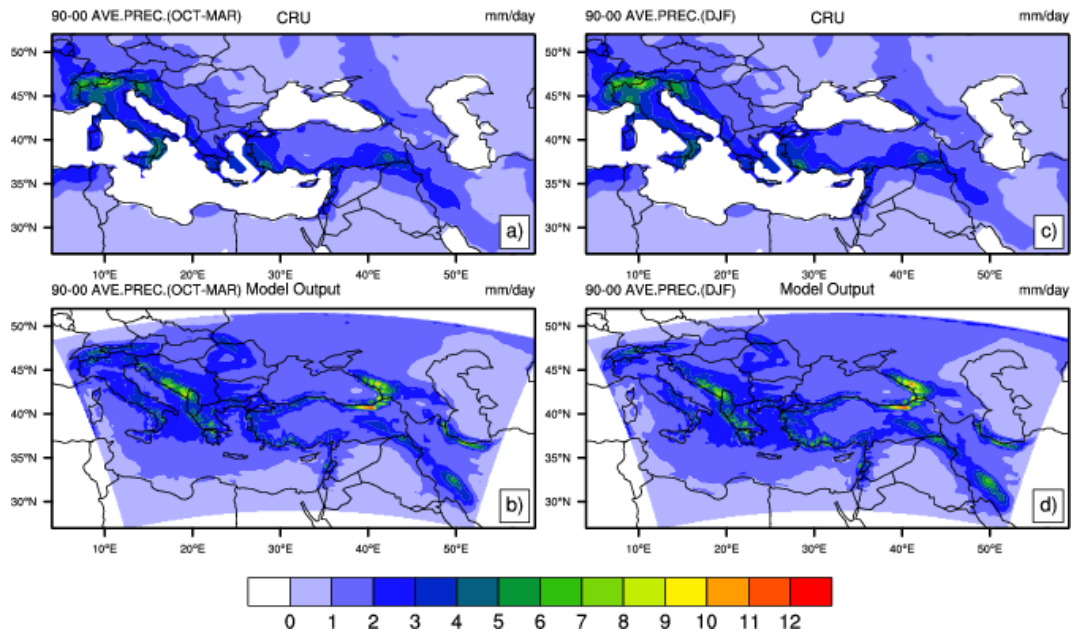


Fig. 2.9. 10-year average precipitation values (mm/day) for ONDJFM and DJF from gridded observations (CRU data) (a),(c) and from RegCM3 model output (b),(d).

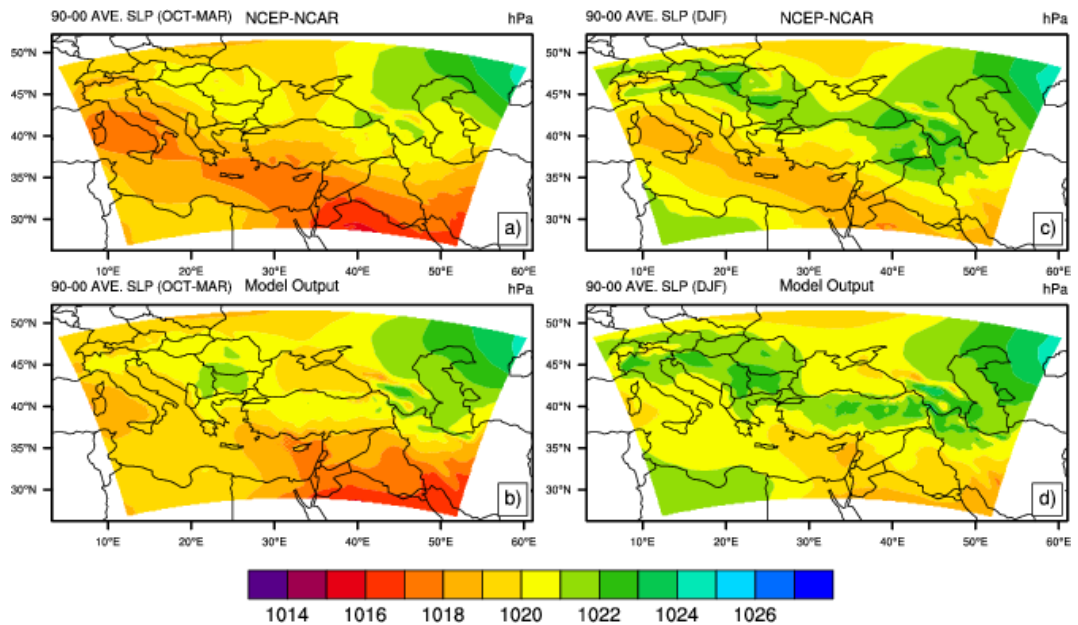


Fig. 2.10. 10-year average SLP values (hPa) for ONDJFM and DJF from NCEP/NCAR Reanalysis (a),(c) and from RegCM3 model output (b),(d).

3. SIMULATION RESULTS

3.1. Aegean Sea Sensitivity Experiment

Fig. 3.1 shows the 10-year average DJF difference in precipitation between perturbation simulations and control simulations with 850hPa wind vectors from the 10-year average control simulations. In addition to this, Student's T-test was applied and if any values that are less than $p < 0.1$ (90% confidence level) were hatched.

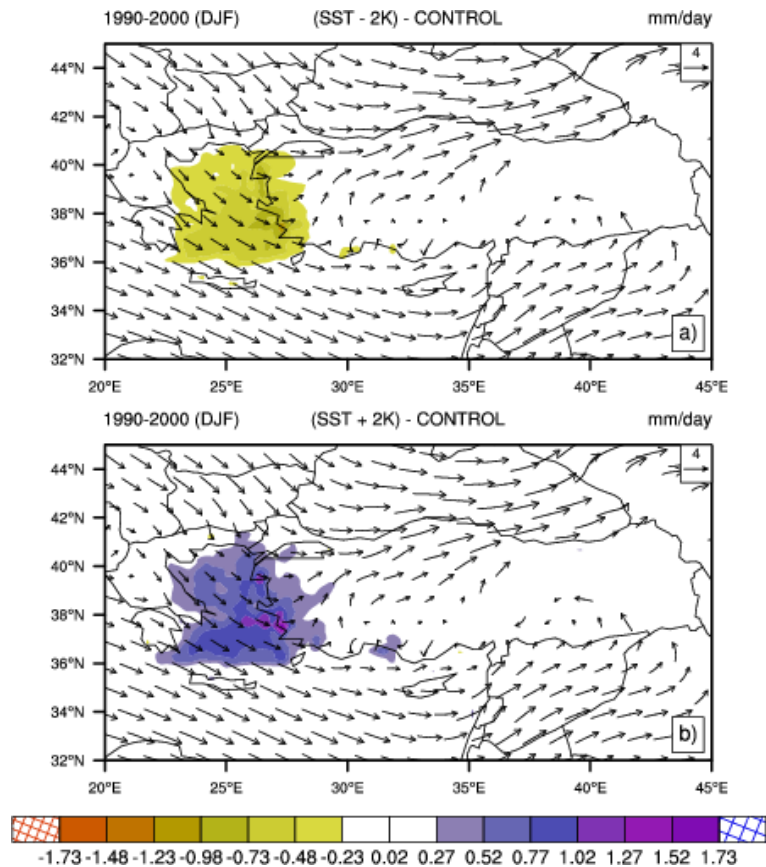


Fig. 3.1. 10-year average DJF difference of precipitation between perturbations and control simulation with 850hPa wind vectors of control simulation. (a) (SST-2K)-Control, and (b) (SST+2K)-Control.

It can be said that decreasing or increasing Aegean Sea surface temperature by 2K affect mostly the precipitation falling or increasing at Aegean Sea and the coastal areas surrounding this sea in winter. Highest changes occur in the westernmost coasts of Turkey. It is also important to emphasize that a decreased SST results in reductions in precipitation and and increased SST results in increases in precipitation, a somewhat quasi-linear relationship.

3.1.1. Changes in surface parameters

In order to explain how the SST perturbations effect precipitation change, some figures depicting other surface variables such as 2m-temperature, sensible heat flux, and latent heat flux are presented.

SST perturbations in Aegean Sea causes changes in 2m-temperature as it is shown in Fig. 3.2. 2m-temperature is decreased when SST of Aegean Sea is decreased by 2K and it is increased when SST is increased by 2K. Changes in 2m-temperature mostly occurred in the Aegean Sea itself and confined to the coastal areas of both Turkey and Greece.

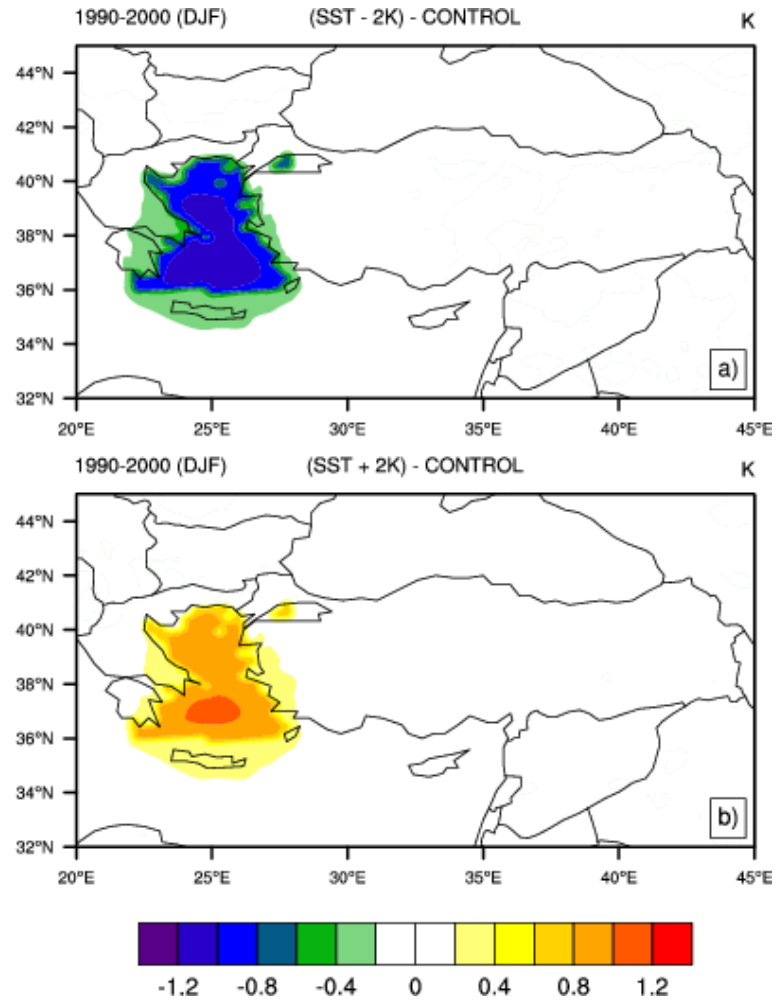


Fig. 3.2. 10-year average DJF difference of 2m-temperature between perturbations and control simulation. (a) (SST-2K)-Control, and (b) (SST+2K)-Control.

Changes in SST also cause changes in sensible heat flux and latent heat flux. Both sensible heat and latent heat fluxes are increased or decreased as the SST of Aegean Sea is increased or decreased (Fig. 3.3, Fig. 3.4).

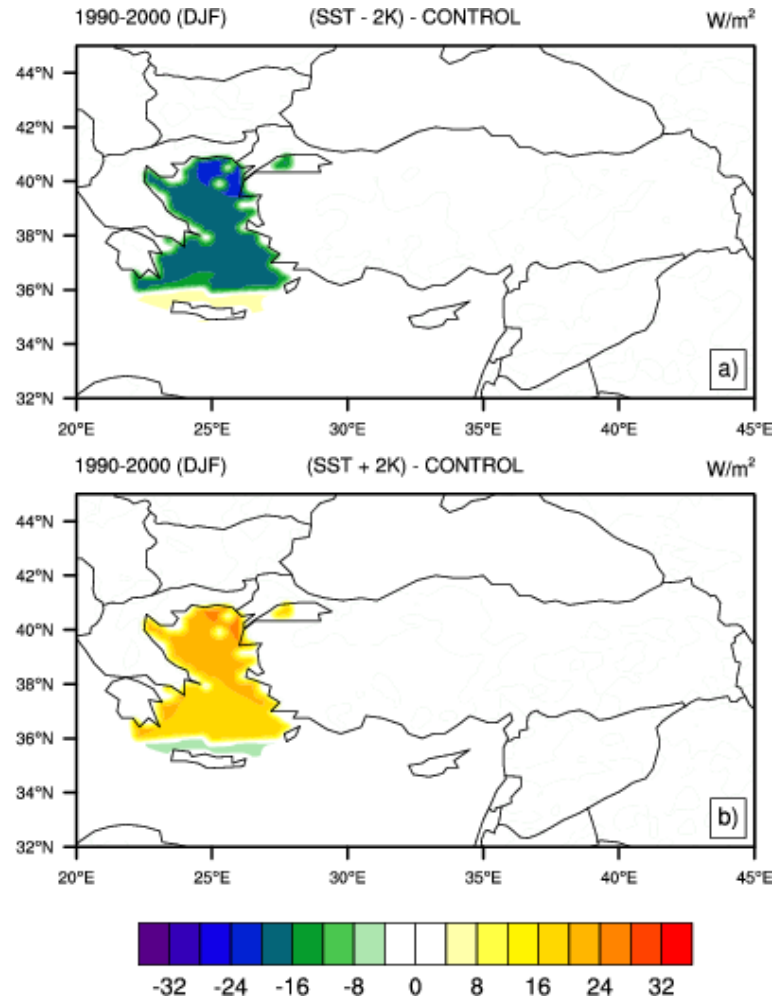


Fig. 3.3. 10-year average DJF difference of sensible heat flux between perturbations and control simulation. (a) (SST-2K)-Control, and (b) (SST+2K)-Control.

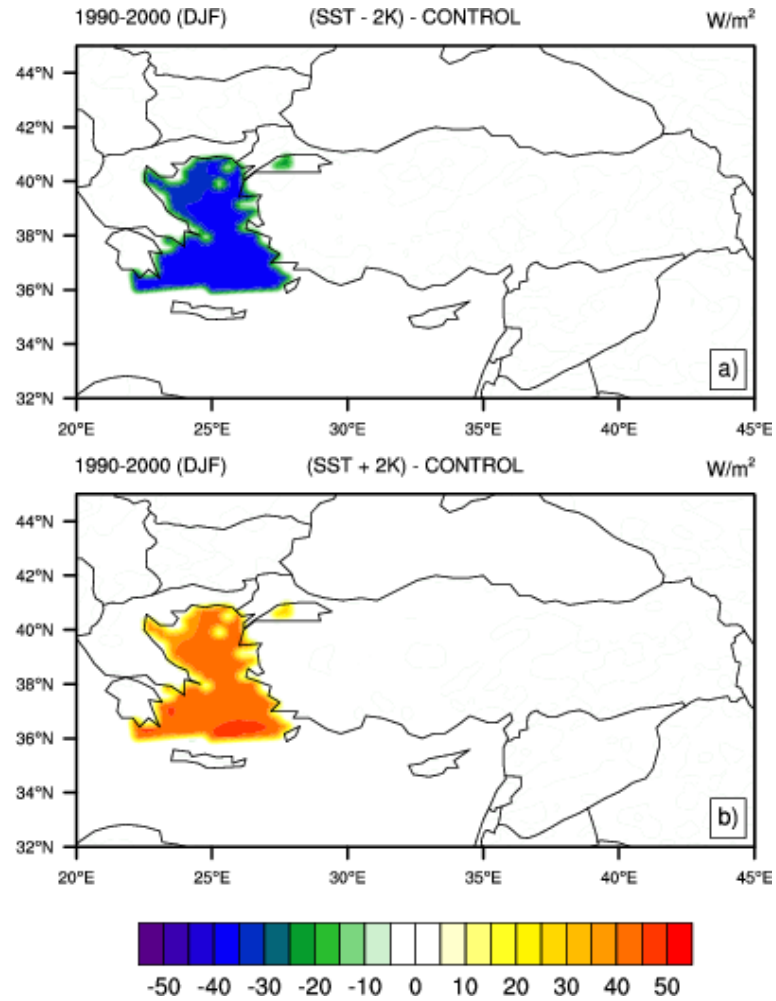


Fig. 3.4. 10-year average DJF difference of latent heat flux between perturbations and control simulation. (a) (SST-2K)-Control, and (b) (SST+2K)-Control.

3.1.2. Changes in upper level parameters

When we look at effect of SST perturbations on air temperature and specific moisture at 925hPa, it is observed that when the SST of Aegean Sea is decreased by 2K, air temperature at 925hPa is decreased especially in Aegean Sea itself and coastal areas of Turkey and Greece. Decrease in air temperature is spreaded to the eastern Mediterranean Sea, region of Marmara and Black Sea with the direction of prevailing wind at 850hPa. When the SST of Aegean Sea is increased by 2K, air temperature at 925hPa is increased in similar regions and spreaded with the direction of prevailing wind as in SST-2K (Fig. 3.5).

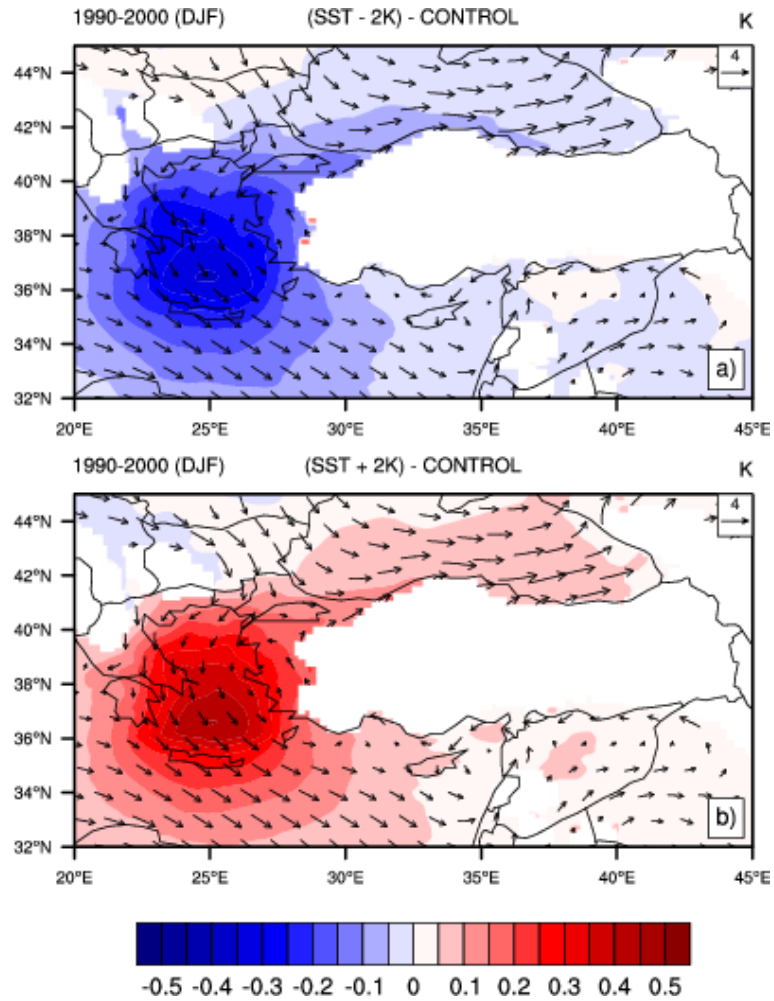


Fig. 3.5. 10-year average DJF difference of air temperature at 925hPa between perturbations and control simulation. (a) (SST-2K)-Control, and (b) (SST+2K)-Control.

Similar changes occur in specific moisture at 925hPa, as SST of Aegean Sea increases it increases too, and as SST of Aegean Sea decreases it decreases too. However, the most striking difference in changes between the air temperature and specific moisture at 925hPa is that changes in specific moisture are mostly confined to the Aegean Sea itself and coastal areas (Fig. 3.6).

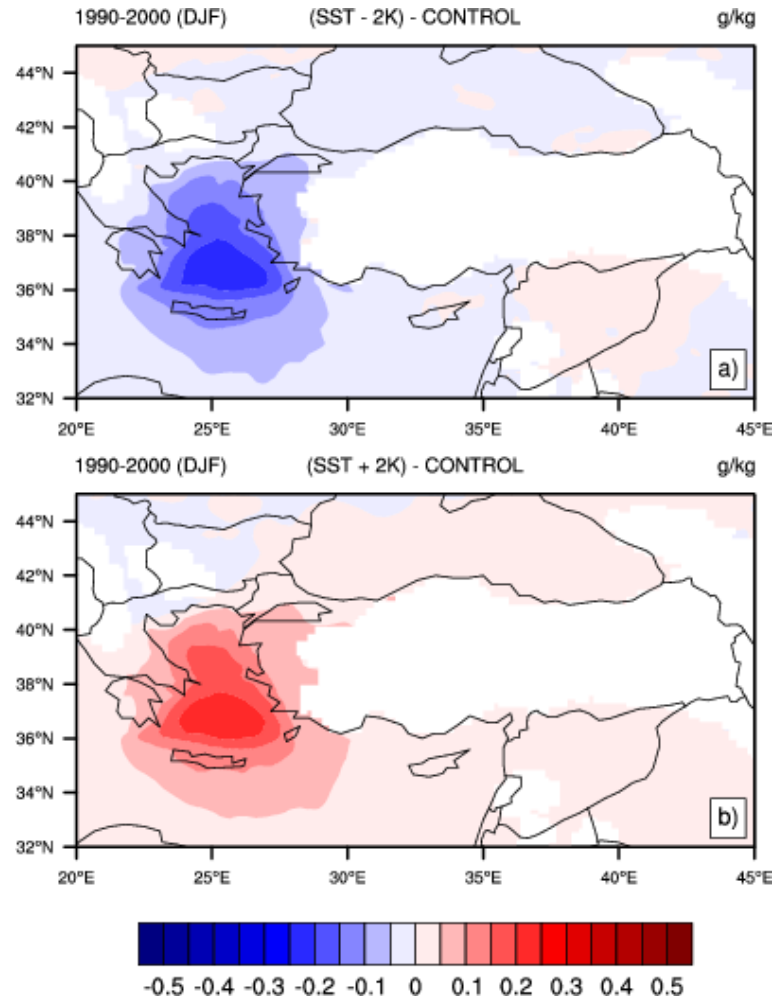


Fig. 3.6. 10-year average DJF difference of specific moisture at 925hPa between perturbations and control simulation. (a) (SST-2K)-Control, and (b) (SST+2K)-Control.

At 850hPa, less changes are occurred in air temperature and specific moisture due to SST perturbations and changes in air temperature cover more regions than of those in specific moisture with the direction of prevailing wind at 850hPa (Fig. 3.7, Fig. 3.8). Especially increase in SST by 2K causes remarkable increase in air temperature in the central part of Turkey (Fig. 3.7(b)).

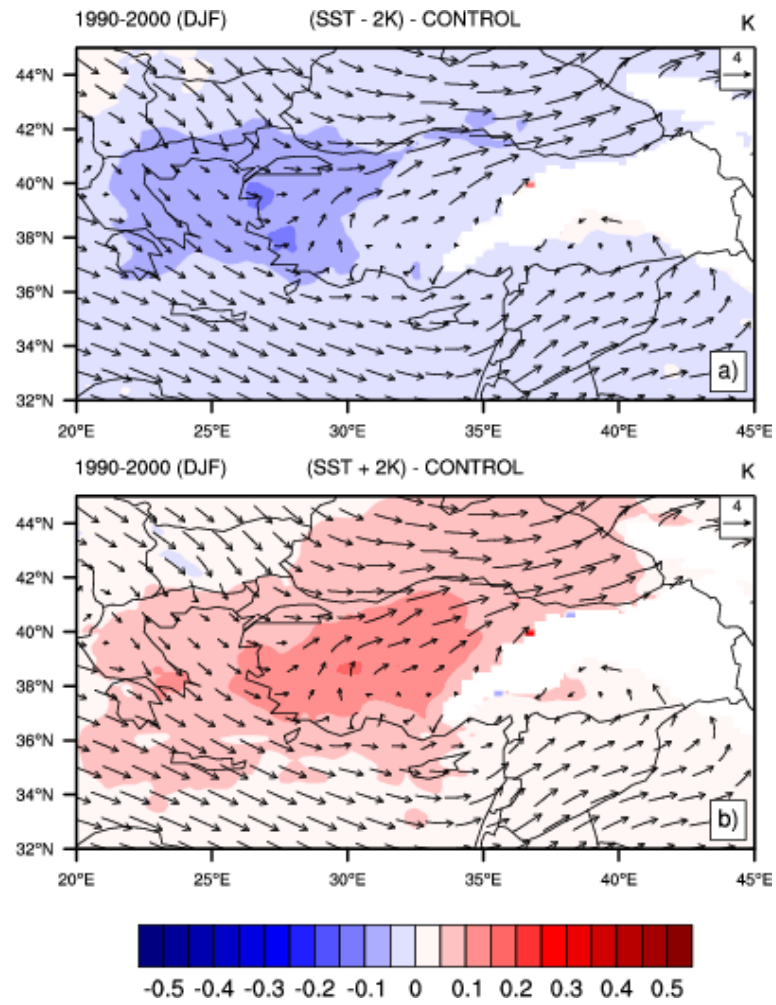


Fig. 3.7. 10-year average DJF difference of air temperature at 925hPa between perturbations and control simulation. (a) (SST-2K)-Control, and (b) (SST+2K)-Control.

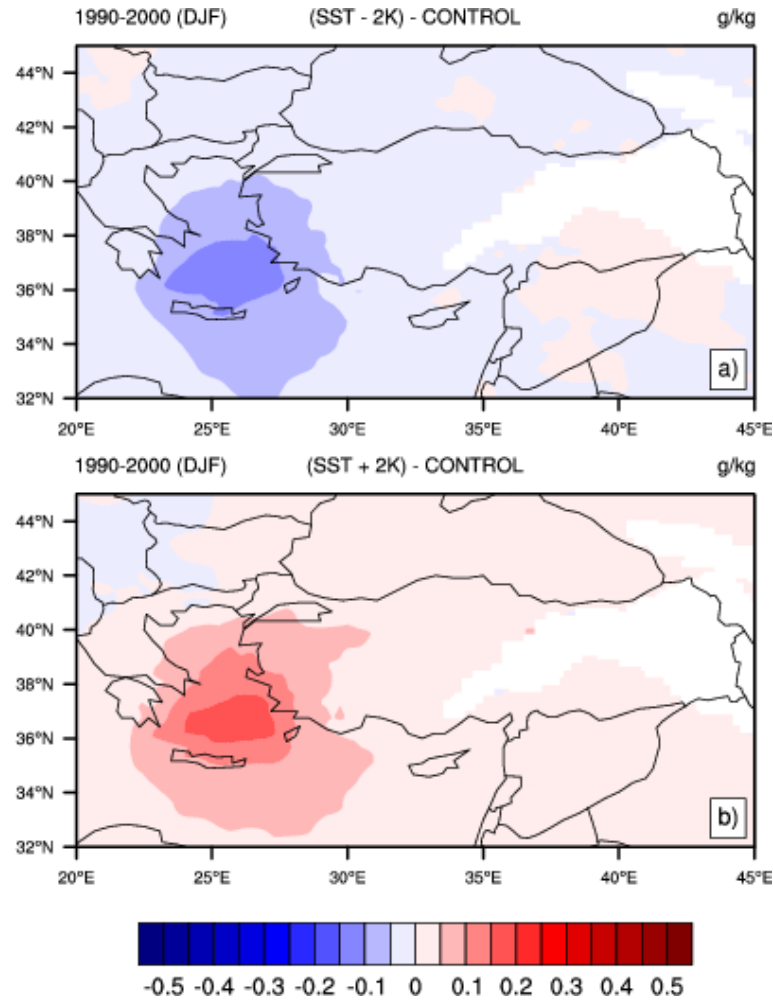


Fig. 3.8. 10-year average DJF difference of specific moisture at 925hPa between perturbations and control simulation. (a) (SST-2K)-Control, and (b) (SST+2K)-Control.

3.1.3. Changes in monthly precipitations

When we look at the individual months for SST-2K perturbation (Fig. 3.9), we can see that the changes in precipitation occur in Aegean Sea and immediate surrounding lands. One of the most striking change takes place in December when reduced SST in Aegean Sea causes substantial declines in rainfall along the westernmost coastal areas of Turkey (Fig. 3.9c). Similar inferences could be stated for SST+2K perturbation (Fig. 3.10). Highest changes in precipitation occur in December in that experiment too (Fig. 3.10c).

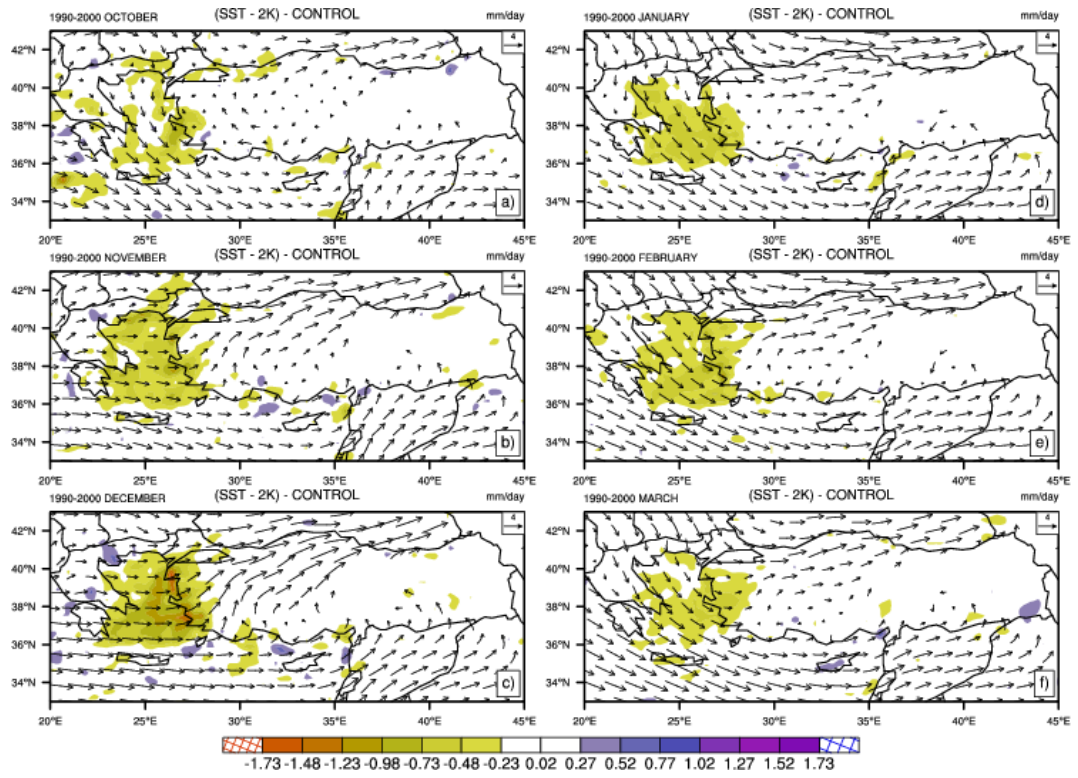


Fig. 3.9. 10-year average monthly difference of precipitation between SST-2K perturbation and control simulation with 850hPa wind vectors of control simulation.

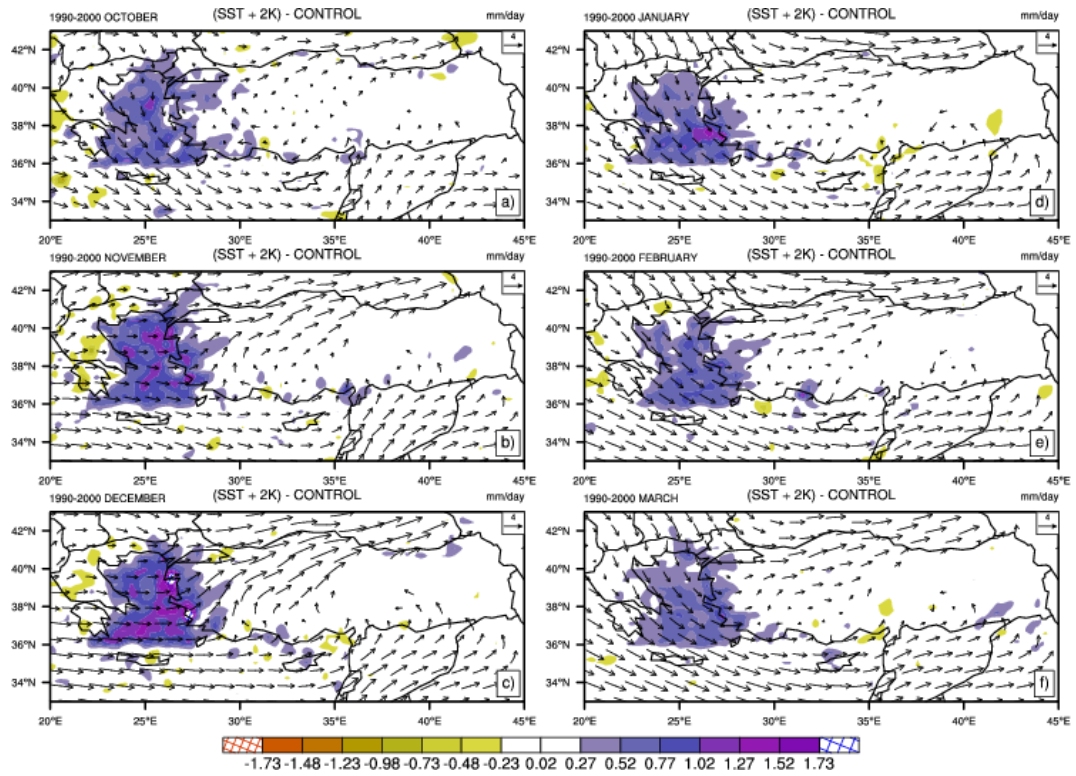


Fig. 3.10. 10-year average monthly difference of precipitation between SST+2K perturbation and control simulation with 850hPa wind vectors of control simulation.

It is also important to emphasize that increase in precipitation by SST+2K perturbation for December months between the years of 1990-2000 is significance when Student's T-test is applied with a 90% confidence level (Fig. 3.11b) while there is no significance reduction in precipitation by SST-2K perturbation (Fig. 3.11a).

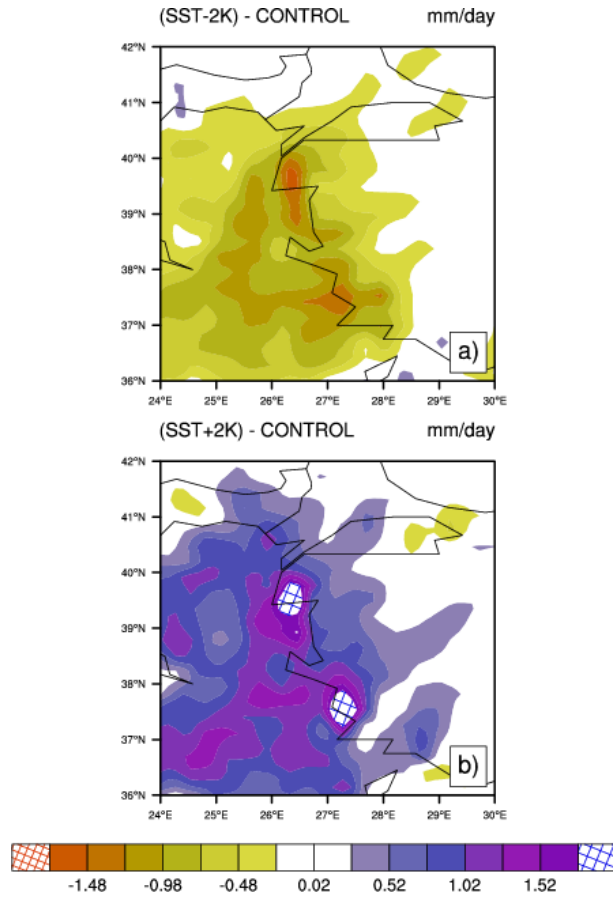


Fig. 3.11. 10-year average December precipitation change with 90% confidence level for both SST-2K (a) and SST+2K (b) perturbations.

Monthly precipitation change of each run indicates that highest precipitation amount occurs in December months between the years of 1990-2000 (Fig. 3.12). Therefore it is accepted as comprehensible reason why the December month has the highest changes. However, when we look at relative changes, percentage changes of each months is close to each other in SST-2K experiment while differences between the each months take place in SST+2K experiment (Fig. 3.13).

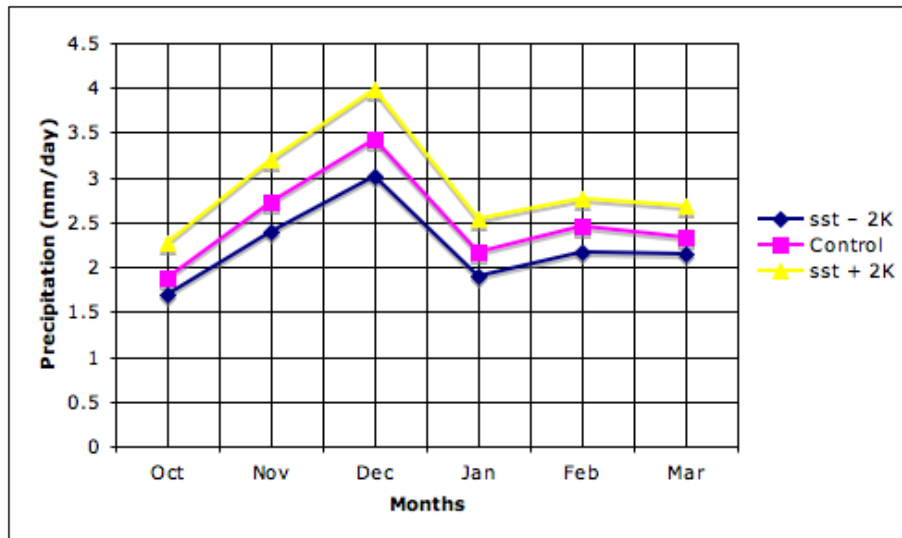


Fig. 3.12. 10-year average monthly precipitation amounts of SST perturbations and control simulation.

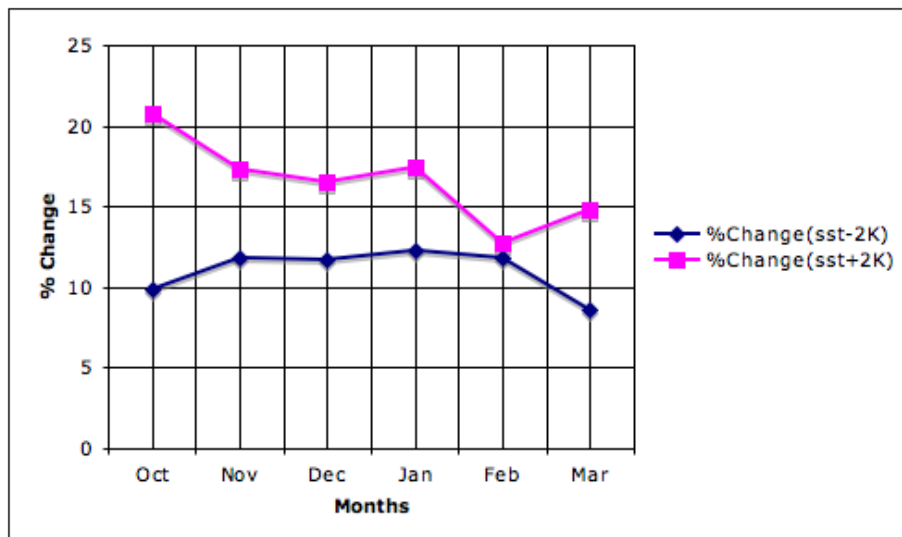


Fig. 3.13. 10-year average relative changes in each month for precipitation.

3.1.4. Wet and dry years comparison

10-year simulation experiment for Aegean Sea take dry and wet as well as normal years into account, thus getting closer to, what's called, climatology. It is necessary to analyze precipitation variability with SST changes in conjunction with climatic phenomenon such as North Atlantic Oscillation (NAO). NAO is a major disturbance of the atmospheric circulation and climate of the North Atlantic-European region. It is defined as fluctuations in the difference of sea level pressure between the Icelandic Low and the Azores High. Pressure difference between various stations on the Iceland and Azores is used to constitute NAO index. If the difference between Icelandic Low and the Azores High is big, then NAO index positive and southern Europe tends to be colder

and drier while northern Europe warmer and wetter (Fig. 3.14). If the NAO index is negative, the opposite occurs (Fig. 3.15).

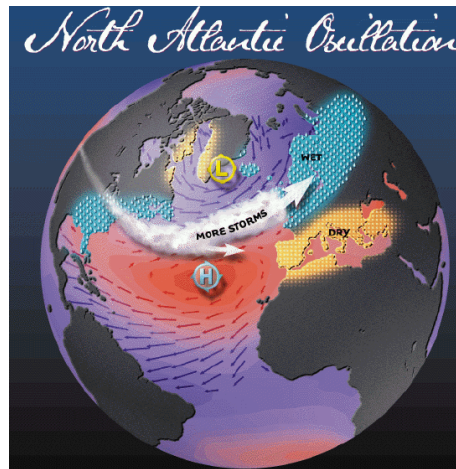


Fig. 3.14. Effects of positive NAO index on North Atlantic and European (<http://www.ldeo.columbia.edu/NAO/>).

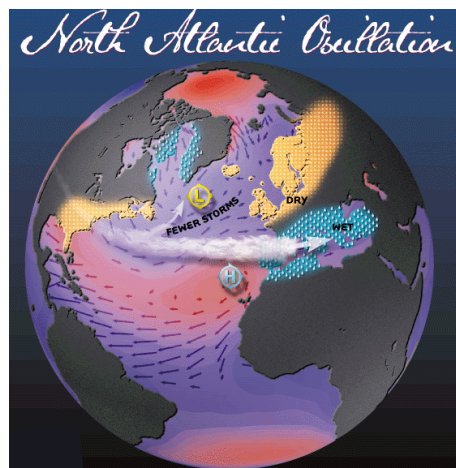


Fig. 3.15. Effects of negative NAO index on North Atlantic and European (<http://www.ldeo.columbia.edu/NAO/>).

In order to demonstrate sensitivity experiment of Aegean Sea for wet and dry years, we chose three wet and three dry years according to both DJF and ONDJFM index of the NAO (Fig. 3.16). For wet years we took 1995-1996, 1996-1997, and 1997-1998 for dry years we took 1992-1993, 1993-1994, and 1994-1995 (Fig. 3.17).

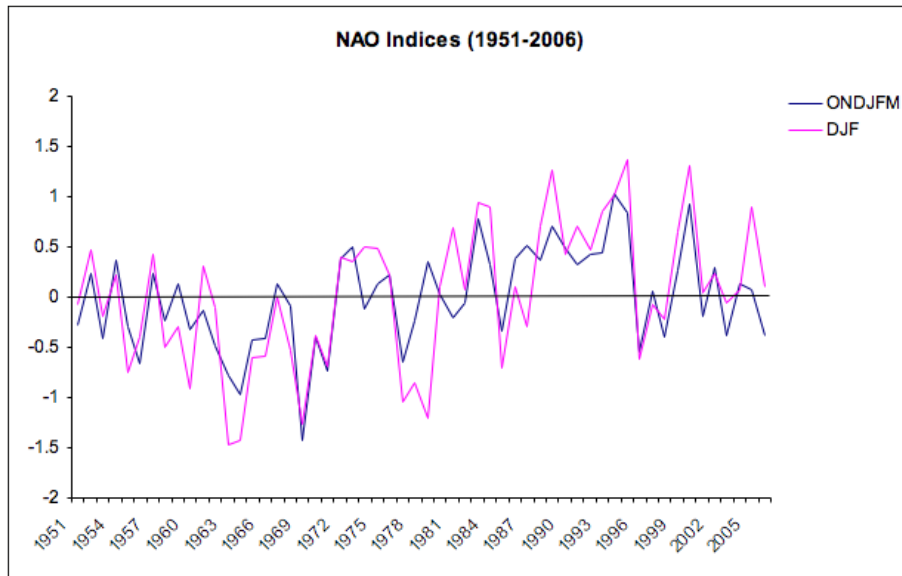


Fig. 3.16. DJF and ONDJFM index of the NAO 1951-2006.

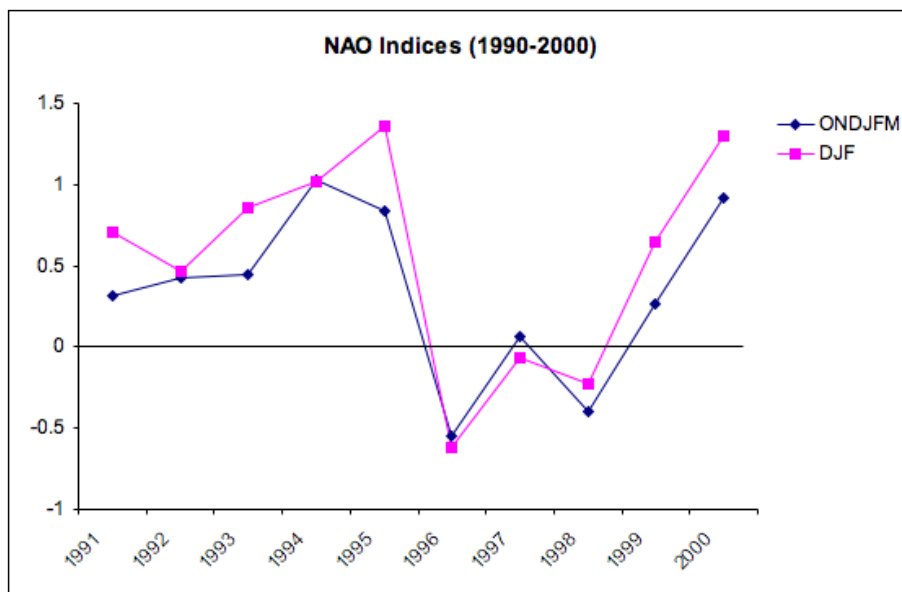


Fig. 3.17. DJF and ONDJFM index of the NAO 1990-2000.

Fig. 3.18 and Fig. 3.19 show precipitation response to SST perturbations for average of three wet and dry years. It is seen that there is no striking differences in response of precipitation change between wet and dry years. However, in wet years, major precipitation change occurs in northern regions of Aegean while it moves to central coastal regions of Aegean in dry years.

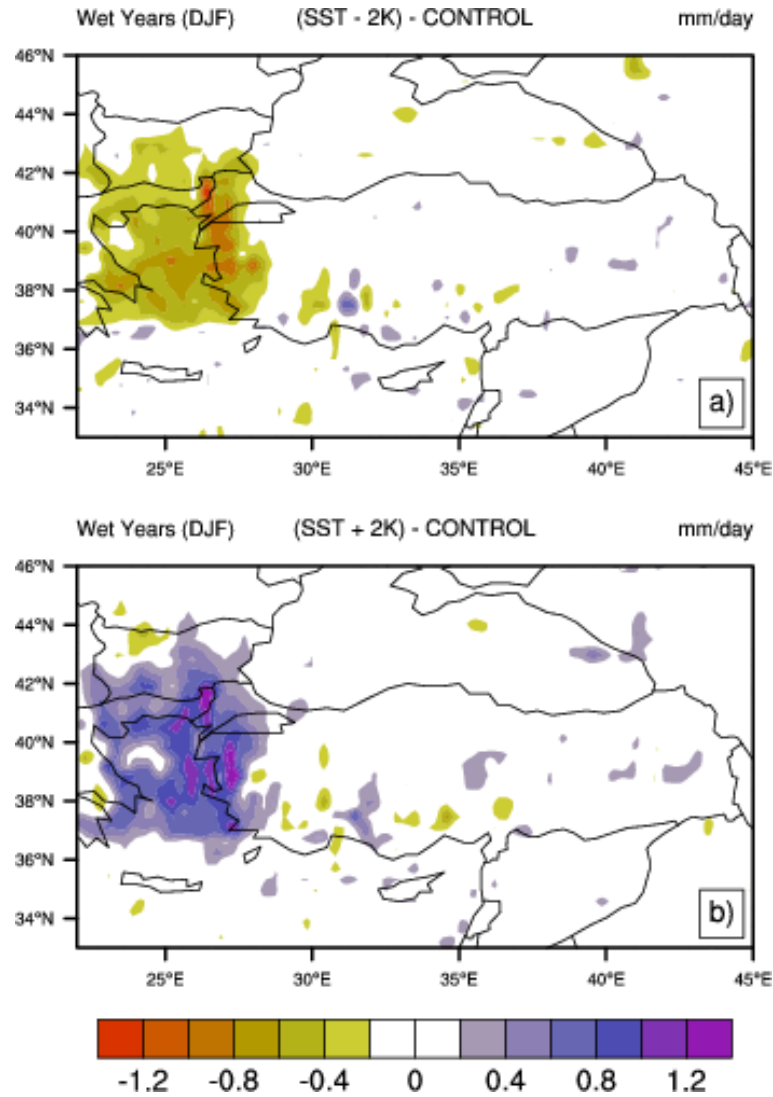


Fig. 3.18. Average wet years (1995-1996, 1996-1997, and 1997-1998) difference of precipitation between perturbations and control simulation. (a) (SST-2K)-Control, and (b) (SST+2K)-Control.

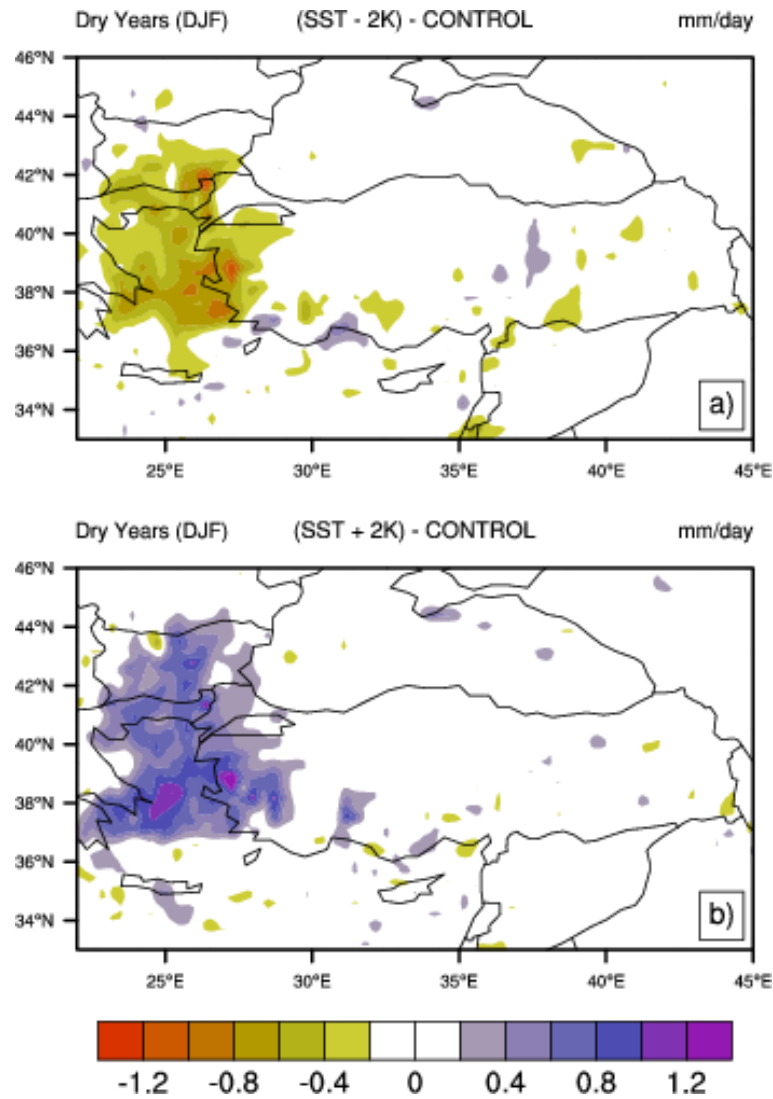


Fig. 3.19. Average dry years (1992-1993, 1993-1994, and 1994-1995) difference of precipitation between perturbations and control simulation. (a) (SST-2°C)-Control, and (b) (SST+2°C)-Control.

3.2. Eastern Mediterranean Sea Sensitivity Experiment

One of the results of Aegean Sea sensitivity experiment is that there is a quasi-linear relationship between change in precipitation due to SST-2K perturbation and SST+2K perturbation. For that reason and due to inadequate hardware, just SST-2K perturbations were performed for the other seas.

Fig. 3.20 shows the DJF precipitation difference between SST-2K perturbation and control for the second region that covers eastern Mediterranean Sea (Fig. 2.5). Results from sensitivity experiment for eastern Mediterranean indicate reductions in rainfall at the region itself, however, highest reductions occur towards eastern and northern boundaries of the region. Reductions take place in the central parts of eastern Turkey too.

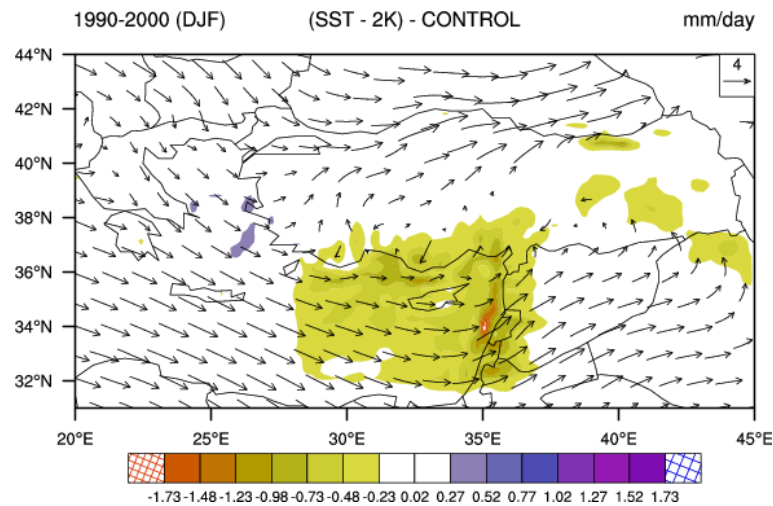


Fig. 3.20. 10-year average DJF precipitation differences between SST-2K perturbation and control for the region of East Mediterranean.

As it is presented in Aegean Sea sensitivity experiment, changes in SST result in changes in surface parameters. Similar results are valid for other seas and changes in surface parameters are confined to the sea itself same as in Aegean Sea sensitivity experiment.

3.2.1. Changes in upper level parameters

Air temperature at 925hPa is mostly decreased at eastern Mediterranean Sea itself when the SST is decreased by 2K. Southern coastal regions of Turkey are also affected from decreasing of SST by 2K. Since the direction of prevailing wind is west to east, decrease in air temperature is spreaded to the Middle East regions. Due to higher topography of Turkey, we are not able to state the regions in which air temperature at 925hPa is changed due to decrease in SST by 2K (Fig. 3.21).

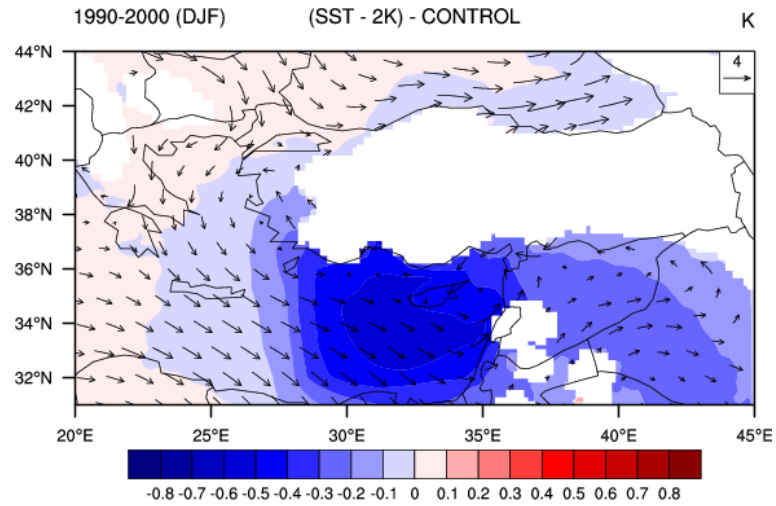


Fig. 3.21. 10-year average DJF difference of air temperature at 925hPa between SST-2K and control simulation.

Decrease in specific moisture at 925hPa is major on eastern Mediterranean Sea itself and it is not able to spread as in air temperature (Fig. 3.22).

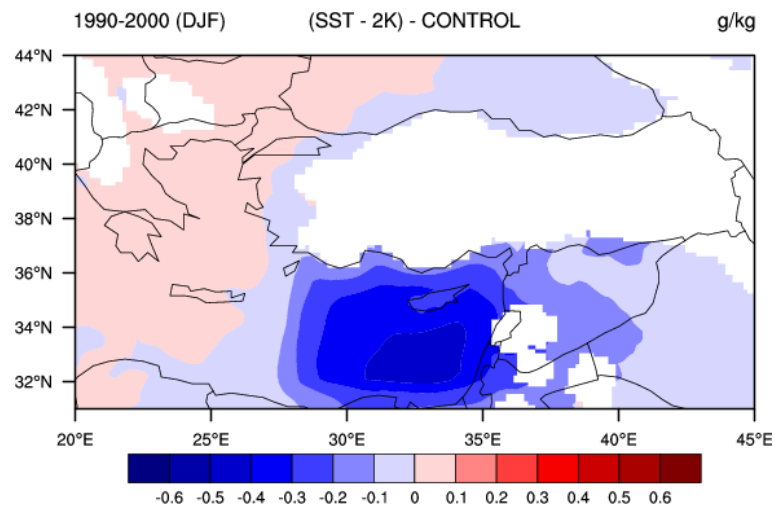


Fig. 3.22. 10-year average DJF difference of specific moisture at 925hPa between SST-2K and control simulation.

At 850hPa, decrease in air temperature and specific moisture due to decrease in SST by 2K is less and changes in air temperature cover more regions than of those in specific moisture with the direction of prevailing wind at 850hPa (Fig. 3.23, Fig. 3.24). Especially decrease in SST by 2K causes more remarkable decrease in air temperature in the southern coastal regions of Turkey and decrease in air temperature can be spreaded to central parts of eastern Turkey.

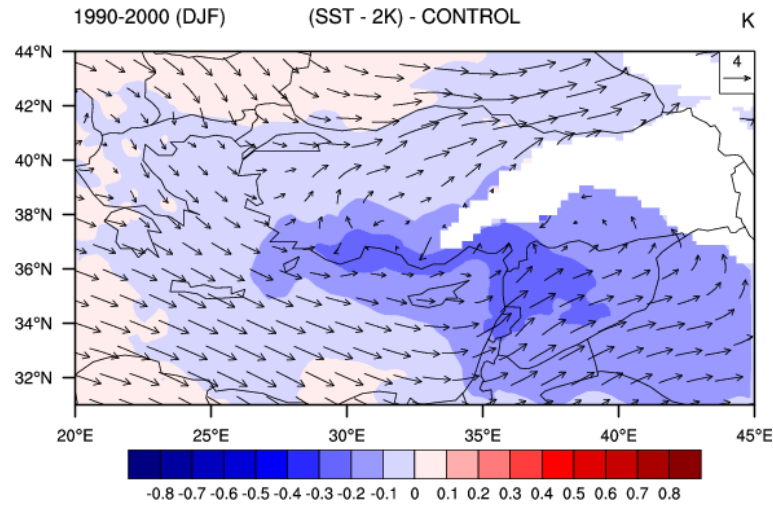


Fig. 3.23. 10-year average DJF difference of air temperature at 850hPa between SST-2K and control simulation.

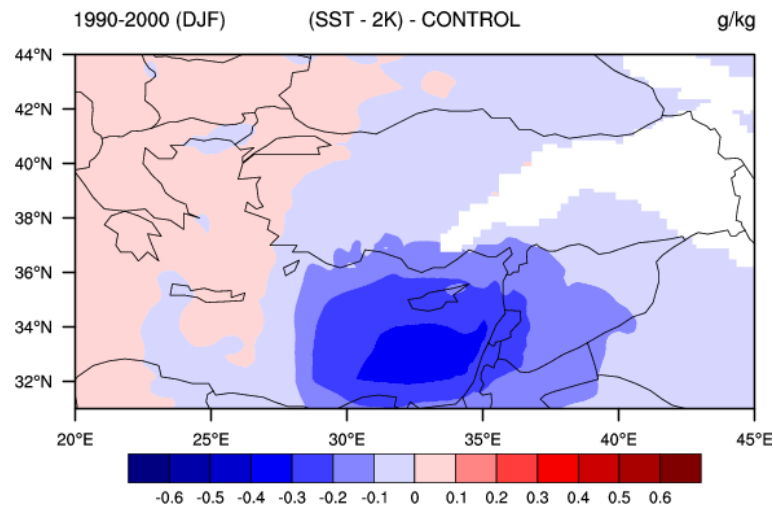


Fig. 3.24. 10-year average DJF difference of specific moisture at 850hPa between SST-2K and control simulation.

3.2.2. Changes in monthly precipitation

When we look at the individual months for SST-2K perturbation (Fig. 3.25), it can be seen that reduced SST in eastern Mediterranean Sea causes substantial declines in rainfall along the southernmost coastal areas and central parts of eastern Turkey especially in December and January. The major reductions in precipitation take places in Antalya, Adana, and Çukurova basin. Especially, reduction in precipitation in Çukurova basin is statistically significant with 90% confidence level in November (Fig. 3.25b). In addition, reduction in precipitation spreads to the eastern parts of Turkey in December and January (Fig. 3.25c).

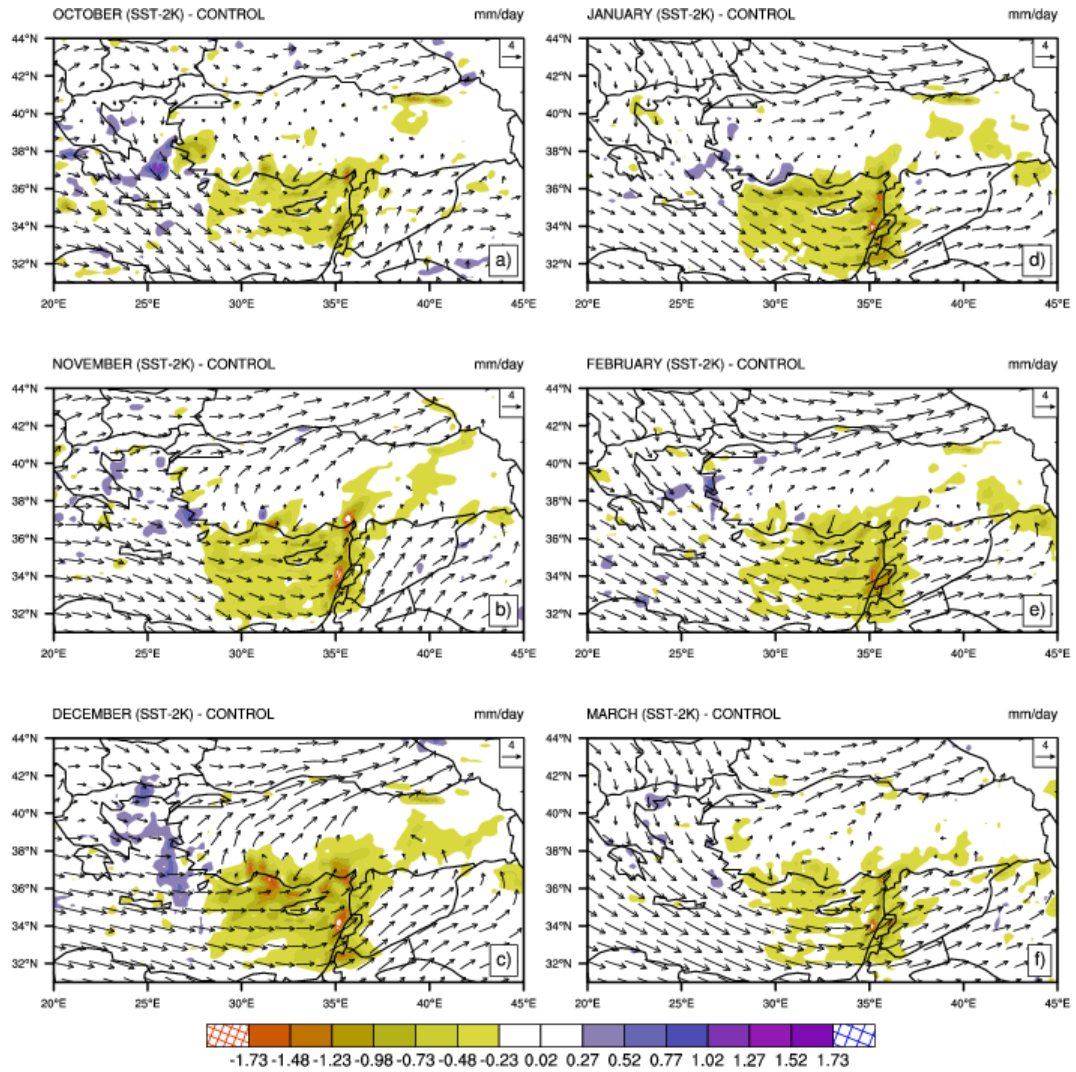


Fig. 3.25. 10-year average monthly difference of precipitation between SST-2K perturbation and control simulation with 850hPa wind vectors of control simulation.

3.2.3. Wet and dry years comparison

As in Aegean Sea sensitivity experiment, changes in precipitation in wet and dry years according to NAO index were performed for Eastern Mediterranean Sea (Fig. 3.26).

In dry years, reductions in precipitation are mostly occurred in southern coastal regions of Turkey and eastern coastal regions of Mediterranean Sea. It is seen that precipitation in central parts of eastern Turkey and eastern coastal regions of Black Sea are also reduced. In wet years, the regions in which precipitation reductions occurred are mostly confined to the eastern Mediterranean Sea itself and southern coastal regions of Turkey especially to Antalya.

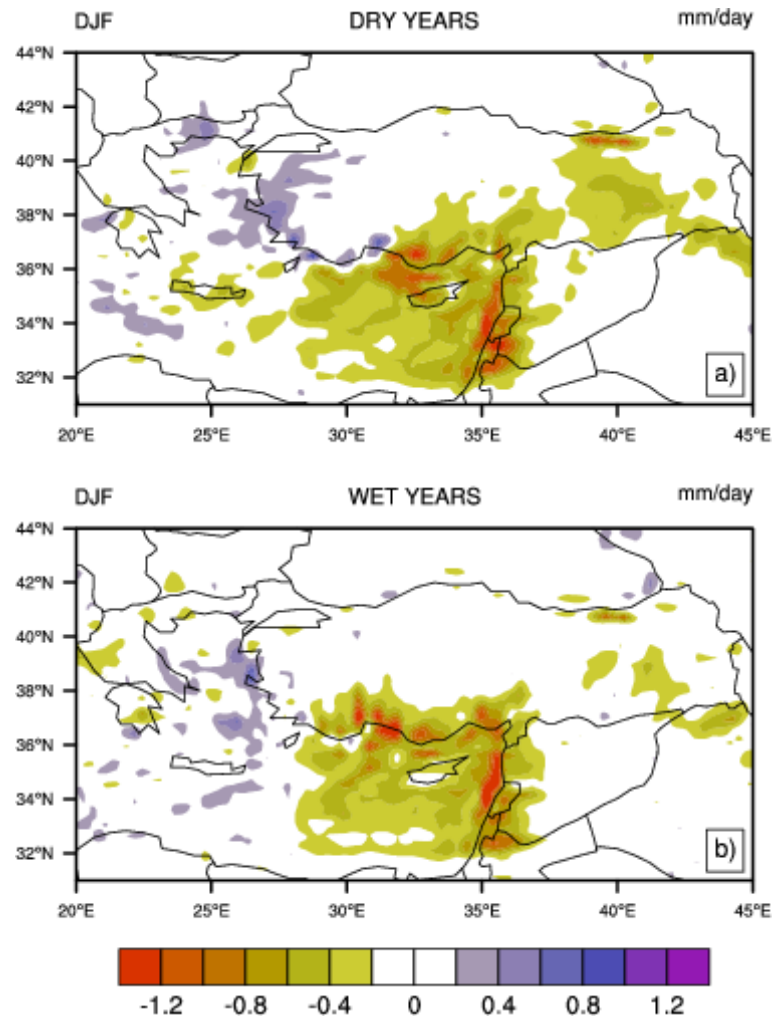


Fig. 3.26. Average dry years (1992-1993, 1993-1994, and 1994-1995) (a) and wet years (1995-1996, 1996-1997, and 1997-1998) (b) difference of precipitation between (SST-2K)-Control and control simulation.

3.3. Western Black Sea Sensitivity Experiment

Fig. 3.27 shows the DJF precipitation difference between SST-2K perturbation and control for the third region that covers western Black Sea (Fig. 2.5). Results indicate that SST perturbation in the western half of Black Sea has little or no effect on Turkish precipitation.

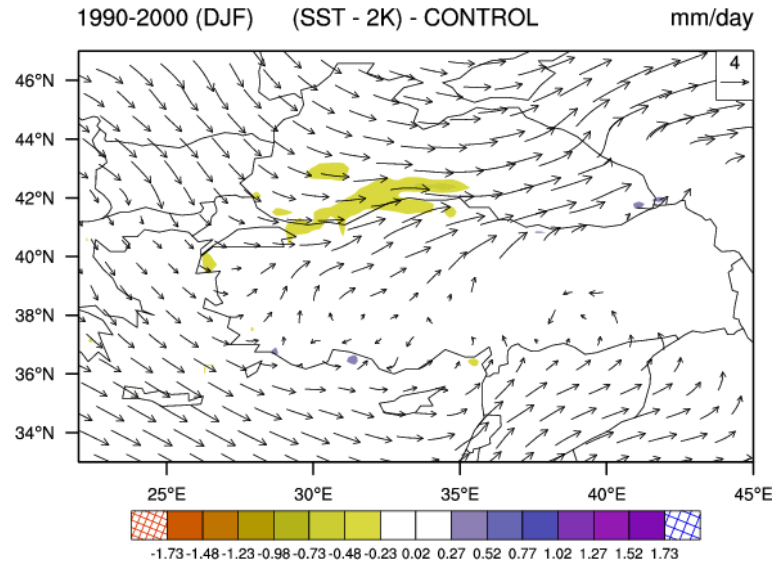


Fig. 3.27. 10-year average DJF precipitation differences between SST-2K perturbation and control for western Black Sea.

3.3.1. Changes in upper level parameters

Air temperature at 925hPa is mostly decreased at western Black Sea itself and coastal regions of it when the SST is decreased by 2K. Since the direction of prevailing wind is north to south and west to east, decrease in air temperature is spreaded to the northwest regions of Turkey, northern parts of Aegean Sea, and eastern Black Sea (Fig. 3.28).

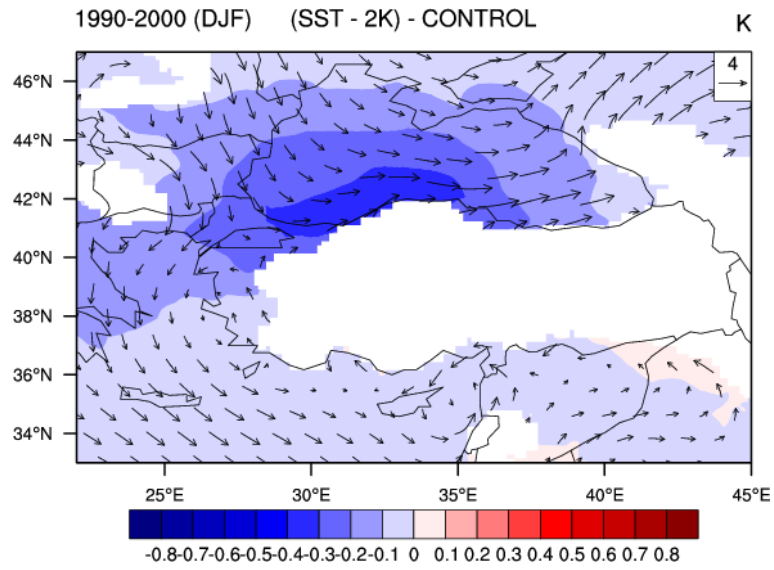


Fig. 3.28. 10-year average DJF difference of air temperature at 925hPa between SST-2K and control simulation.

Decrease in specific moisture at 925hPa is major on eastern Mediterranean Sea itself and it is not able to spread as in air temperature (Fig. 3.29).

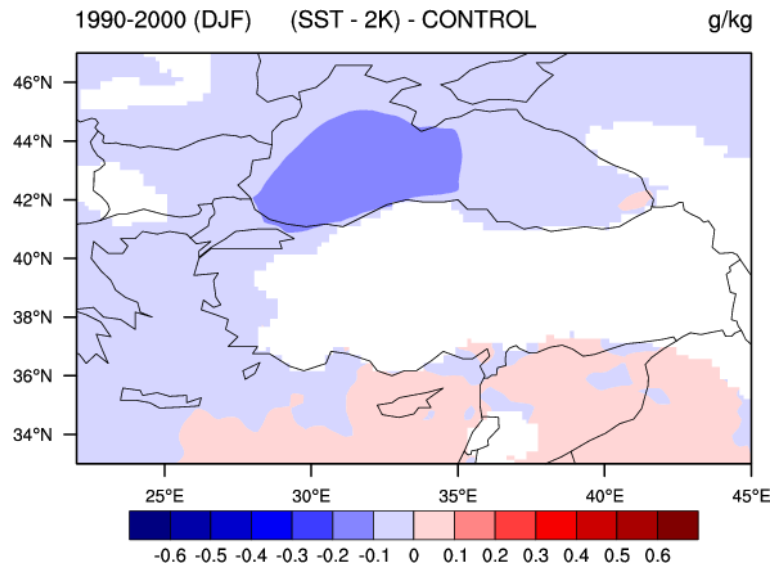


Fig. 3.29. 10-year average DJF difference of specific moisture at 925hPa between SST-2K and control simulation.

At 850hPa, decrease in air temperature and specific moisture due to decrease in SST by 2K is less and changes in air temperature cover more regions than of those in specific moisture with the direction of prevailing wind at 850hPa (Fig. 3.30, Fig. 3.31). Especially decrease in SST by 2K causes more remarkable decrease in air temperature in the southern coastal regions of Turkey and decrease in air temperature can be spreaded to central parts of eastern Turkey.

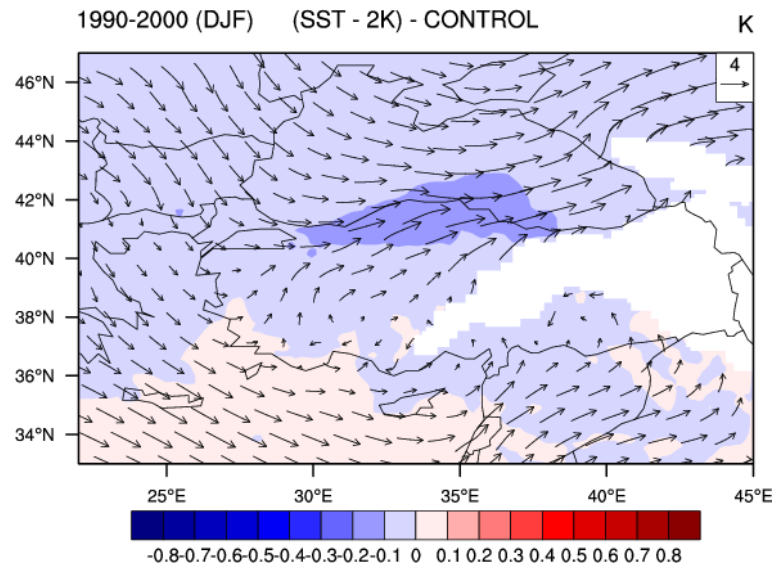


Fig. 3.30. 10-year average DJF difference of air temperature at 850hPa between SST-2K and control simulation.

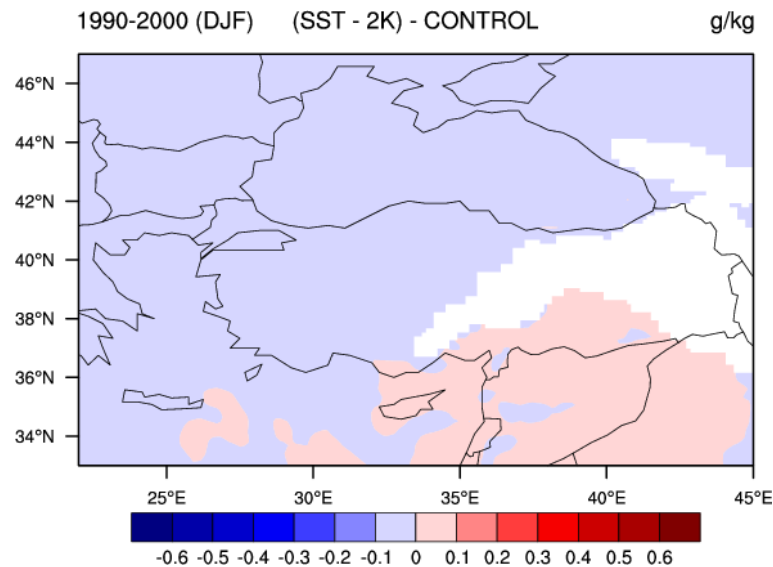


Fig. 3.31. 10-year average DJF difference of specific moisture at 850hPa between SST-2K and control simulation.

3.3.2. Changes in monthly precipitation

When we look at the individual months for SST-2K perturbation (Fig. 3.32), it can be seen that there is no remarkable reduction in Turkish precipitation when the SST of western Black Sea is decreased by 2K. Reductions are mostly occurred in sea itself especially in October.

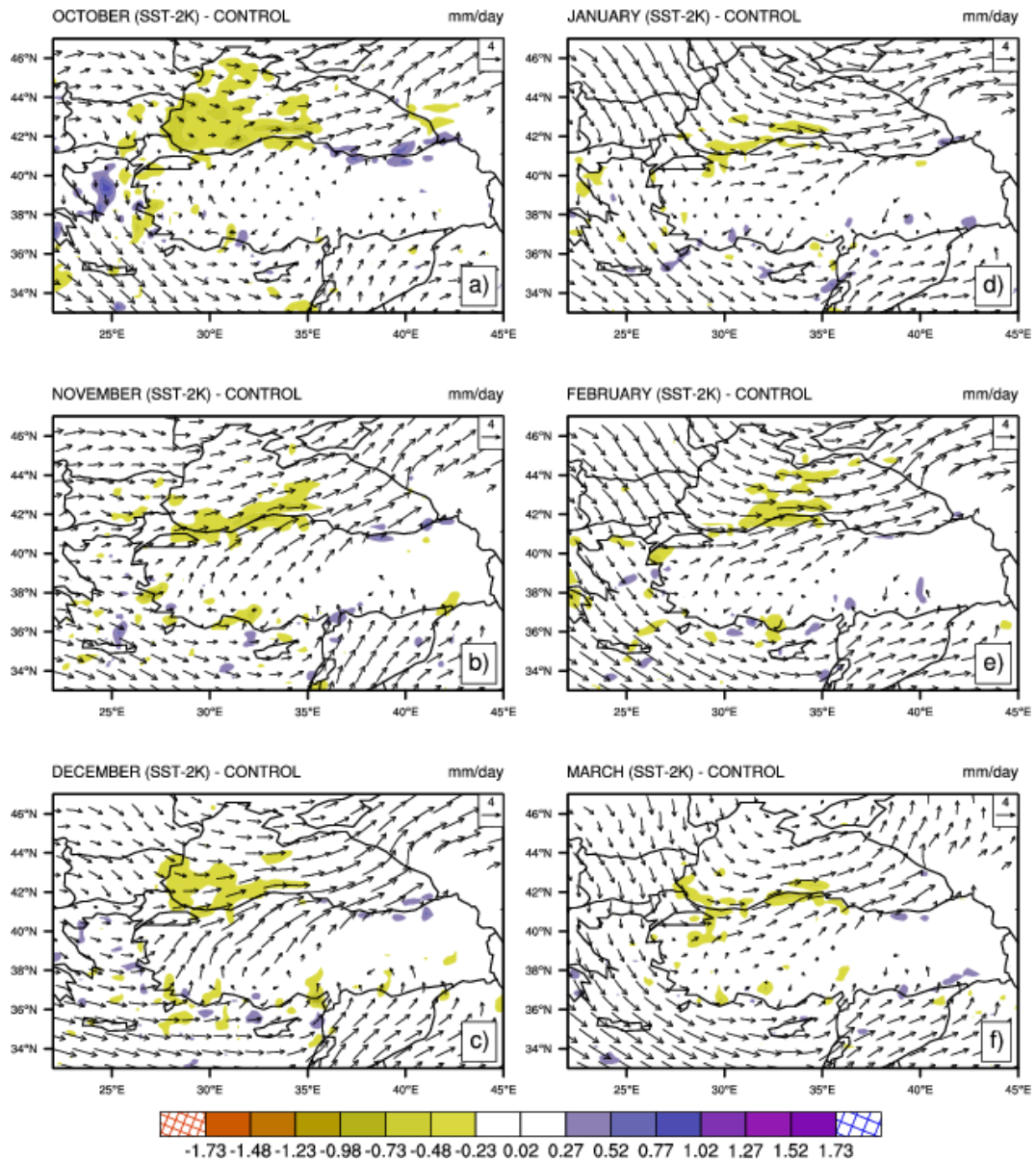


Fig. 3.32. 10-year average monthly difference of precipitation between SST-2K perturbation and control simulation with 850hPa wind vectors of control simulation.

3.3.3. Wet and dry years comparison

Precipitation reduction in both dry and wet years is almost similar and is confined to the western coastal regions of Black Sea (Fig. 3.33).

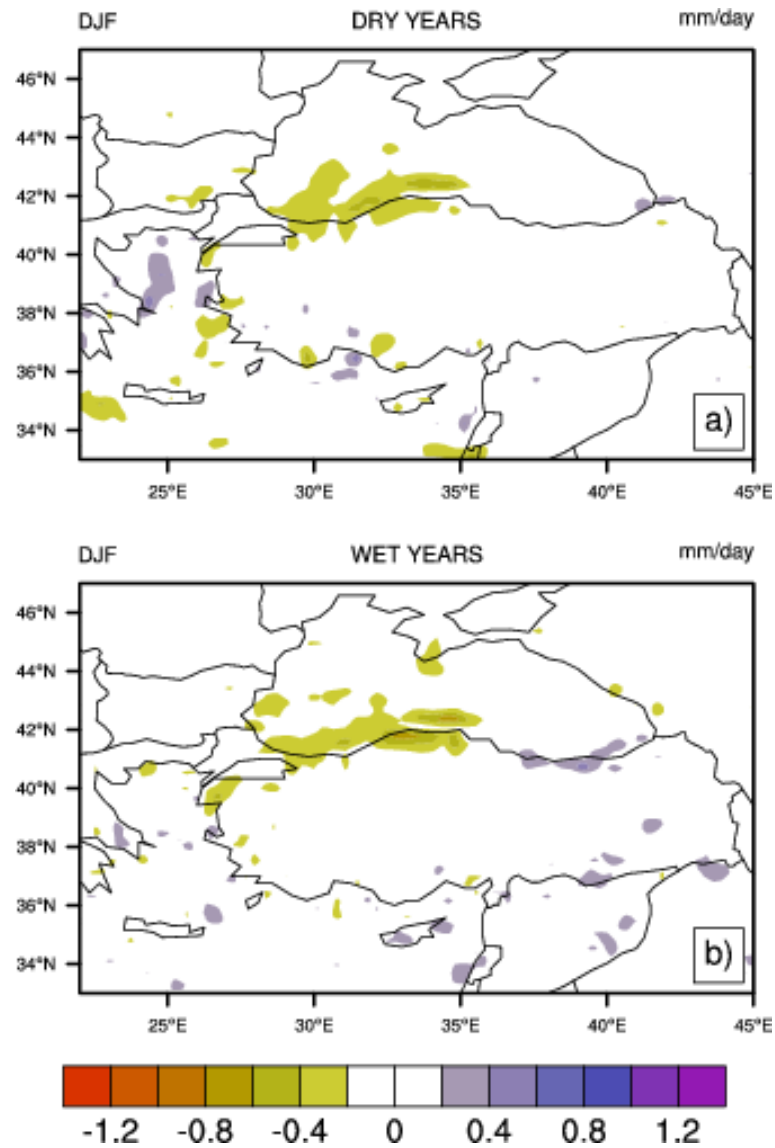


Fig. 3.33. Average dry years (1992-1993, 1993-1994, and 1994-1995) (a) and wet years (1995-1996, 1996-1997, and 1997-1998) (b) difference of precipitation between (SST-2K)-Control and control simulation.

3.4. Eastern Black Sea Sensitivity Experiment

Fig. 3.34 shows the DJF precipitation difference between SST-2K perturbation and control for the fourth region that covers eastern Black Sea (Fig. 2.5). Results indicate that SST perturbation in the eastern half of Black Sea has little or no effect on Turkish precipitation. Eastern and northeastern coastal regions of Black Sea are the regions in which reduction in precipitation takes place.

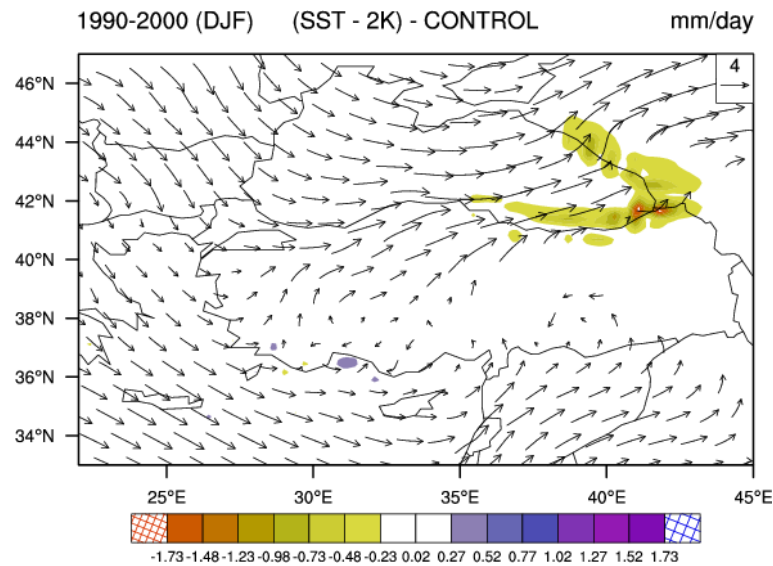


Fig. 3.34. 10-year average DJF precipitation differences between SST-2K perturbation and control for eastern Black Sea.

3.4.1. Changes in upper level parameters

Air temperature at 925hPa is mostly decreased at eastern Black Sea itself and spreaded from west to east with the direction of prevailing wind at 925hPa (Fig. 3.35).

Decrease in specific moisture at 925hPa is occurred on eastern Black Sea itself (Fig. 3.36).

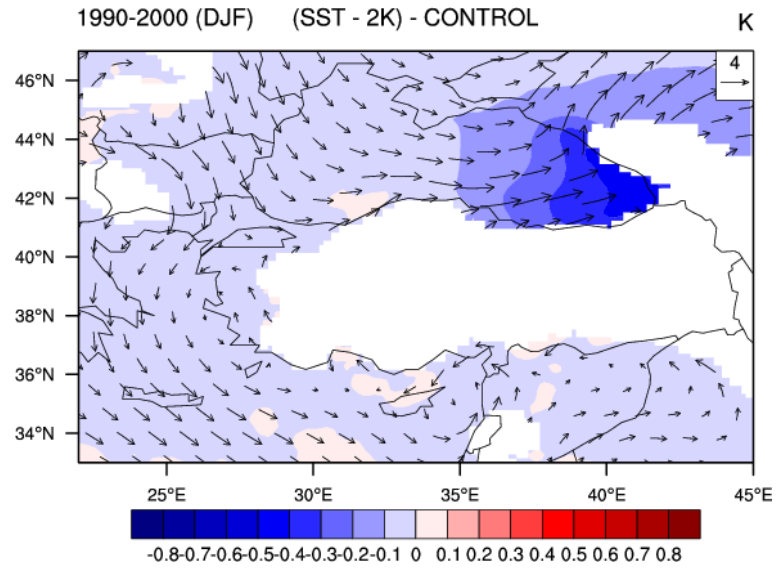


Fig. 3.35. 10-year average DJF difference of air temperature at 925hPa between SST-2K and control simulation.

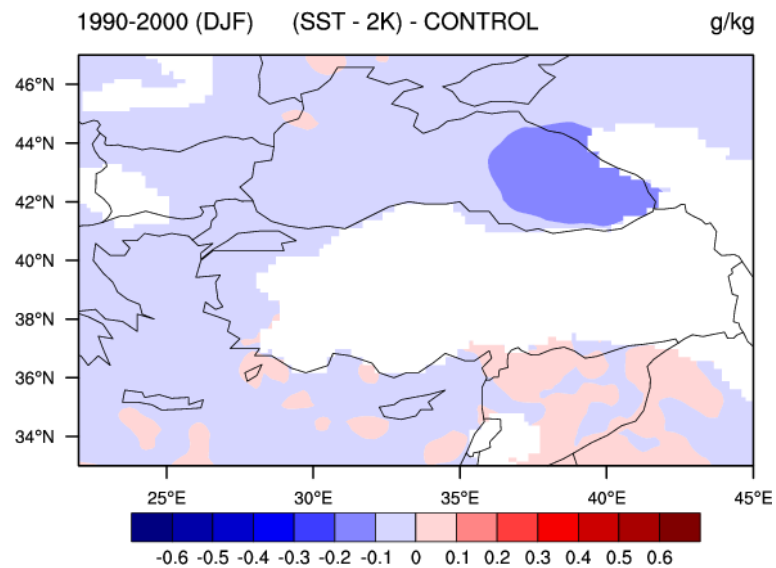


Fig. 3.36. 10-year average DJF difference of specific moisture at 925hPa between SST-2K and control simulation.

At 850hPa, decrease in air temperature is less and spreaded with the direction of prevailing wind at 850hPa (Fig. 3.37). There is no or very little change in specific moisture at 850hPa (Fig. 3.38).

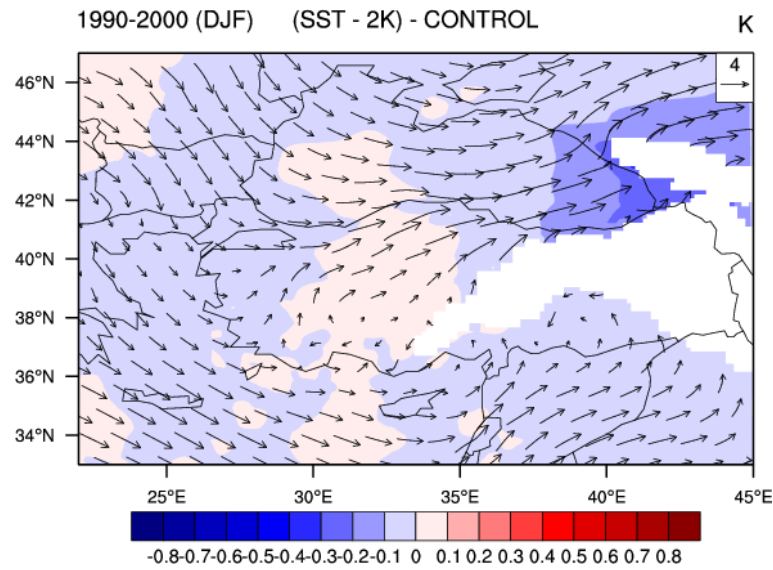


Fig. 3.37. 10-year average DJF difference of air temperature at 850hPa between SST-2K and control simulation.

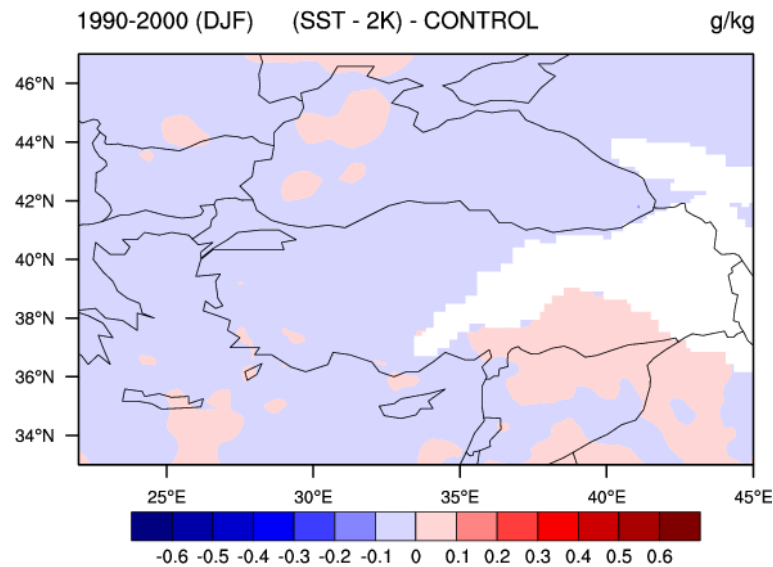


Fig. 3.38. 10-year average DJF difference of specific moisture at 850hPa between SST-2K and control simulation.

3.4.2. Changes in monthly precipitation

When we look at the individual months for SST-2K perturbation (Fig. 3.39), it can be seen that there is no remarkable reduction in Turkish precipitation as it is in western Black Sea experimen. Reductions are mostly occured in sea itself especially in October and take place in the coastal regions of eastern Black Sea in other months.

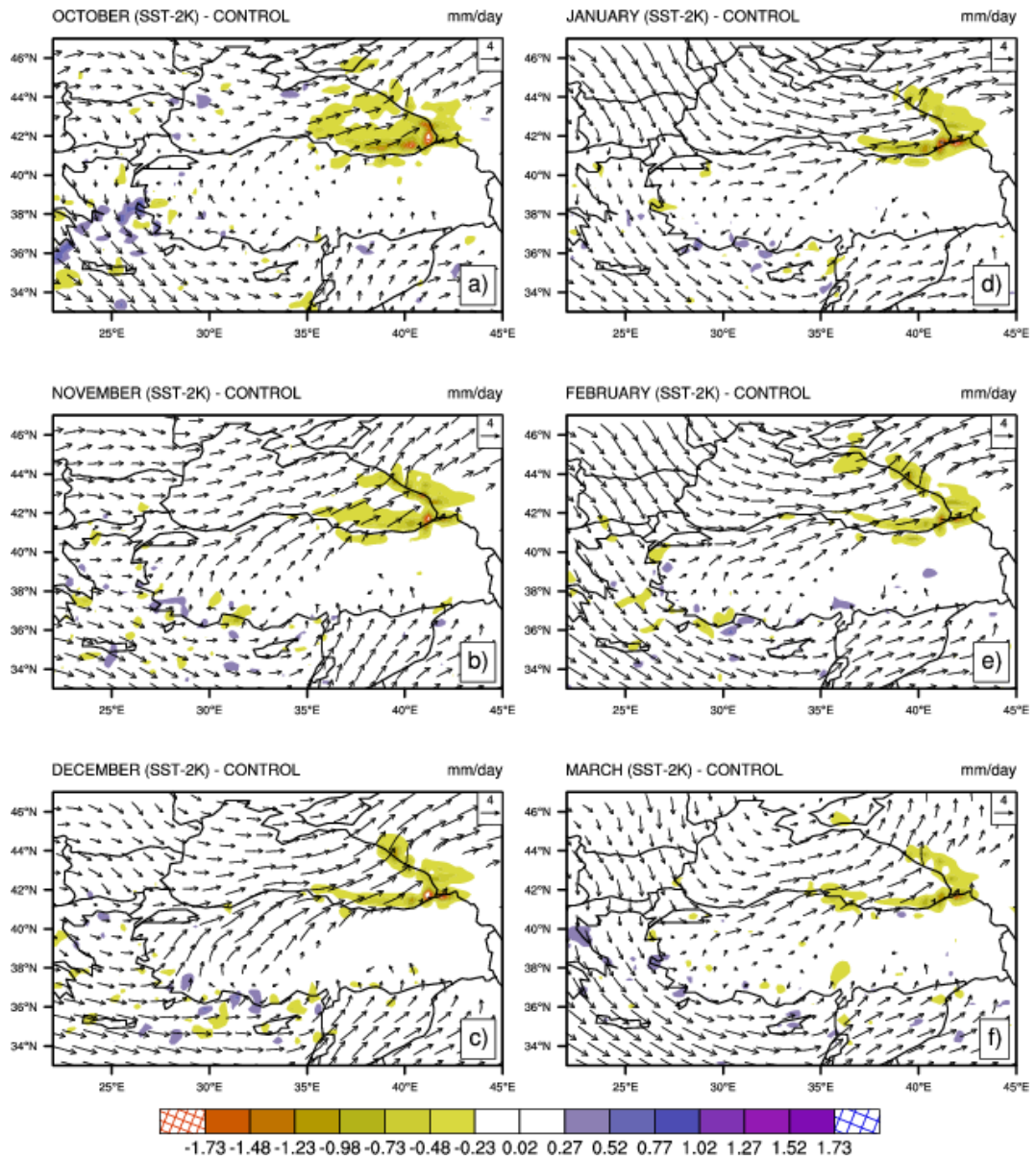


Fig. 3.39. 10-year average monthly difference of precipitation between SST-2K perturbation and control simulation with 850hPa wind vectors of control simulation.

3.4.3. Wet and dry years comparison

Precipitation reduction in both dry and wet years is almost similar and is confined to the coastal regions of eastern Black Sea (Fig. 3.40).

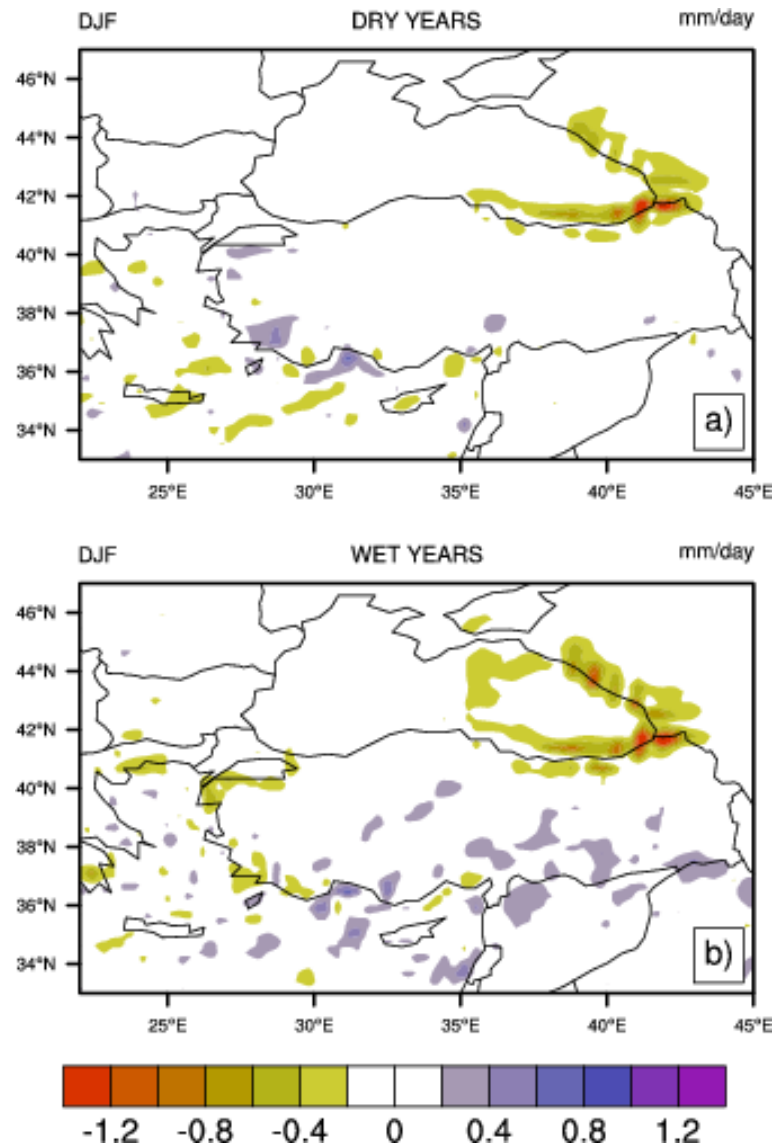


Fig. 3.40. Average dry years (1992-1993, 1993-1994, and 1994-1995) (a) and wet years (1995-1996, 1996-1997, and 1997-1998) (b) difference of precipitation between (SST-2K)-Control and control simulation.

3.5. Central Mediterranean Sea Sensitivity Experiment

Fig. 3.41 shows the DJF precipitation difference between SST-2K perturbation and control for the fifth region that covers central Mediterranean Sea (Fig. 2.5). Results indicate that SST perturbation in the central Mediterranean Sea causes precipitation reduction in mostly sea itself and Greece. It has little effect on precipitation in western parts of Turkey and there is almost no change in precipitation in other parts of Turkey.

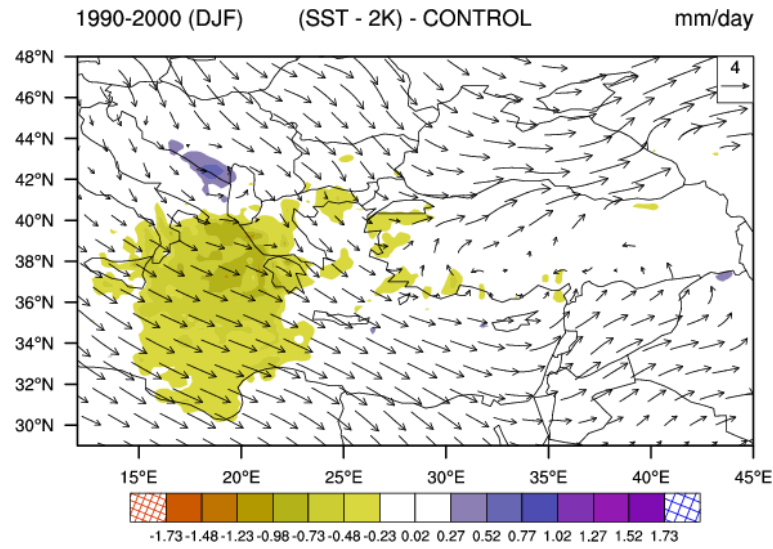


Fig. 3.41. 10-year average DJF precipitation differences between SST-2K perturbation and control for central Mediterranean Sea.

3.5.1. Changes in upper level paramaters

Air temperature at 925hPa is mostly decreased in central Mediterranean itself and spreaded from west to east with the direction of prevailing wind at 925hPa (Fig. 3.42). It can be seen that change in air temperature has also effect on Turkey.

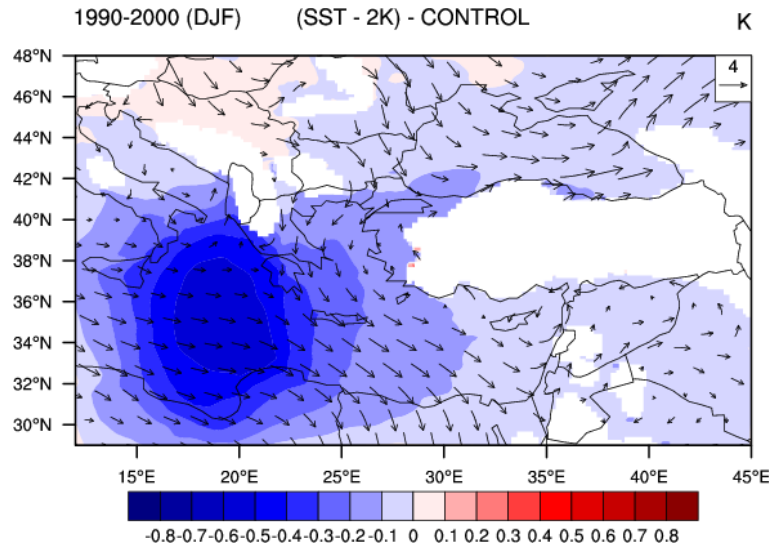


Fig. 3.42. 10-year average DJF difference of air temperature at 925hPa between SST-2K and control simulation.

Decrease in specific moisture at 925hPa is mostly occurred on central Mediterranean Sea itself and there is no effect on Turkey (Fig. 3.43).

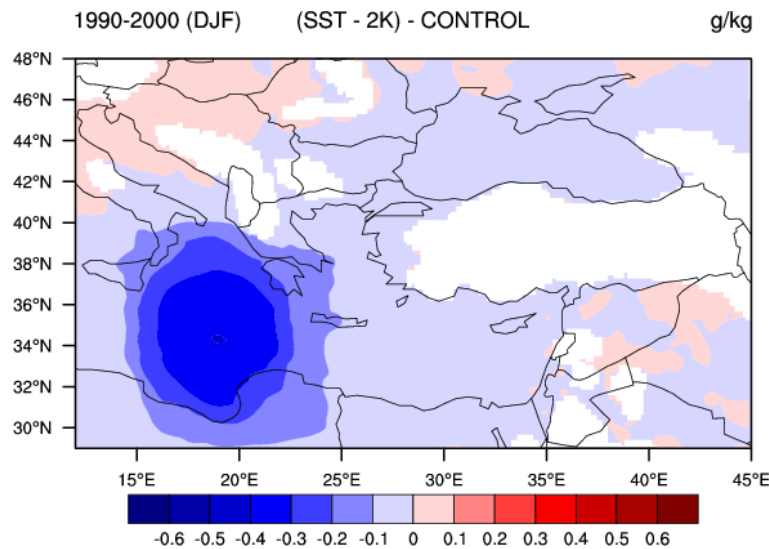


Fig. 3.43. 10-year average DJF difference of specific moisture at 925hPa between SST-2K and control simulation.

At 850hPa, decrease in air temperature is ranged over a wide field covering

western and northern parts of Turkey (Fig. 3.44). As it is in 925hPa, change in specific moisture at 850hPa is confined to the central Mediterranean Sea (Fig. 3.45).

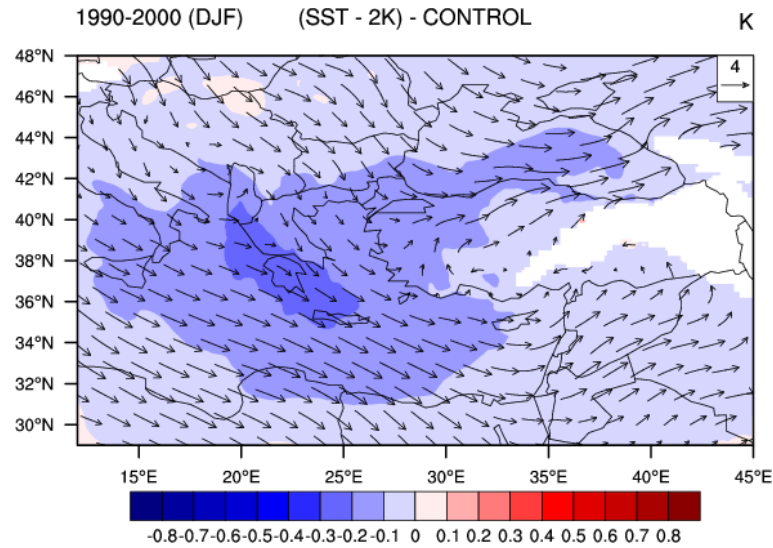


Fig. 3.44. 10-year average DJF difference of air temperature at 850hPa between SST-2K and control simulation.

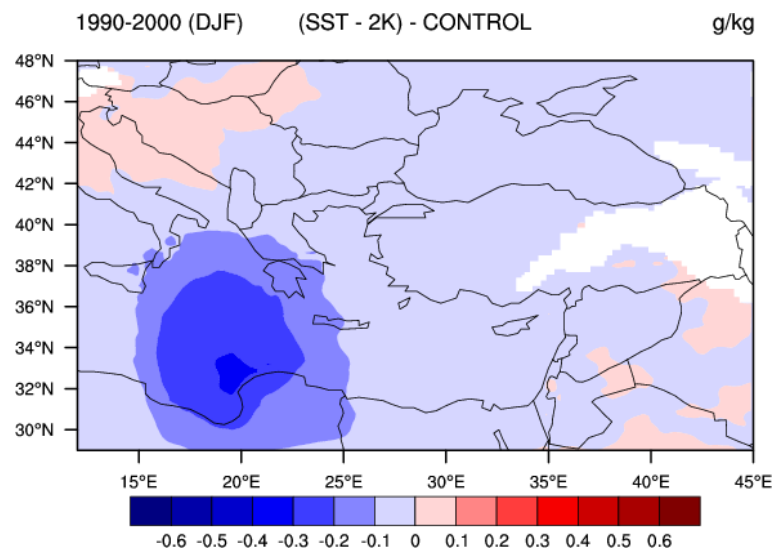


Fig. 3.45. 10-year average DJF difference of specific moisture at 850hPa between SST-2K and control simulation.

3.5.2. Changes in monthly precipitation

When we look at the individual months for SST-2K perturbation (Fig. 3.46), major reductions in precipitation occur in sea itself especially October, November, and December months. Precipitation in certain regions of Turkey such as Antalya, Muğla, and Çanakkale is reduced especially in December.

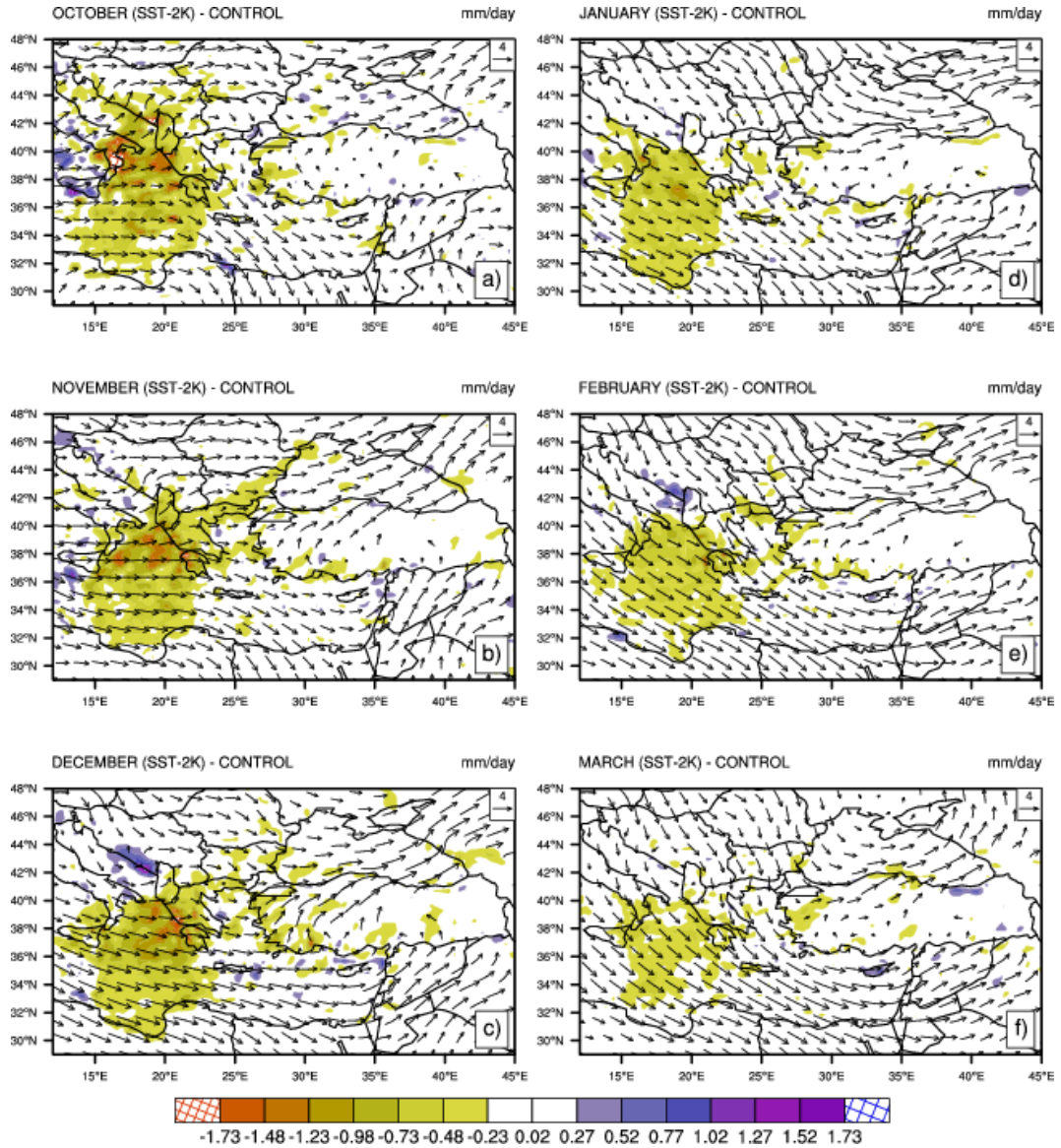


Fig. 3.46. 10-year average monthly difference of precipitation between SST-2K perturbation and control simulation with 850hPa wind vectors of control simulation.

3.5.3. Wet and dry years comparison

Precipitation reduction in both dry and wet years is almost similar, however, since three years are used to analyze wet and dry years it is highly possible to encounter noises (Fig. 3.47).

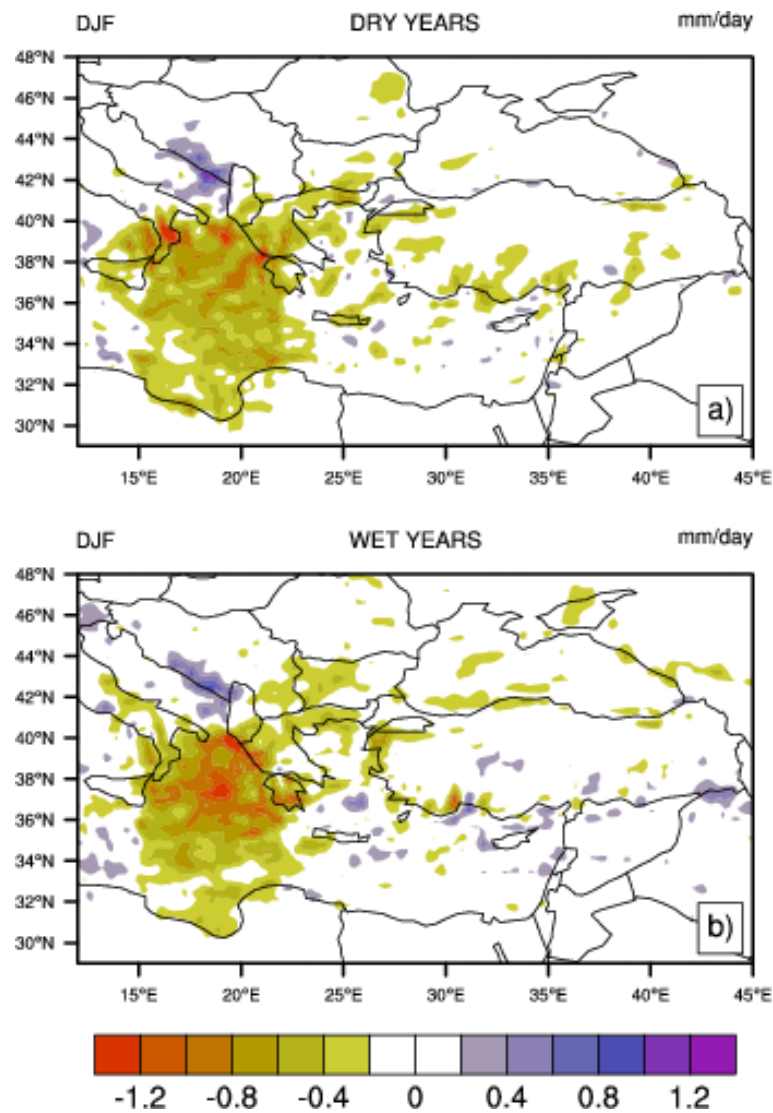


Fig. 3.47. Average dry years (1992-1993, 1993-1994, and 1994-1995) (a) and wet years (1995-1996, 1996-1997, and 1997-1998) (b) difference of precipitation between (SST-2K)-Control and control simulation.

4. CONCLUSIONS and DISCUSSION

Previous studies have investigated precipitation variabilities of Turkey in conjunction with large-scale circulation patterns and atmospheric teleconnections. This study investigates the linkage between precipitation variability in Turkey and sea surface temperature variability in surrounding seas through sensitivity experiments using a state-of-the-art regional climate model.

In general, the results of the sensitivity experiments show that the response of Turkish precipitation to SST changes in the surrounding seas is limited and mostly confined to the coastal areas in Turkey. In addition to this precipitation response to SST perturbations is statistically insignificant. Aegean Sea perturbation experiments indicate that rainfall changes mostly in Aegean Sea and westernmost areas of Turkey in winter. Increasing SST, in general, increases rainfall in these areas, and reducing it decreases rainfall. SST perturbations in the eastern Mediterranean regions affect immediate sea and land areas in winter. Winter precipitation in Turkey seems to be not affected by the SST perturbations in Black Sea. SST perturbation in the central Mediterranean region has more influence on precipitation in Greece than those of in Turkey. According to monthly results Turkish precipitation is mostly affected from perturbations especially in Eastern Mediterranean Sea and Aegean Sea in December which may be related to cyclone tracks and frequency in this month. Monthly results also indicate that there are a few areas where SST changes may have potentially more impact on precipitation. These results are more or less related to the climatology, but the picture for the response of precipitation to SST in cases of individual precipitation events could be very different.

For the future, we are planning to look into how the individual severe precipitation events in Turkey are affected by these SST perturbations. In addition to this, we are also planning to construct a cyclone tracking algorithm in order to understand and demonstrate changes in cyclone tracks, frequency, and density by explaining the interactions between the SST and cyclones.

REFERENCES

- Anthes, R. A.**, 1977. A cumulus parameterization scheme utilizing a one-dimensional cloud model. *Mon. Weather Rev.*, **117**, 1423–1438.
- Arakawa, A. and Schubert, W.**, 1974. Interaction of a cumulus cloud ensemble with the large-scale environment, Part 1. *Journal of Atmospheric Sciences*, **31**, 674–701.
- Arpe, K., Dümenil, L., Giorgetta, M. A.**, 1998. Variability of Indian Monsoon in the ECHAM3 Model: Sensitivity to Sea Surface Temperature, Soil Moisture, and Stratospheric Quasi-Biennial Oscillation. *Journal of Climate*, **11**, 1837–1858.
- Barret, B. S.**, 2006. Relationship between sea surface temperature anomalies and precipitation across Turkey. In Ünal, Y., Kahya, C., Bari, D. D. (Eds.), *Proceedings of the International Conference on Climate Change and the Middle East: Past, Present and Future*. Istanbul Technical University, Istanbul.
- Bolle, H. J. (Editor)**, 2003. Mediterranean Climate - Variability and Trends. Springer Verlag, Berlin, Heidelberg, New York, 372pp.
- Dickinson, R. E., Kennedy, P. J., Hendersen-Sellers, A., Wilson, M.**, 1986. Biosphere-Atmosphere Transfer Scheme (BATS) for the NCAR Community Climate Model. *NCAR Technical Note, NCAR / TN-275+STR, National Center for Atmospheric Research*.
- Dickinson, R. E., Errico, R., Giorgi, F., and Bates, G.**, 1989. A regional climate model for the western united states. *Climate Change*, **15**, 383–422.
- Dickinson, R. E., Henderson-Sellers, A., and Kennedy, P.**, 1986. Biosphere-Atmosphere Transfer Scheme (BATS) version 1e as coupled to the NCAR Community Climate Model. *NCAR Technical Report, National Center for Atmospheric Research*.
- Emanuel, K. A.**, 1991. A scheme for representing cumulus convection in large-scale models. *Quart. J. Roy. Meteor. Soc.*, **48**, 2313–2335.
- Emanuel, K. A. and Zivkovic-Rothman, M.**, 1999. Development and evaluation of a convection scheme for use in climate models. *J. Atmos. Sci.*, **56**, 1766–1782.
- Fritsch, J. M., and Chappell, C. F.**, 1980. Numerical prediction of convectively driven mesoscale pressure systems. part i: Convective parameterization. *Journal of Atmospheric Sciences*, **37**, 1722–1733.

- Giorgi, F., Marinucci, M. R., and Bates, G. T.**, 1993a. Development of a second generation regional climate model (RegCM2), I, Boundary layer and radiative transfer processes. *Mon. Weather Rev.*, **121**, 2794–2813.
- Giorgi, F., Marinucci, M. R., De Canio, G., and Bates, G. T.**, 1993b. Development of a second generation regional climate model (RegCM2), II, Convective processes and assimilation of lateral boundary conditions. *Mon. Weather Rev.*, **121**, 2814–2832.
- Goodess, C. M., Jones, P. D.**, 2002. Links between circulation and changes in the characteristics of Iberian rainfall. *Int. J. Climatol.*, **22**, 1593–1615.
- Grell, G. A.**, 1993. Prognostic evaluation of assumptions used by cumulus parameterizations. *Monthly Weather Review*, **121**, 764–787.
- Grell, G. A., Dudhia, J., and Stauffer, D. R.**, 1994b. A description of the fifth generation Penn State/NCAR Mesoscale Model (MM5). *NCAR Technical Note, NCAR / TN-398+STR*, 121pp.
- Hack, J. J., Boville, B. A., Briegleb, B. P., Kiehl, J. T., Rasch, P. J., Williamson, D. L.**, 1993. Description of the NCAR Community Climate Model (CCM2). *NCAR Technical Note, NCAR / TN-382+STR, National Center for Atmospheric Research, Boulder, Colorado.*, 108pp.
- Holtstlag, A., de Bruijn, E., and Pan., H. L.**, 1990. A high resolution air mass transformation model for short-range weather forecasting. *Monthly Weather Review*, **118**, 1561–1575.
- Holtstlag, A., Boville, B. A.**, 1993. Local versus nonlocal boundary-layer diffusion in a global climate model. *Journal of Climate*, **6**, 1825–1842
- Hsie, E. Y., Anthes, R. A., and Keyser, D.**, 1984. Numerical simulation of frontogenesis in a moist atmosphere. *J. Atmos. Sci.*, **41**, 2581–2594.
- Janicot, S., Harzallah, A., Fontaine, B., Moron, V.**, 1998. West African Monsoon Dynamics and Eastern Equatorial Atlantic and Pacific SST Anomalies (1970-88). *Journal of Climate*, **11**, 1874–1882.
- Karaca, M., Deniz, A., and Tayanç, M.** 2000. Cyclone track variability over Turkey in association with regional climae. *Int. J. Climatol.*, **20**, 122–136.
- Kiehl, J., Hack, J., Bonan, G., Boville, B., Breigleb, B., Williamson, D., and Rasch, P.** 1996. Description of the NCAR Community Climate Model (CCM3). *NCAR Technical Note, NCAR / TN-420+STR, National Center for Atmospheric Research.*
- Krichak, S. O., Alpert, P.**, 2005a. Decadal trends in the East Atlantic/West Russia pattern and the Mediterranean precipitation. *Int. J. Climatol.*, **25**, 183–192.
- Krichak, S. O., Alpert, P.**, 2005b. Signatures of the NAO in the atmospheric circulation during the wet winter months over the Mediterranean region. *Theor. Appl. Climatol.*, **82**, 27–39.

- Leung, L. R., Ghan, S. J., Zhao, Z. C., Luo, Y., Wang, W. C., and Wei, H. L.**, 1999. Intercomparison of regional climate 30 simulations of the 1991 summer monsoon in eastern Asia. *J. Geophys. Res.*, **104**, 6425–6454.
- Li, L.Z. X.**, 2006. Atmospheric GCM response to an idealized anomaly of the Mediterranean sea surface temperature. *Climate Dynamics*, **27**, 543–552.
- Maheras, P., Flocas, H., Patrikas, I., and Anagnostopoulou, Ch.**, 2001. A 40 year objective climatology of surface cyclones in the Mediterranean region: Spatial and temporal distribution. *Int. J. Climatol.*, **21**, 109–130.
- Maracchi, G., Crisci, A., Grifoni, D., Gozzini, B., Meneguzzo, F.**, 1999. Relationships between extreme convective events and sea surface temperature anomalies in coastal regions of the Mediterranean. In A. Amendola and J. Linnerooth-Bayer (Eds.), *Proceedings of the euroconference on global change and catastrophe risk management: Flood risks in Europe*. Laxenburg, Austria.
- McGregor, J. L.**, 1997. Regional Climate Modeling. *Meteorol. Atmos. Phys.*, **63**,
- Messenger, C., Gallee, H., Brasseur, O.**, 2004. Precipitation sensitivity to regional SST in a regional climate simulation during the West African monsoon for two dry years. *Climate Dynamics*, **22**, 249–266.
- Pal, J., Small, and Eltahir, E.**, 2000. Simulation of regional-scale water and energy budgets: Representation of subgrid cloud and precipitation processes within regcm. *Journal of Geophysical Research-Atmospheres*, **105(D24)**, 29579–29594.
- Pinet, P. R.**, 1996. Invitation to Oceanography. *St Paul, MN, West Publishing Co., ISBN (3rd ed.)*, p.202
- Roads, J., Chen, S., Cocke, S., Druyan, L., Fulakeza, M., LaRow, T., Lonergan, P., Qian, J. H., and Zebiak, S.**, 2003. International Research Institute/Applied Research Centers (IRI/ARCs) regional model intercomparison over South America. *J. Geophys. Res.*, **108:4425**, doi:10.1029/2002JD003201.
- Rowell, D. P.**, 2003. The impact of Mediterranean SSTs on the Sahelian rainfall season. *Journal of Climate*, **16**, 849–862.
- Sundqvist, H., Berge, E., and Kristjansson, J.**, 1989. The effects of domain choice on summer precipitation simulation and sensitivity in a regional climate model. *Journal of Climate*, **11**, 2698–2712.
- Takle, E. S., Gutowski Jr., W. J., Arritt, R. W., Pan, Z., Anderson, C. J., da Silva, R. R., Caya, D., Chen, S. C., Giorgi, F., Christensen, J. H., Hong, S. Y., Juang, H.M. H., Katzfey, J., Lapenta, W. M., Laprise, R., Listen, G. E., Lopez, P., McGregor, J., Pielke Sr., R. A., and Roads, J. O.**, 1999. Project to intercompare regional climate simulations (PIRCS): Description and initial results. *J. Geophys. Res.*, **104**, 19443–19461.

- Trigo, I. F., Davies, T. D., and Bigg, G. R.**, 2000. Decline in Mediterranean rainfall caused by weakening of Mediterranean cyclones. *Geophys. Res. Lett.*, **27**, 2913–2916.
- Trigo, R., and 21 coauthors.**, 2006. Relations between variability in the Mediterranean region and mid-latitude variability (lead author of Chapter 3), in: *The Mediterranean Climate: an overview of the main characteristics and issues*, Ed. P. Lionello, P. Malanotte-Rizzoli, and R. Boscolo. *Elsevier*, 179–226.
- Xoplaki, E., González-Rouco, J. F., Luterbacher, J., Wanner, H.**, 2004. Wet season Mediterranean precipitation variability: influence of large-scale dynamics and trends. *Journal of Climate*, **11**, 2628–2644.

VITA

Deniz Bozkurt was born in Samandağ, Hatay on 28 June 1980. He finished Kadir Has High School in 1998. Having joined to Environmental Engineering Department of Engineering Faculty at Marmara University in 1999, he transferred to Environmental Engineering Department of Engineering Faculty at Middle East Technical University in 2001 and graduated from this department in June 2004. He started to his Master of Sciences in Eurasia Institute of Earth Sciences in 2005 and he has been a research assistant in the Eurasia Institute of Earth Sciences since November 2005.